3-2020

Detonation Confinement in a Radial Rotating Detonation Engine

Kavi Muraleetharan

DETONATION CONFINEMENT IN A RADIAL ROTATING DETONATION ENGINE

THESIS

Kavi Muraleetharan, Second Lieutenant, USAF

AFIT-ENY-MS-20-M-273

DEPARTMENT OF THE AIR FORCE
AIR UNIVERSITY

AIR FORCE INSTITUTE OF TECHNOLOGY

Wright-Patterson Air Force Base, Ohio

AFIT-ENY-MS-20-M-273

DETONATION CONFINEMENT IN A RADIAL ROTATING DETONATION ENGINE

THESIS

Presented to the Faculty

Department of Aeronautics and Astronautics

Graduate School of Engineering and Management

Air Force Institute of Technology

Air University

Air Education and Training Command

in Partial Fulfillment of the Requirements for the

Degree of Master of Science in Aeronautical Engineering

Kavi Muraleetharan, B.S.

Second Lieutenant, USAF

March 2020

AFIT-ENY-MS-20-M-273

DETONATION CONFINEMENT IN A RADIAL ROTATING DETONATION ENGINE

Kavi Muraleetharan, B.S.
Second Lieutenant, USAF

Committee Membership:

Marc D. Polanka, PhD
Chairman

Frederick R. Schauer, PhD
Member

Major Levi M. Thomas, PhD
Member

Abstract

Radial Rotating Detonation Engines (RRDE) have provided an opportunity for use of a pressure-gain combustor in a more compact form compared to an axial RDE. A successfully tested RRDE has operated over a wide range of test conditions and produced detonation modes with one, two, and three waves. The presence of multiple waves located the detonation waves to the outer radius, while one wave modes operated closer to the inner radius. Locating the detonation wave closer to the inner diameter resulted in less time for combustion prior to the radial turbine. Subsequently, this tended to decrease efficiency. To attempt to alleviate this, the detonation chamber area was modified from its constant area design to a decreasing area design as the flow travelled radially inward to confine the detonation wave to a more radially outward position. The detonation chamber featured a flat channel plate that reduced the flow's effective cross-sectional area by almost 65% from its inlet to the turbine inlet plane. The constant channel height improved total pressure loss as high as 92% over the constant area geometry for similar flow conditions and increased the RRDEs ability to operate at larger channel heights. Guide vanes were introduced downstream of the combustion section by modifying the flat channel plate with modular channel plates. This configuration attempted to provide a combustion section with a confined detonation and a transition section to the guide vanes and nozzle. While in this configuration, the RRDE operated at both detonative and acoustic wave modes. Thin-filament pyrometry (TFP) was also performed to measure transient temperature responses during operation. The successful implementation of the filaments provided temperature measurements during detonative modes up to 2194 K at the guide vanes and frequency responses captured through TFP between 1.6-5.9 kHz.

Acknowledgements

I would like to thank my advisor, Dr. Marc Polanka, for providing me the guidance to accomplish the objectives of this research. Furthermore, he has been selflessly committed to providing mentorship to a young engineer as I start my professional career. The remaining members of my committee, faculty members of AFIT, and the entire team at D-Bay have also been helpful in providing their technical expertise towards the research and my professional development. I would also like to thank my fellow student co-workers and friends who have provided encouragement as we endured the academic vigor in the lab and classroom. Most importantly, I would like to thank my family. My father and sisters have provided me the courage to achieve success as they promote my continuous journey in education and innovation. Despite her own academic and professional workload, my fiancée has provided continued love and support towards all my endeavors. I am eternally grateful for her sacrifices and hope to reciprocate that devotion as she pursues her dreams. Finally, my mother's primary values of perseverance and compassion have allowed me to overcome all obstacles while committing to help those around me. I strive to become my best self for her, and this work is dedicated to her loving memory.

Kavi Muraleetharan

Table of Contents

Page

List of Figures

List of Tables

List of Abbreviations

Abbreviation		Page
fps	Frames per Second	71
CFD	Computational Fluid Dynamics	74
RTV	Room-Temperature-Vulcanizing	85

List of Symbols

DETONATION CONFINEMENT IN A RADIAL ROTATING DETONATION ENGINE

I. Introduction

The Rotating Detonation Engine (RDE) is a device that uses detonative combustion to potentially improve the performance of gas-turbine engines, with application as an efficient and sustainable system for power and propulsion. RDEs are considered pressure-gain combustion devices that increase the amount of work potential due to the higher thermodynamic state of the products. Therefore, RDEs can provide a more efficient replacement to deflagrative combustors within gas-turbine engines [1]. As an integral part of the turbomachinery cycle, a combustor with a higher work potential would decrease energy consumption to allow for more power to be developed over a given cycle.

While the design of the RDE is relatively simple, the physical phenomenon within the combustion chamber creates a flowfield difficult to understand and model. Fundamentally, an RDE operates by initiating a detonation wave that travels cyclically within a chamber to combust reactants. Shown in Figure 1, two configurations of RDEs have been tested. The axial RDE, shown in Figure 1a, has been studied extensively and features reactants and products traveling axially through the combustion chamber. However, recent efforts have been made to examine the use of a more compact Radial RDE (RRDE), shown in Figure 1b, where the detonated products flow radially before exhausting axially through a nozzle. Initial work by Nakagami et al. [2] injected the fuel and oxidizer from the outer annulus before reacting with the detonation wave and exhausting axially near the centerline. Their results showed

comparable detonation structures in the RRDE to axial RDEs [2].

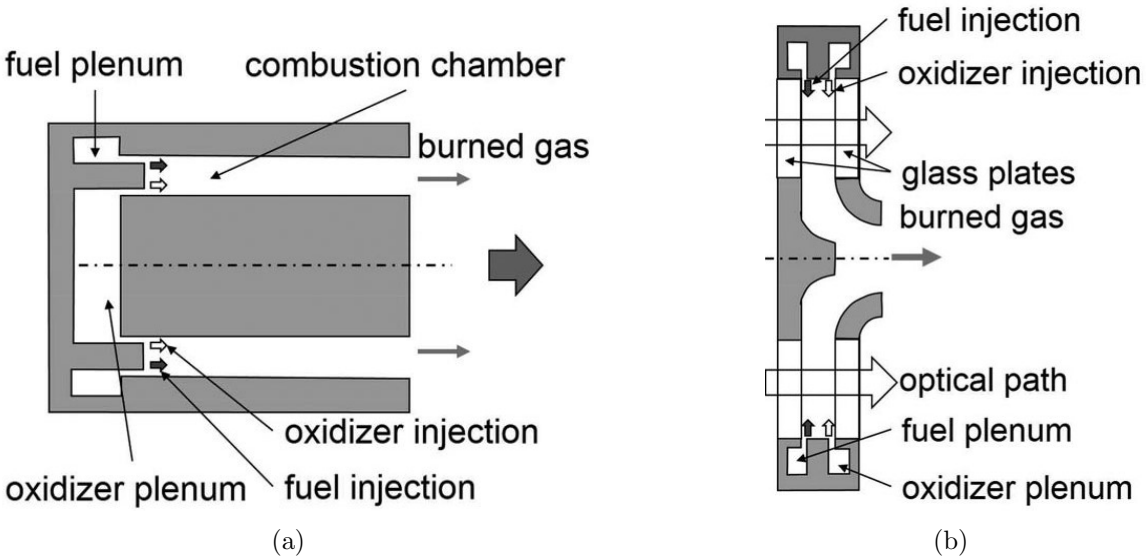

Figure 1. Basic comparison between an (a) Axial and (b) Radial RDE [2].

1.1 Motivation

The motivation of the current research is to investigate the use of an RRDE as a compact auxiliary power unit (APU) onboard aircraft. An RDE has a relatively high power density compared to a traditional gas-turbine with a deflagrative combustor due to the length savings from a transitional combustor. The Radial RDE specifically has increased length savings since the flow and detonation wave is oriented radially before it is turned axially, providing a useful solution onboard aircraft where the axial length of a device must be limited. This overall weight and size reduction and higher power density provides the potential for the RRDE as a compact APU.

Huff et al. [3] developed a novel RRDE using a modular design that controlled the injection area ratio between the reactant throat and detonation channel, as well as the nozzle area ratio between the detonation channel and exit nozzle. This RRDE, given in Figure 2a, was designed to have a constant area detonation chamber with

initially channel heights of 3.5, 4.0, and 4.5 mm and had operability over a wide range of mass fluxes between $50\frac{kg}{m^2s}$ and $200\frac{kg}{m^2s}$ and equivalence ratios between 0.5 and 1.0. The device, considered as a stand-alone combustor due to an absence of turbomachinery, exhibited a variety of wave modes as a function of the operating conditions, with higher waves present for larger mass fluxes and lower equivalence ratios. While the RRDE was able to detonate successfully at multiple flow conditions, the device operated with an average static pressure loss around 30% from the plenum to the inlet of the nozzle, which was incongruous with the pressure-gain goal. When guide vanes and a radial inflow turbine were introduced to the exit of the device, the RRDE was considered to be in the bleed air turbine (BAT) configuration shown in Figure 2b. The initial channel height increased from 4.5 mm to 6.5 mm to allow guide vanes upstream of the turbine. With this increase in the combustion chamber's volume, the BAT RRDE had limited detonable operability and thermal efficiencies less than 40% [4].

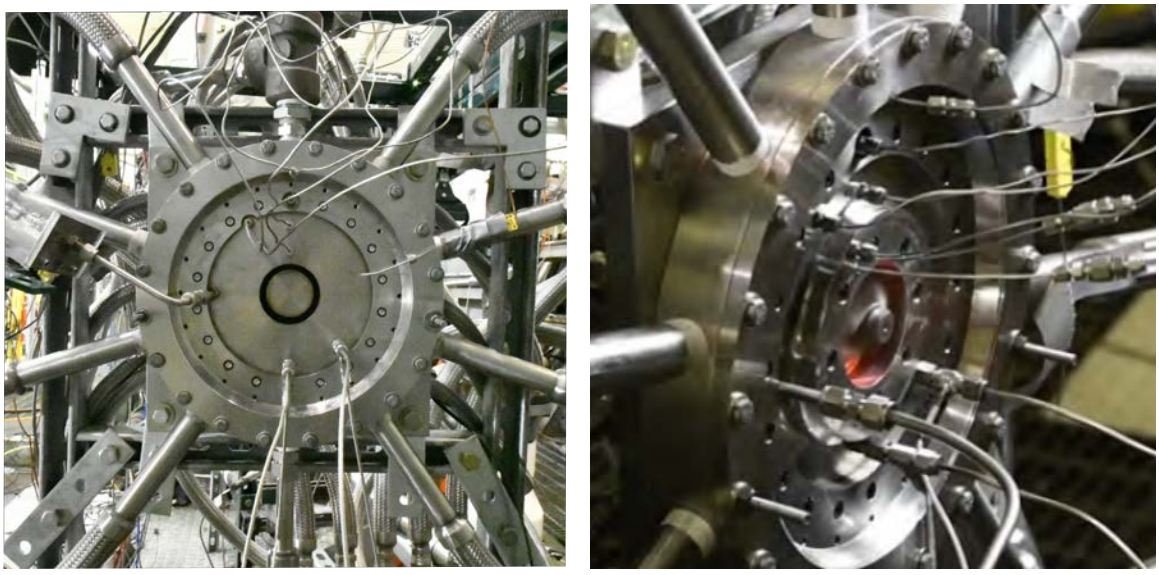

(a) (b)

Figure 2. Constant area RRDE tested as (a) stand-alone combustor and (b) with radial-inflow turbine [5].

For both configurations, the RRDE was tested by Huff et al. [3] with steel channel plates that prevented optical access into the detonation chamber to examine the flowfield. Boller et al. [6] explored the flow behavior, shown in Figure 18, within this constant area stand-alone RRDE by implementing a polycarbonate, clear channel plate to determine the wave modes for given flow conditions. While operating with a single wave, the RRDE's detonation wave was located closer to its inner radius, while multiple waves moved the detonation's location to the outer radius. This outer radial location provided a geometric constraint that limited the number of expansion fans per detonation wave. Furthermore, the outer detonation location increased the distance to the integrated turbomachinery at the center [6]. This would increase the residence time for combustion while keeping the heat release from the detonation away from the airfoils. Despite the success of visualizing the detonation chamber in the RRDE, the setup suffered from consistent ablation of the polycarbonate during testing which provided uncertainty in the operating conditions and its correlation to the steel channel plate testing.

These benefits of an outer detonation wave provided inspiration to examine det-

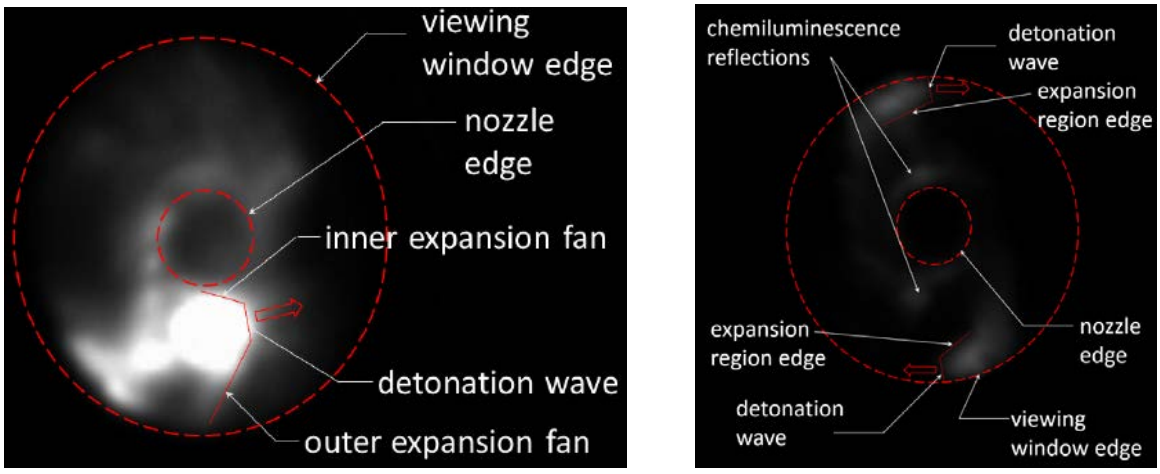

(a) (b)

Figure 3. Comparison of (a) one wave mode operation and (b) two wave mode operation [6].

onation confinement through a different detonation chamber geometry. The present research employed a constant height, decreasing area detonation chamber to attempt to confine the detonation wave to the outer radial location of the device. The results for this constant height geometry at different channel heights, throat area ratios, and nozzle restrictions were compared to the constant area geometry and analyzed to determine an optimal configuration.

1.2 Objectives

The first objective was to enforce detonation confinement in the RRDE to the outer radial location of the device. This was attempted to separate the combustion section of the RRDE from integrated turbomachinery at the center of the device. A flat channel plate was used to create a constant height detonation chamber to create an area restriction to force confinement. Detonation confinement was monitored through static pressure measurements at various radial locations through a steel channel plate and with high-speed visualization of the detonation confinement through a clear, polycarbonate channel plate.

The second objective was to determine the modal operability of the constant height geometry RRDE in the stand-alone combustor configuration. This was accomplished to configure the constant height RRDE compared to the constant area RRDE that operated with one, two, and three wave modes. Based on previous flowfield visualization demonstrating the outer radial location for two wave modes, increasing the number of waves compared to the constant area RRDE at the same given flow condition was desired to promote detonation confinement. Operation maps were developed by analyzing high-speed pressure measurements on the channel plate. In addition, high-speed visualization with a clear channel plate was used to confirm the trends suggested by the frequency obtained through the pressure measurements.

The third objective was to drive toward pressure gain combustion in the stand-alone combustor configuration that was not previously achieved in the constant area geometry. Accomplishing this objective would prove the device's effectiveness to perform as a pressure-gain combustor in an APU. In the constant area geometry, pressure loss was seen for all conditions. Reconfiguring the detonation chamber to the constant height geometry attempted to create pressure gain combustion by accelerating the flow to increase the equivalent available pressure downstream of the detonation. In addition, the throat height was increased to lower the pressure loss across the injector. The same experimental setup and flow conditions from the modal operability study were used to determine the pressure change from the plenum to the end of the detonation chamber. Static pressure measurements were taken throughout the detonation chamber and in the plenum and were corrected to total pressure values based an assumed choked condition downstream of the detonation and the flow effective area.

The fourth objective was to successfully detonate and maintain detonation confinement within the RRDE in the BAT configuration. Previously, the constant area BAT configuration had a relatively low thermal efficiency due to insufficient turning by the guide vanes into the radial inflow turbine. Furthermore, the detonation was shown to be radially close to the turbomachinery which provided a low residence time upstream of the turbine. The configuration was distinguished by the inclusion of guide vanes aft of the desired combustion section. The guide vanes were redesigned to promote more efficient turning into the turbine. The turbine channel plate was also redesigned to promote detonation confinement. The design considered flow conditions that were set by the selected radial inflow turbine which required a mass flow rate of 0.32 $\frac{kg}{s}$.

The final objective was to determine if thin-filament pyrometry (TFP) is a viable

technique to characterize the temperature of the flow downstream of the detonation event and if TFP is able to capture the transient temperature response due to a rotating detonation event. Measuring the temperature provides the thermodynamic properties of the flow downstream of the detonation event and at the inlet of the turbine. If the viability of TFP can be confirmed in this device, the results can provide confidence that TFP can be used in other RDEs.

1.3 Thesis Description

This document provides the relevant background and experimental setup for testing the stated objectives. Chapter II provides a description of the background and theory developed for the RDE. The motivation and foundation of pressure gain combustors and RDEs is given in further detail. The development of the constant area Radial RDE is also discussed to include its modal operability, performance in terms of pressure loss, and its implementation with high-speed flowfield visualization techniques that were used to determine the detonation wave's radial location for the constant area geometry. In addition, previous attempts to integrate RDEs with turbomachinery are discussed to provide a background that was used to attempt detonations with the constant height RRDE with guide vanes. Lastly, this chapter provides a literature review of measurement techniques that have been developed and used which are unique to the RDE and this research.

Chapter III provides an overview of the experimental setup used for the current research. The facility used for testing, as well as the testing procedures, are described in detail in this chapter. The previously tested constant area RRDE is described as relevant to the current research, specifically the components that were shared between the constant area and current research's constant height geometry. The stand-alone combustor and bleed air turbine configurations are individually described, and the

new components designed are detailed. This includes the channel plates that were designed to attempt detonation confinement and pressure gain through the device, as well as the guide vanes that were used to integrate turbomachinery into the RRDE to attempt detonation while in BAT configuration and to implement filaments for TFP. In addition, the enactment of measurement techniques is discussed to include constant capillary tube average pressure measurements to measure confinement and pressure performance, infinite tube pressure measurements and high-speed visualization to determine modal operability, and TFP to measure the RRDE's output temperature.

The results and discussion of the research is given in Chapter IV. First, detonation confinement in the constant height RRDE as a stand-alone combustor is confirmed. The resulting operating modes are compared to the constant area geometry, as well as the performance increase seen for the constant height geometry. The results from testing with the bleed air turbine configuration is also provided, with the viability of TFP confirmed and its results discussed. Lastly, Chapter V provides overall conclusions obtained from the research and how well this research achieved its objectives.

II. Literature Review

Understanding the fundamentals of a Radial Rotating Detonation Engine (RRDE) allows for the appreciation of its novel technology and the methods implemented to confine the detonation and implement turbomachinery into the device. Section 2.1 provides the basics for the operation of Rotating Detonation Engines (RDE), to include the fundamentals concerning detonation physics and structures. Previous efforts on creating and characterizing the Radial RDE (RRDE) are given in Section 2.2. Section 2.3 provides summaries of research efforts to integrate RDEs and RRDEs with turbomachinery to provide motivation for the use of an RRDE as an Auxiliary Power Unity (APU). To understand the current measurement techniques possible to quantify the extreme conditions within the RDE, an explanation of various pressure and temperature measurement methods are provided in Section 2.4.

2.1 Theory of Rotating Detonation Engines

Detonation based propulsion and power systems include unique devices designed to improve the performance of conventional engines by increasing the amount of available work through a pressure-gain, heat addition process. This is through the use of the detonation combustion mode rather than the deflagrative combustion mode, with the former characterized by a combustion wave propagating at supersonic speeds. A Rotating Detonation Engine (RDE) is an example of such a device that functions by harnessing a continuous, self-sustaining detonation wave rotating within an annulus to combust its fuel and oxidizer. The device itself refers to the combustion chamber where the pressure and temperature increase, but the RDE can theoretically provide the heat addition process for various propulsion and power systems such as turbines, rockets, and scramjets. Both numerical and experimental studies that explain the

phenomena that occur within the device are summarized in Section 2.1.1. It is also important to understand the fundamentals behind detonations, which are described as they pertain to RDEs in Section 2.1.2. Furthermore, the theoretical work potential for RDEs is outlined through thermodynamic cycle analyses given in Section 2.1.3.

2.1.1 Rotating Detonation Engines

Detonation engines are ideally pressure-gain combustion (PGC) devices, in contrast to combustors in conventional gas-turbines which experience pressure loss. However, to use detonations involves fixing systematic issues created from very high pressures, shock waves, and high velocities different from those in conventional gas-turbine applications. Moreover, detonations must be generated consistently and efficiently. The materials to handle the extreme environment would also need to be developed to contain the detonation. Two devices of note that have been tested while operating using detonation waves are the Pulse Detonation Engine (PDE) and the Rotating Detonation Engine (RDE). The PDE operates by filling a tube with reactants, initiating the combustion event to detonate the mixture, and purging the products from the tube to repeat this three-step process continuously. However, the unsteadiness and cyclic nature of this fill-fire-purge method, as well as loss of work potential due to the short amount of time spent on the detonation event, led to the development of the RDE [1].

The RDE functions by mixing air and fuel from a plenum into a detonation chamber. Typically, they are fed separately (i.e. not premixed) as shown in the cross-section of a typical RDE given in Figure 4. The two feeds are positioned to allow mixing between the two as they settle into the detonation channel, and the areas before the reactants reach the detonation channel are constricted to limit the amount of backflow that occurs due to the overpressure created by the detonation. The setup

is relatively simple, but the performance can vary based on the channel width, or the distance between the center-body and the outer-body, the injection area where the reactants enter the detonation chamber, and the blockage area which is controlled by the aerospike nozzle in the schematic shown in Figure 4.

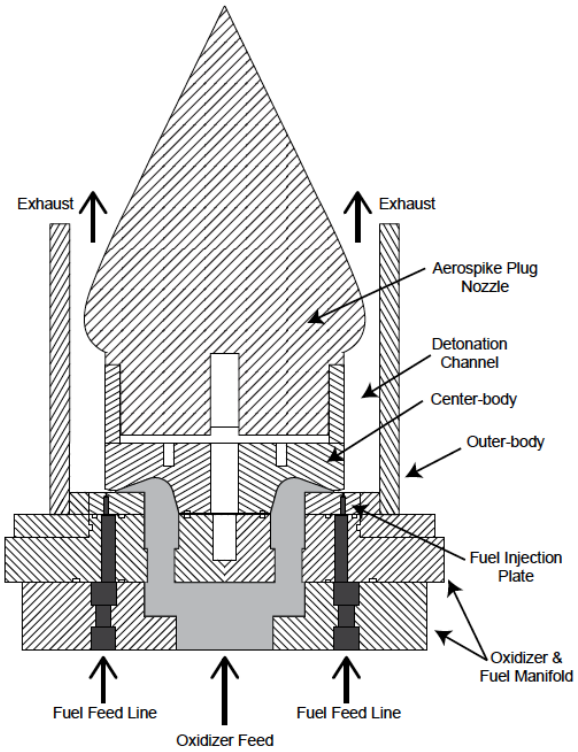

Figure 4. Cross-section of typical RDE configuration showcasing reactant feed lines, center-body, and outer-body, with aerospike nozzle to affect nozzle area ratio [7].

In the detonation chamber, shown in Figure 5, a detonation wave is initiated that runs around the annulus, consuming the reactants. Reactants are introduced to the detonation chamber at the bottom. A detonation wave, initially introduced using a pre-detonation system, passes through the reactants, combusting the reactants into products as they continue to flow axially towards the exhaust. As the detonation wave propagates, an oblique shock is created by the expansion of the detonated products. The detonation wave is characterized by the increase in both pressure and temperature.

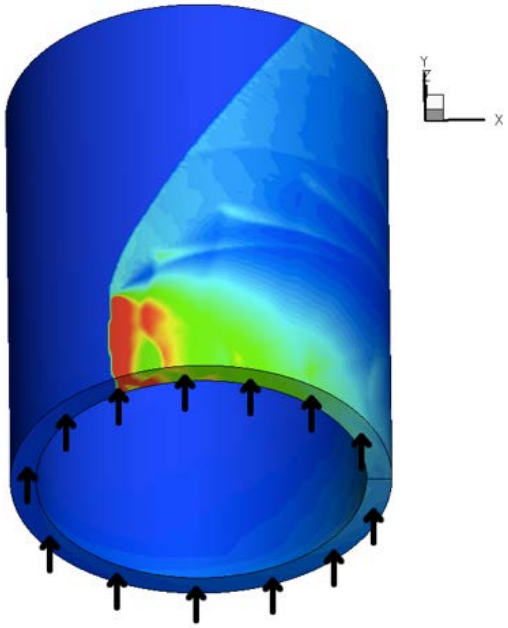

Figure 5. Typical annular RDE setup with reactant inflow from the bottom of the image expanding axially up after detonation [8].

By linearly unrolling the annular channel, as shown in Figure 6, the structures within the annulus can be studied [9]. The detonation wave front is shown by Point A, with the oblique shock given at Point B and a secondary shock wave in Point D. In addition to the detonation event, surface burning, or slip lines, can occur between the recently detonated products and 'older product', as well as fresh reactants and the products, shown in Point C and E, respectively. Point F is the region of backpressure into the reactant nozzles due to the detonation, while Point G is the area of mixed reactants. The flow resumes from the nozzles once the post-detonation pressure lowers to the inlet pressure.

These events have been confirmed using visual techniques such as mid-infrared imaging by Naples et al. [10] for hydrogen-air mixtures. Naples et al. conducted a study on the flowfield characteristics within an RDE to compare to numerical work [10]. This was accomplished by creating an optically clear RDE based on a successfully tested RDE, shown in Figure 7. The initiator was moved from the outer body

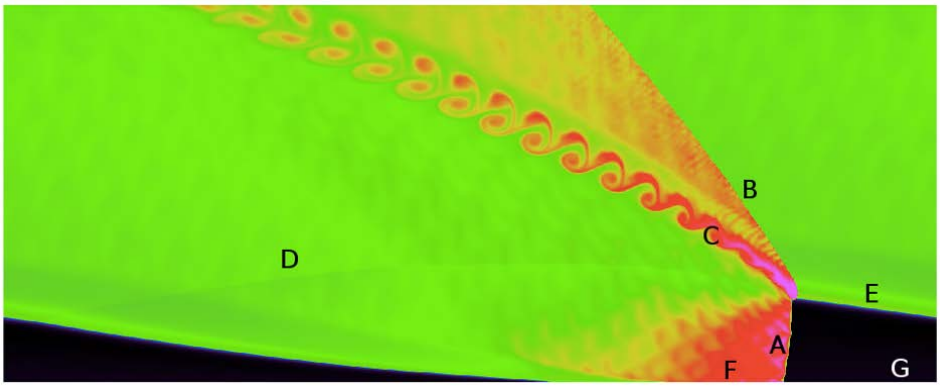

Figure 6. Unrolled schematic of RDE wave structure [9].

in the metal through the exit flow, providing evidence of an invariable pre-detonation location. With the clear outer body for the detonation chamber annulus, chemiluminescence was used to obtain images of the basic wave structure.

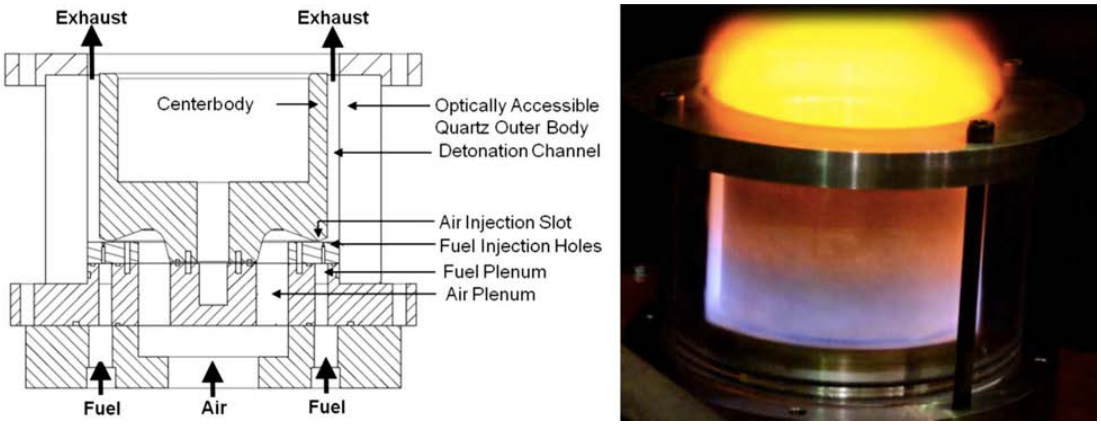

Figure 7. Optically clear RDE used to observe basic detonation flow structure [10].

Using the optically-clear RDE, Figure 8 was created to compare to the unrolled image given in Figure 6 with estimated labeled structures identifying the: (A) oblique shock wave, (B) shear layer, (C) detonation wave, (D) and contact region between products and fresh reactants after the detonation wave has passed by. The angle of the oblique shock wave (α) and the shear layer (β) were measured from the detonation structure given different mass flow rates, but no trends were determined due to large

error. While chemiluminescence provided a general overview of the flowfield, it is not the most accurate due to optic-dependent variables such as light variation due to flame quenching. The error could also be due to variability of the tested RDE rather than the measurement techniques. More accurate methods proposed include Planar Laser Induced Fluorescence (PLIF), Particle Image Velocimetry (PIV), and Schlieren Imaging [10].

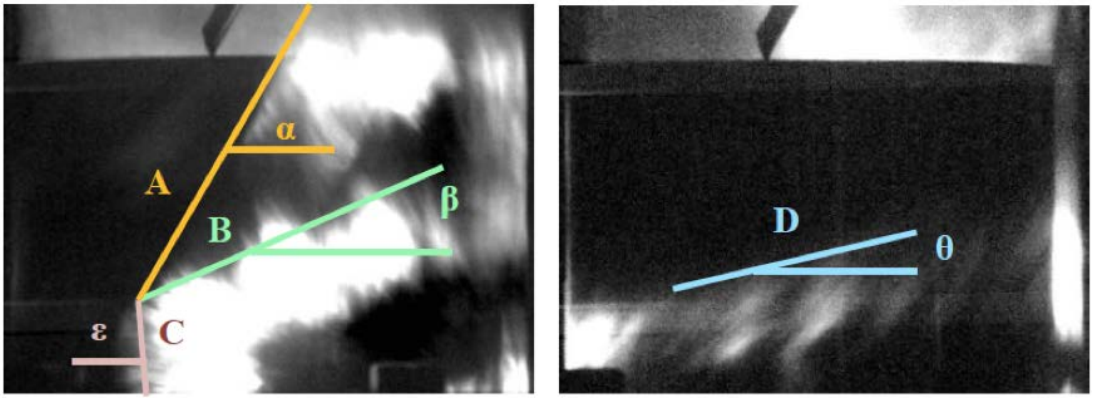

Figure 8. Detonation wave structure within RDE showing (A) oblique shock wave, (B) shear layer between gases of previous and current detonation cycles, (C) detonation wave, (D) contact region between detonated products and fresh reactants [10].

2.1.2 Detonation Theory

As the driving mechanism for the pressure-gain within the RDE, it is also important to characterize the detonation event. A detonation consists of a shock wave that is sustained by the energy from the combustion process. The combustion is initiated by the shock-wave compression. Ideally, the processes of the shock wave and the combustion complement each other to create a self-sustaining process with a continued flow of reactants. The properties of the combusted gases can be related to properties outlined through normal shock theory [11].

Most mathematical relationships defining the detonation event are created through one-dimensional analysis. While detonations are fully three-dimensional, the one-

dimensional analysis provides a foundation for flow understanding. The equation set to solve for the gas properties use the mass, momentum, and energy conservation equations, as well as state relationships. The Rayleigh line solves the continuity and momentum conservation equations, which provides a relationship between the pressure and specific volume. The slope of the line is the mass flux, with limits between zero and infinity (where negative mass flux is non-physical) [11].

The Rankine-Hugoniot curve includes the continuity and momentum conservation equations with the energy equation, shown in Figure 9. The amount of heat release, pressure, and specific volume specifies the curve. Points on the Hugoniot are given by the Rayleigh line intersecting with the Rankine-Hugoniot curve. The upper tangent point of the Rayleigh line to the Hugoniot curve provides the upper Chapman-Jouguet (CJ) point. At this point, the burned gas velocity is sonic and the process produces the minimum entropy. In contrast, the lower tangent point of the Rayleigh line to the Hugoniot provides the lower CJ point which provides maximum entropy. The burned gas velocity is also sonic. Most detonations in RDEs occur below the upper CJ point [11].

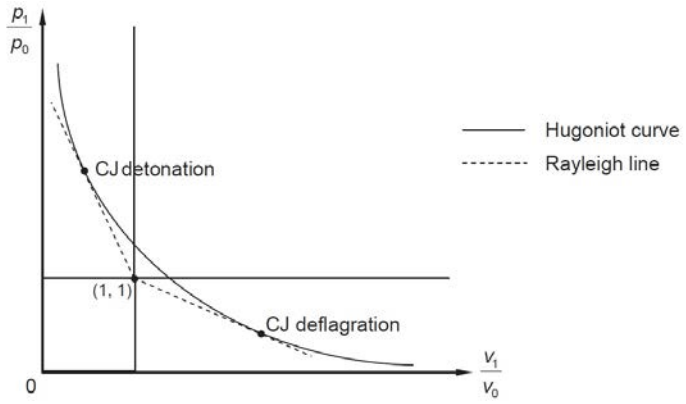

Figure 9. Hugoniot curve with Rankine tangent lines at upper and lower CJ points [12].

The structure of the detonation wave can be simplified as a leading shock wave

followed by a reaction zone. This is considered the Zeldovich, von Neumann, and Doring (ZND) structure, shown in Figure 10. The shock wave is considered infinitesimally small, with no combustion processes across the shock. In real experiments, the ZND structure does not exist due to its one-dimensional assumption. A detonation wave has been found to contain several shock fronts, which intersect to form what is called the triple point. The ZND model for detonations helps describe the three processes that would be experienced by pressure sensors during experimentation of RDEs, which are the shock, induction, and heat release zones. The shock creates a sharp rise in pressure and temperature. The induction zone, where the radicals of the fuel and oxidizer are generated, leads to the heat release where they recombine and provide another increase in temperature with a decrease in pressure. Understanding the true characteristics of the detonation waves allows for the correct implementation of sensors. The most important characteristics of a detonation to account for are the lead and first transverse waves.

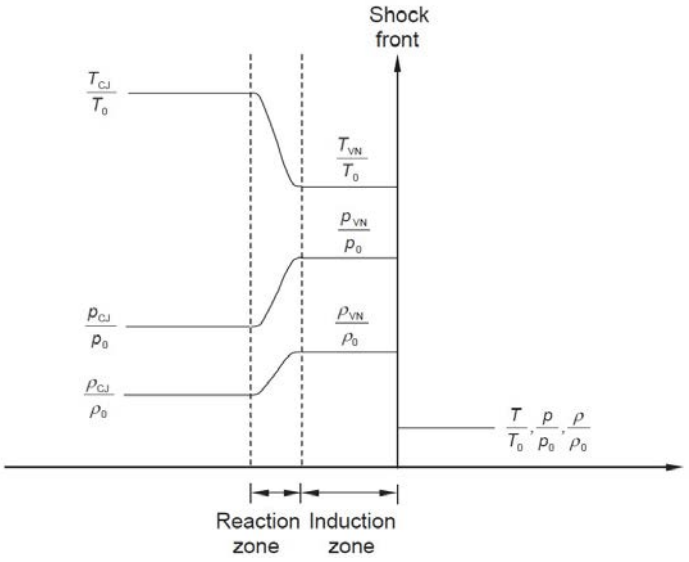

Figure 10. ZND structure characterized by three zones [12].

2.1.3 Thermodynamic Cycles of Detonations

Thermodynamic cycle analysis is important for engines in understanding the general heat transfer and work expected in a system based on basic thermodynamic law of energy conservation, where no change in system energy exists over the entire cycle. Understanding the thermodynamic cycle of the RDE helps with the design of the device. This can include evaluating the thermodynamic benefits of reducing the amount of back pressure into the reactant inflow to allow adequate filling and mixing of air and fuel before combustion. In addition, the effects of reducing deflagration between fresh reactants and detonated products on the thermodynamic efficiency can be examined. Furthermore, developing a thermodynamic cycle that corresponds to a typical operating RDE helps to develop and validate numerical modeling of an RDE.

In contrast to the Brayton cycle, which models gas turbines using isobaric (constant pressure) combustion, the detonation cycle operates using isochoric (constant volume) combustion. Evident through the pressure-specific volume (P-v) diagram shown in Figure 11, the detonation cycle offers more available work to be extracted compared to the Brayton cycle. The operating pressure ratio (OPR) for each cycle is given in the figure as well, based on example engines from Schwer and Kailasanath [13]. The Brayton cycle engine uses an $OPR = 10$ between the beginning and end of the compressor, while the proposed detonation cycle engine would only have a single-spool $OPR = 2$ compressor. Therefore, the detonation cycle would still be able to produce more work with limited turbomachinery.

Historically, the Atkinson or Humphrey thermodynamic cycles have been used to characterize PGC devices including the RDE [1]. The Atkinson and Humphrey cycles have a higher post-combustion temperature and lower post-combustion entropy. This lower entropy generation leads to a higher thermal efficiency. The unsteady combustion typical in RDEs can be related to an unsteady Atkinson/Humphrey cycle, which

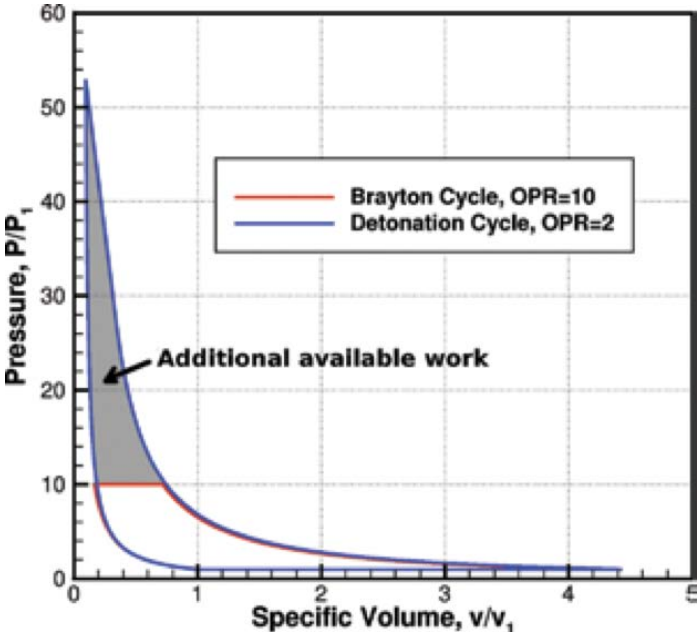

Figure 11. P-v diagram of Brayton and detonation cycles, including each cycle's typical operating pressure ratio (OPR) [13].

still provides an advantage over the Brayton cycle, with some loss in performance compared to a steady Atkinson/Humphrey cycle.

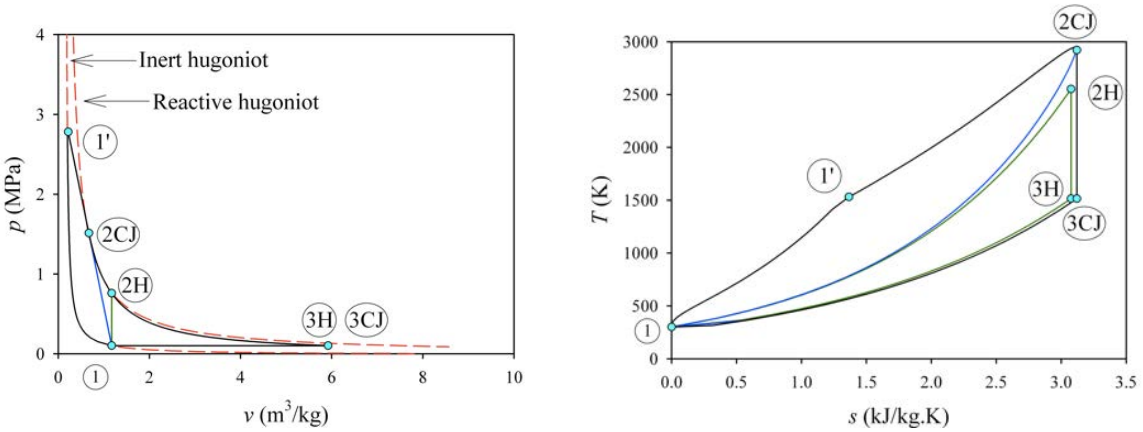

(a) (b)

Figure 12. Humphrey Cycle (1-2H-3H-1), Fickett-Jacobs Cycle (1-2CJ-CJ-1), and ZND Cycle (1-1'-2CJ-3CJ-1) shown in (a) P-v and (b) T-s diagrams [14].

The Fickett-Jacobs (FJ) cycle, based on CJ theory and developed separately from Zeldovichs theories, has also been proposed as an indicator for the thermodynamic

processes within a detonation engine [15]. The cycle is demonstrated by Wintenberger et al. in Figure 13 by considering a closed system within a cylinder and pistons [15]. The fluid is compressed through a non-equilibrium process which can be assumed to be in local thermodynamic equilibrium. The detonation is initiated due to the external work of the piston. The detonation propagates from one piston to the other through the reactants. Then, the entire system moves once the detonation wave reaches the farther piston. The detonation products are at rest while the distance between the pistons remains the same. The products are isentropically expanded to initial pressure, which are then cooled to extract heat through a reversible process. Finally, the products are converted to reactants for the cycle to restart.

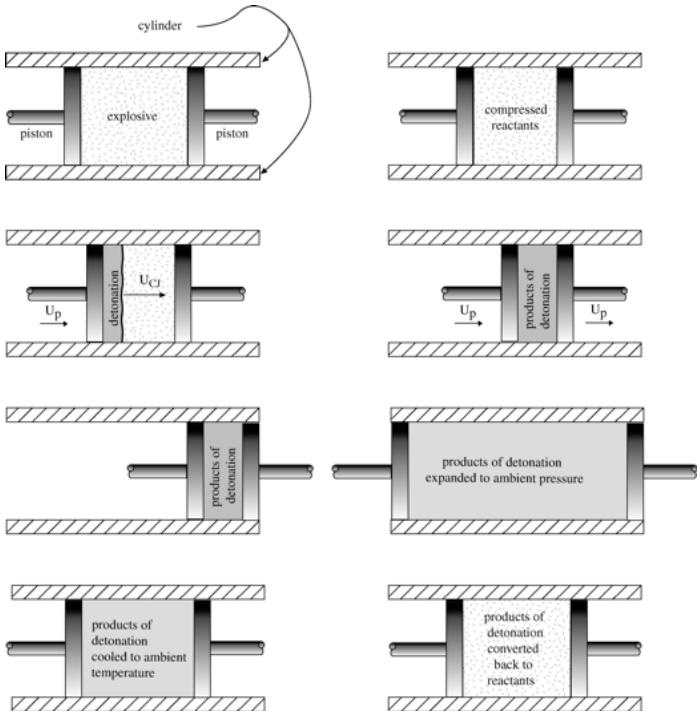

Figure 13. Fickett-Jacobs cycle outlined by a closed cylinder/pistons system [15].

The upper and lower CJ points act as the bounds of the cycle, shown in Figure 12 as 2CJ and 3CJ for the upper and lower points, respectively. This analysis can provide an upper bound of thermal efficiency for detonation devices, which can be

expressed as the ratio of the change of enthalpy between States 1 and 5, and States 1 and 6. The thermal efficiency increases with CJ Mach number.

ZND theory, as described in Section 2.1.2, is used to capture what is occurring through the physical theory of a one-dimensional detonation wave. This model accounts for the energy from the shock wave unlike the Humphrey and FJ cycles, while using the same CJ points outlined through the FJ cycle. Unlike the FJ cycle, the ZND theory accounts for the von Neumann spike where the shock raises the pressure to the ZND point before decreasing to the CJ value through supersonic Rayleigh heating. Vutthivithayarek considers the ZND cycle the most appropriate for detonation engines since it considers this von Neumann pressure spike, and subsequent decrease to the CJ value, rather than just an increase to the CJ point [14].

Rankin et al. proposed a specific thermodynamic analysis of an unsteady Humphrey cycle used in an RDE [1]. This was modeled based on the main features affecting RDE combustion to include: detonation combustion, deflagration combustion, a secondary shock, and mixing between the detonated and deflagrated flows, shown in Figure 14. Elements of these RDE combustion events show relative thermodynamic advantages between each section of an RDE. From the figure, it can be seen that reducing deflagration between the fresh reactants and detonated products from previous cycles would improve the thermal efficiency of the RDE.

2.2 Development of the Radial RDE

Recent efforts have been made to examine the use of a more compact Radial RDE (RRDE), shown in Figure 15b, where the detonated products flow radially before turned axially with a nozzle through its exhaust. Nakagami et al. [2] initiated research into this concept through their disk RDE. In their design, the fuel and oxidizer were injected from the outer annulus before reacting with the detonation

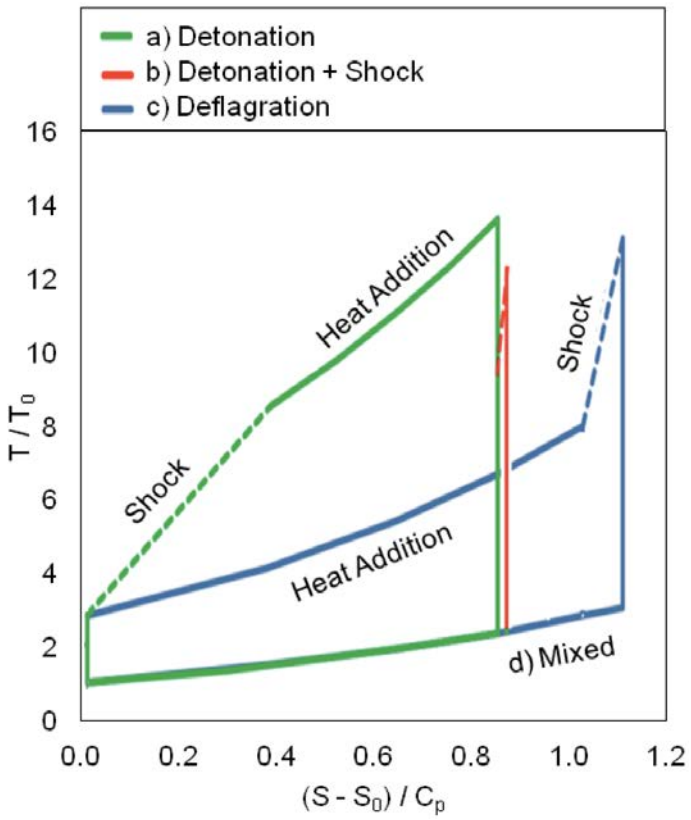

Figure 14. Elements within an RDE thermodynamic cycle, to include detonation, detonation and shock, deflagration, and a mixing process [1].

wave and exhausting axially near the centerline, with their results showing comparable detonation structures in the RRDE to axial RDEs.

As the physical phenomena of detonation waves continue to be studied, other characteristics inherent to an RDE/RRDE have also been explored. Due to the local pressure increase created by the detonation wave against the fuel and air nozzles, flow reversal occurred in both [2]. In the RRDE used by Nakagami et al. [2], it was observed that the oxidizer resumed flow around one-sixth of a cycle after the detonation wave passed while the fuel resumed flow after two-thirds of a cycle. This leads approximately one-third of a cycle period for the reactants to mix before the detonation wave passes through again. Due to the high frequency of the detonation waves, mechanical valves cannot be used to control the flux of reactants while blocking

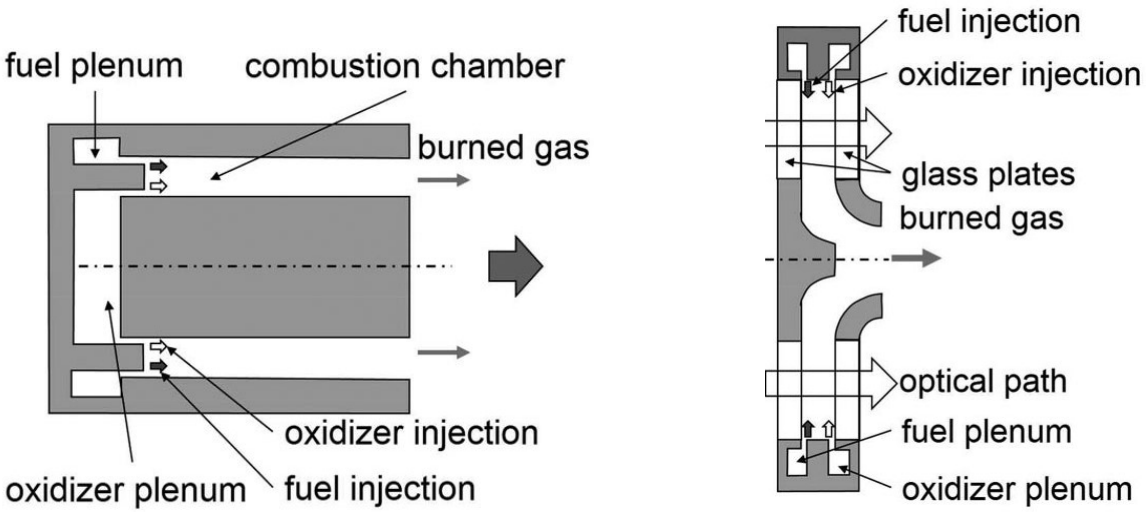

Figure 15. Basic comparison between an (a) Annular and (b) Radial RDE [2].

backpressure. This promotes a possible area of research interest to improve the time for mixing and propagation of the reactants before the detonation wave returns.

Huff et al. [3] initiated a novel RRDE using a modular design that controlled the injection area ratio between the reactant throat and detonation channel, as well as the nozzle area ratio between the detonation channel and exit nozzle. The design of this device, shown in Figure 16, was considered to be in a stand-alone combustor configuration since the thrust or potential power from a radial-inflow turbine was not measured. The detonation channel, shown in yellow in Figure 16, was constrained by the channel plate, shown in green, and the base plate given in black. The device maintained a constant area effective chamber area (A_c) as the flow travelled radially inward; therefore, the channel height (h_c) also increased as the radial distance from the centerline (C_L) decreased. The injection was controlled by the throat ring, given in cross-hatched yellow, to provide a restriction between the plenum upstream of this throat ring and the detonation chamber. This throat ring could be shimmed to provided different injection ratios (AR_t) between the area at the throat (A_t) and A_c. The blockage was modified by the nozzle, given in purple in Figure 16, to provide an

area restriction that was quantified as the ratio (AR_n) between the area at the exit of the nozzle (A_n) and A_c. Full details of the device can be seen in the thesis completed by Huff [5] and the function of the various components of the modular design are provided in Section 3.1.2 as they pertain to the current research's design.

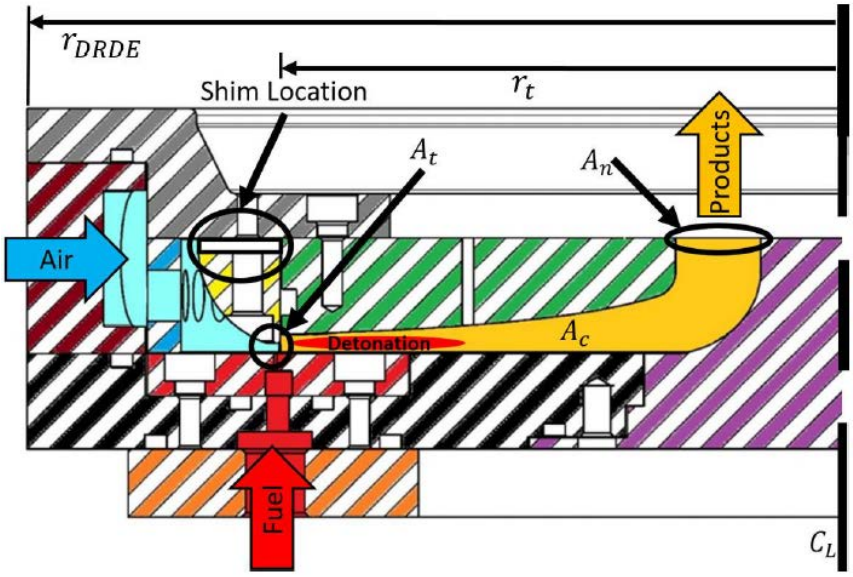

Figure 16. Cross-section view of the constant area RRDE in stand-alone combustor configuration from Huff [5].

The device tested by Huff et al. successfully detonated at mass fluxes between $50\frac{kg}{m^2s}$ and $200\frac{kg}{m^2s}$ and equivalence ratios between 0.5 and 1.0 [3]. The RRDE was characterized by three channel heights of 3.5, 4.0, and 4.5 mm, throat area ratios between 0.2-0.4, and nozzle area ratios between 0.5-0.6 [5]. An example of the operability of this RRDE is given in Figure 17. The example geometry given in Figure 17 was used in the current research as the baseline for performance and operability for the constant area RRDE. A variety of wave modes as a function of the operating conditions were seen based on the high-speed pressure signals, with higher waves present for larger mass fluxes and lower equivalence ratios. While the RRDE was able to detonate successfully at multiple flow conditions, the device operated with an

average static pressure loss around 30% from the plenum to the inlet of the nozzle, which was incongruous with the pressure-gain goal.

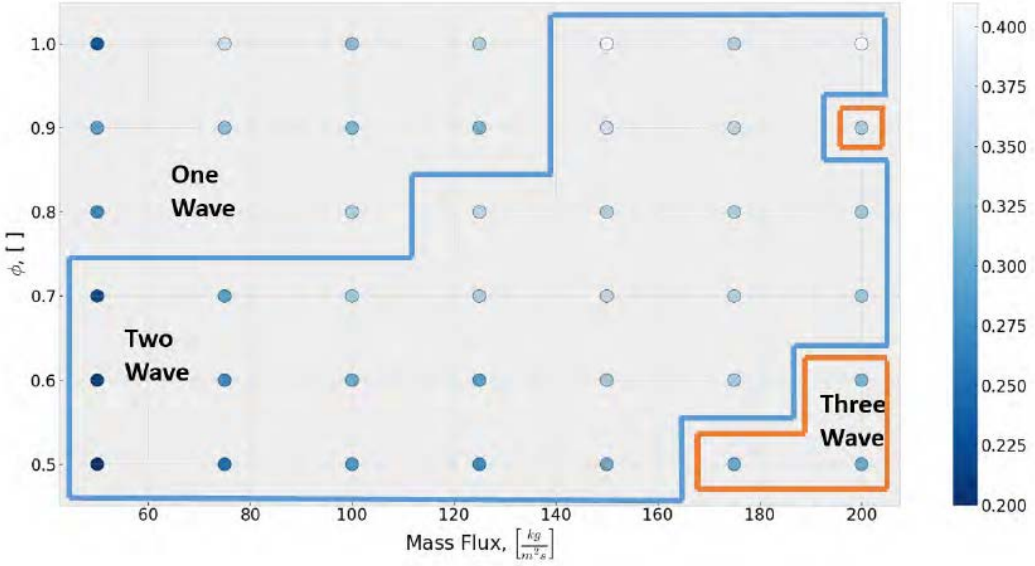

Figure 17. Operability map, color coded with pressure loss, of constant area RRDE with $h_c = 4.5$ mm, $AR_t = 0.2$, and $AR_n = 0.6$ as tested by Huff [5].

The configuration developed by Huff et al. [3] was further characterized through flowfield visualization by Boller et al. [6]. This was accomplished by using a polycarbonate channel plate in place of the stainless steel channel plate was used to define the detonation chamber. The visualization study was accomplished using a high-speed camera that confirmed many of the operating modes suggested by the pressure measurements on the steel channel plate [16]. In addition, the nature of the multiple waves within the detonation chamber was able to be captured. These waves have been seen to either propagate in the same direction, or clap back and forth once they met each other. In addition to studying these multiple waves, Boller et al. [6] also examined the variables affecting the radial location of where the detonation waves propagated, shown in Figure 18. In general, for the two wave mode, the radial position was 20% larger (further from the centerline) than the one wave mode.

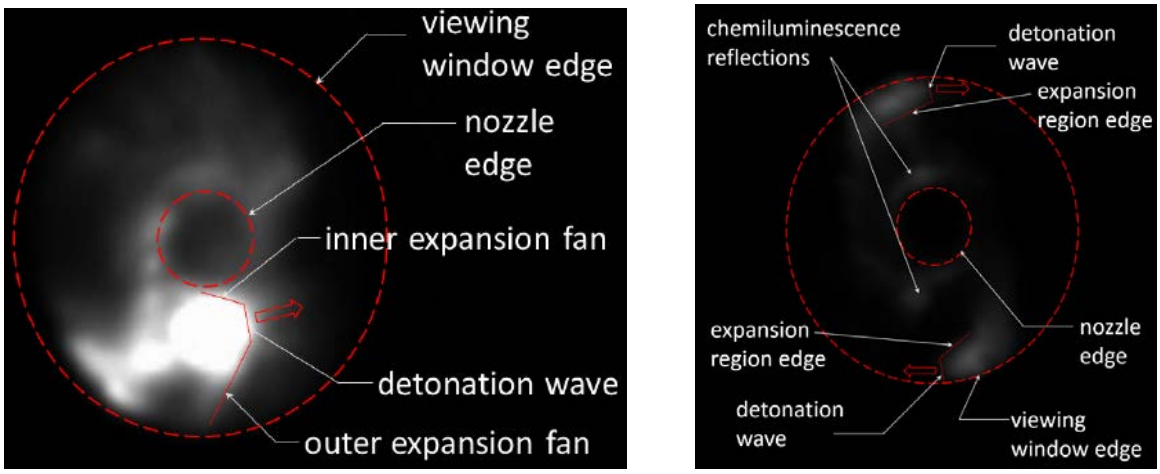

(a) (b)

Figure 18. Comparison of (a) one wave mode operation and (b) two wave mode operation for constant area RRDE [6].

The RRDE provides an opportunity to examine radial variations of the detonation wave, in contrast to an axial RDE, due to its radial inflow configuration. Boller [16] hypothesized that detonations occurring away from the outer wall in the RRDE, which occurred for one-wave tests, allowed expansion from the detonation on either side of the detonation wave front, shown in Figure 18a. Confining the detonation wave to the outer wall, as was seen for the two wave mode shown in Figure 18b, would provide a physical barrier on one side of the wave, but could provide higher backpressure to the inlets. Therefore, results from an RRDE with a decreasing effective flow area would also provide insight into the physical interactions between the detonation wave location and the product gas expansion as it attempts to backpressure the detonation area and into the reactant source inlets.

2.2.1 Detonation Confinement

In the context of this research, detonation confinement refers to constraining the detonation wave to a specific location that does not propagate in the direction of the flow. Cho et al. examined the confinement of a detonation wave to examine the

difference in wavespeed observed between experimental results and numerical models based on the CJ speed [17]. Experimentally, there is usually a difference between the theoretical CJ velocities and measured velocities. Understanding the deficit will also help make preliminary assumptions on the wavespeed once the factors that reduce the wavespeed from the theoretical speed are understood.

It was hypothesized that various factors could affect the CJ velocity. This included heat loss, the changing direction of the fluid, non-stationary gas, deflagration of reactants and detonated products, and lateral relief. Lateral relief, for this experiments, referred to the lack of solid confinement against a detonation wave, and the effects of lateral relief of a detonation wave within a thin channel were examined.

The results from Cho et al. showed that the wavespeed difference was greater for the setup with lateral relief, with the measured wavespeed nominally around 85% of the calculated CJ speed. The wavespeed for the confined section wave was nominally around 95% of the CJ speed. The difference was dependent on the equivalence ratio for both cases, with a higher equivalence ratio also leading to a greater difference between wavespeed and CJ speed for that equivalence ratio. Considering an RDE application, wavespeeds closer to CJ speeds could show active confinement within a detonation chamber.

A numerical study by Reynaud et al. also examined the confinement of a detonation wave due to a high-temperature compressible layer. The applicability of this study to an RDE relates the combusted products as the inert high-temperature layer simulated in this study, and the results are shown in Figure 19. The influence of the inert compressible layers temperature was examined on the detonation area. It was found that increasing the temperature of the confining layer increased the detonations velocity. Expansion of detonated gases to its upper layer, due to temperature differences of the two layers, created a decrease in velocity. In addition, higher inert

temperatures created an increase in the oblique shock angle produced. In general, vortices were formed between inert and detonated gases. Based on the figures, it appears that greater mixing occurred from the larger Kelvin-Helmholtz instabilities being produced for the lower inert gas temperature [18].

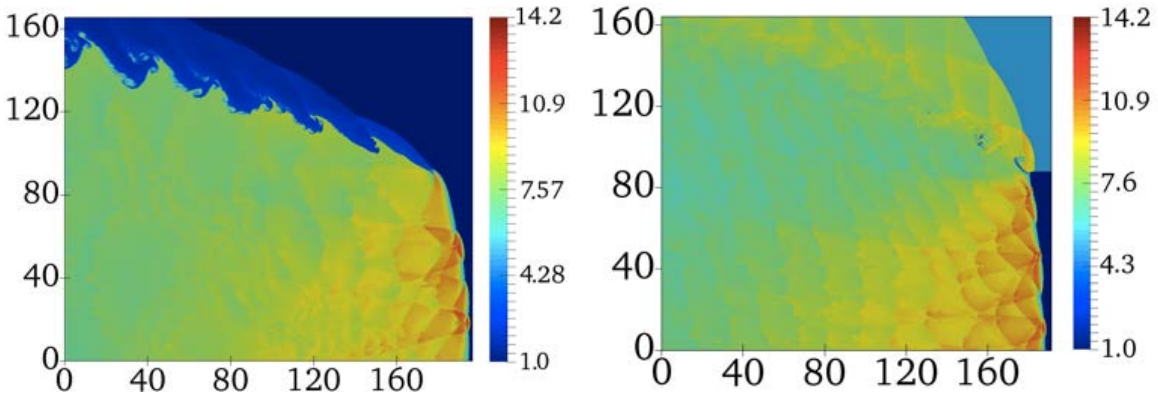

Figure 19. Compressible layer confinement with an inert gas temperature of (a) 295 K and (b) 1400 K. [18].

2.3 Integration of RDEs with Turbomachinery

Research into RDEs must also consider its integration with modern turbomachinery technology to establish potential operationality as a propulsion system or an APU. To consider the feasibility of an RDE with turbomachinery, it is important to understand terminology concerning combustors for gas turbine propulsion, given in Section 2.3.1. There are multiple performance parameters that are implemented for a combustor and turbine. The implementation of RDEs and RRDEs with existing turbomachinery is given in Section 2.3.2.

2.3.1 Turbomachinery Performance Variables

When examining conventional combustors, total pressure loss, which is normally around 2-5%, is typically used to examine the combustor's performance, with a lower

pressure drop desired. However, this performance criteria is not applicable for PGC devices since their goal is to also increase pressure. Instead, the temperature profile and pattern factor could be considered instead. The temperature profile can be examined to determine the efficacy of operation of a combustor. Temperature uniformity from the combustor into the turbine helps with thermal stress and to meet expected performance. This can be measured through multiple ways such as high-temperature thermocouples or gas-sampling techniques [19]; this research will use thin-film pyrometry which will be discussed in detail in Section 2.4.

Pattern factor (PF) is also another performance parameter that is a simplified analysis from the exit temperature data, and is calculated from the following equation:

$$PF = \frac{T_{t,max} - T_{t,av}}{T_{t,av} - T_{t,in}} \tag{1}$$

where $T_{t,max}$ is the maximum exit temperature measured, $T_{t,av}$ is the average temperature at the exit plane, and $T_{t,in}$ is the average temperature at the inlet plane. This variable quantitatively measures the combustors thermal gradient performance, with a lower PF value indicating that the maximum temperature from the combustor is close to the average temperature. PF is typically determined in front of the turbines first-stage stationary airfoils, or nozzle guide vanes (NGV). Typical PF values are between 0.250.45, but modern PF values closer to 0.15-0.25 for new high-temperature-rise main burners have been seen [19].

Profile factor (P_f) is used to characterize the main burners average exit temperature profile, and is given by the following equation:

$$P_f = \frac{T_{t,max,av} - T_{t,in}}{T_{t,av} - T_{t,in}} \tag{2}$$

where $T_{t,max,av}$ is the maximum circumferential average temperature. Average profile

factors are between 1.04 and 1.08, with 1.06 being a common design goal. The P_f is determined on the turbine first-stage's rotating airfoils exposed to the average temperatures after the NGV.

Nozzle guide vanes (NGV) are important for turbines to help direct, or turn, the flow to extract energy through the turbine. Figure 20 provides angles and terminology used for cascading airfoils which are found in guide vanes. Solidity (σ) is the ratio of the airfoils chord to the spacing between each airfoil. Typically, the solidity is near unity but can be an important parameter, in addition to the flows velocity and incidence angle, to affect the performance of the turbine. Total pressure loss coefficient (Φ_c) is used to quantify the drop in total pressure over the incoming flows dynamic pressure. Other terms include the Diffusion factor (D) which is measured based on the amount of diffusion as a function of the inlet/exit velocities and solidity. A direct correlation exists between the diffusion factor and the total pressure loss coefficient [19].

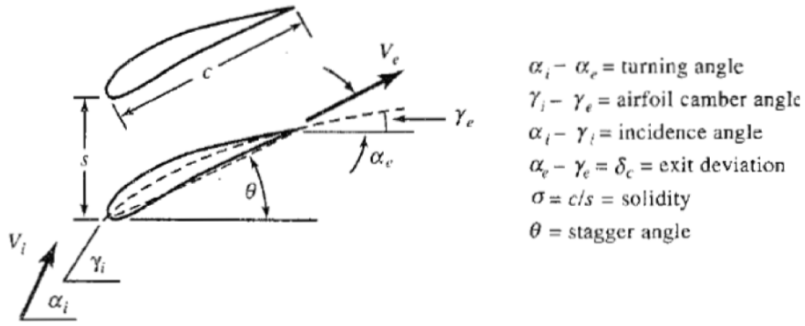

Figure 20. Terminology of cascading airfoils [19].

While these variables are important in characterizing the NGVs typically found in gas-turbines, the use of a radial-inflow turbine (RIT) with the RRDE makes use of a guide vane ring that operates slightly differently than the guide vanes used in axial turbines. The velocity triangles for the guide vanes into an RIT is given in Figure 21. The given velocity triangles are helpful in fundamentally understanding the absolute

and relative components of the flow as it transitions through turbomachinery.

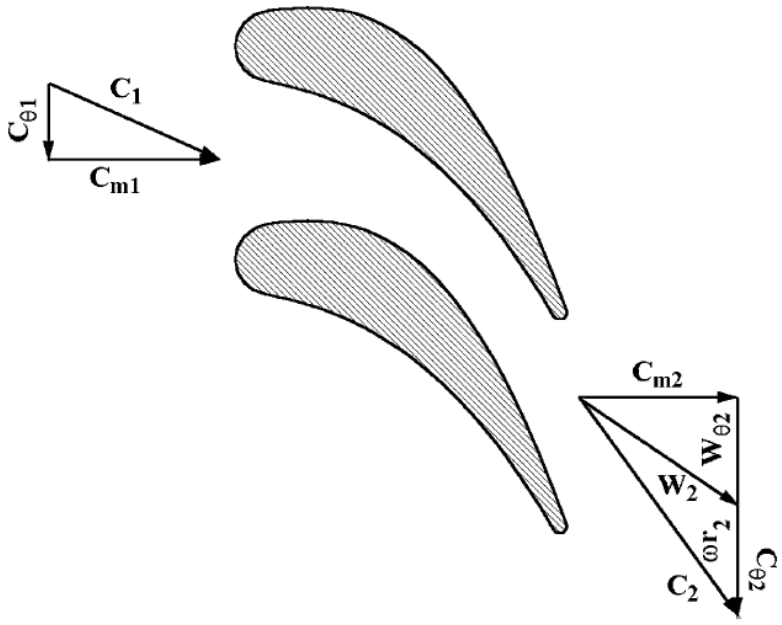

Figure 21. Velocity triangles at the inlet and discharge of a nozzle [20].

The meridional velocity component is an important component of the velocity since it is equivalent to the radial velocity that is seen by the RIT. This is given as W through the following equation [20]:

$$W = \sqrt{{C_m}^2 + {W_\theta}^2} \tag{3}$$

where C_m and W_θ are determined based on the velocity triangle aft of the guide vane given in Figure 21. The flow angle is determined based on the tangential direction of the stationary frame of reference [20] and calculated as:

$$\alpha = \arctan(C_m/C_\theta). \tag{4}$$

The combination of the meridional velocity and flow angle are important in setting up the flow to allow the RIT to operate efficiently and along its operating maps. These

values are developed further in Section 3.3.1 as they were used to design the guide vanes used in this study.

2.3.2 Implementation of RRDE with Radial Turbine

Huff et al. has provided successful integration of an RRDE with a radial turbine [21] [4]. Figure 22 provides the configuration of the RRDE as a Bleed Air Turbine (BAT) to demonstrate potential as a compact APU. The use of an RRDE over an annular RDE was considered to increase power density, or the amount of power produced for a given volume. Geometric studies were done by back-pressuring the turbine with plates to obtain different exit area ratios, as well as back-pressuring the compressor exhaust through a ball valve. As discussed in Section 2.2, the RRDE has previously been tested successfully as a stand-alone combustor over a range of equivalence ratios and mass fluxes. The BAT configuration used the RRDE with an off-the-shelf automotive turbocharger, with a proof on concept shown through the ability of the turbine to provide a significant amount of shaft power of over 70 kW. Based on this previous work, an exhaust duct was added as a flow straightener to combat the radial expansion of the exhaust gases [22].

Figure 22. RRDE integrated with radial turbine in BAT configuration [4].

When testing, the combustion mode was confirmed as detonation, rather than deflagration modes, through the use of infinite tube pressure (ITP) measurements on the combustion chamber. The mode was defined by a sharp pressure spike followed by

a pressure relaxation. This method of high-speed pressure measurement is explained in Section 2.4.2. However, while the stand-alone combustor provided a large range of operability, only the $75\frac{kg}{m^2 s}$ mass flux with an equivalence ratio of 0.6 worked with the turbine. Lower and higher mass fluxes at different equivalence ratios did not detonate and it was assumed that the operability of the device decreased to the larger channel height that was implemented to allow the implementation of guide vanes[4].

These guide vanes, given in Figure 23, were tested at different turning angles that were designed using a program developed from the equations and velocity triangles given by Aungier [20]. Each guide vane ring featured 17 vanes to avoid excitation with the 10 bladed turbine. Of the three guide vanes tested, the 32° turning angle vane set led to the highest specific power from the turbine [5]. However, it was noted that the guide vanes might not have been optimized for the RIT selected for the BAT configuration, and it was assumed that the guide vanes were providing a choke condition upstream of the turbine [4]. It was suggested that a detailed study be conducted to optimize the blade number, geometry, and turning angle to improve performance based on efficiency and power extraction [4].

Back-pressuring the compressor exhaust through a manual ball valve instigated an increase in output work to compensate for the greater compressor work needed. Higher back-pressure conditions pushed over the surge line of the published data for the compressor. Back-pressuring the turbine provided a scenario similar to multiple turbine stages, or using an exhaust duct through a nozzle. This back-pressuring led to a decrease in power output due to the decrease in the turbine's operating pressure ratio [4].

Two lean equivalence ratios of 0.5 and 0.6 were tested, with $\phi = 0.5$ corresponding to an acoustic mode and $\phi = 0.6$ resulting in a detonative mode. An increase in turbine efficiency occurred at the lower equivalence ratio running in an acoustic mode,

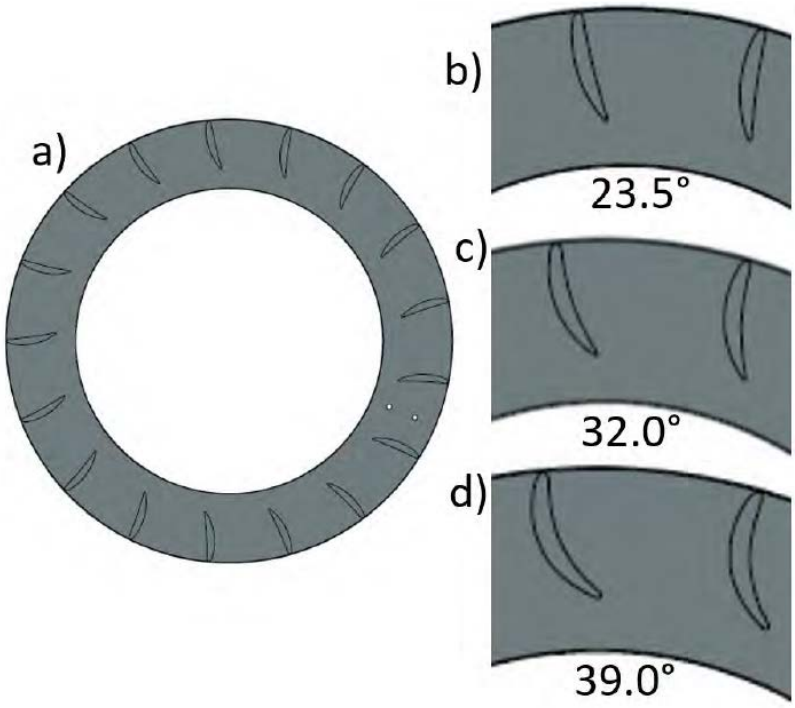

Figure 23. Guide vane ring designs used by Huff in the constant area chamber BAT configuration [5].

compared to higher equivalence ratios running in a detonative mode. However, an increase in thermal efficiency for the detonative mode operation occurred despite the lower turbine efficiency. The exhaust had higher energy flow that could be harnessed to improve turbine efficiency. Possible losses that affect the turbine efficiency could have occurred through the interaction between the combustor section and the NGVs. The integration of the turbine compared the stand-alone combustor device saw an increase in channel height and different back-flow conditions. This also leads to possible issues in the backpressure, detonation area, and injector ratio in changing the operability of the RRDE [4].

2.4 Measurement Techniques for RDEs

While the extreme conditions within RDEs have created problems in integrating instrumentation, such as to measure temperature and pressure, various methods have been developed to allow for both time-accurate and precise measurements. Techniques employed at the Air Force Research Laboratory (AFRL) are examined to determine the optimal setup for accuracy. Flow metering was established using sonic nozzles which are discussed in Section 2.4.1. To measure the pressure magnitude of the signal, capillary tube average pressure (CTAP) measurements are employed and are discussed in Section 2.4.2. In addition, infinite tube pressure (ITP) measurements, which measure the transient pressure signal, are also discussed in Section 2.4.2. Thin-filament pyrometry is an optical measurement technique that can measure hot gas temperatures with minimal intrusion and is discussed in Section 2.4.3.

2.4.1 Flow Metering using Sonic Nozzles

The RRDE made use of sonic nozzles to determine the mass flow rate of the air and fuel into the device. Sonic nozzles are simple Venturi tube devices that are used for compressible gas flow metering [23]. Figure 24 provides a cross-sectional profile of a typical sonic nozzle. As the name implies, the sonic nozzle accelerates the flow to a choked condition at the nozzle's throat where the Mach number is 1.0, or sonic. With this sonic condition, the mass flow rate is calculated based on orifices of known areas within the device and the thermodynamic properties of the flow such that:

$$\dot{m} = C_D \frac{P_0 A^\star}{\sqrt{T_0}} \sqrt{\frac{\gamma}{R} \left(\frac{2}{\gamma+1}\right)^{\frac{\gamma+1}{\gamma-1}}} \tag{5}$$

where $\dot{m}$ is the mass flow rate in kg/s, P_0 is the stagnation pressure in Pa, T_0 is the total temperature in K, $A^\star$ is the area at the sonic condition in m^2, γ is the ratio

of specific heats for the fluid, and R is the specific gas constant. In addition, the non-dimensional discharge coefficient (C_D) is needed to quantify the viscous losses through the sonic nozzle, where a discharge coefficient of $C_D = 1$ represents an ideal case with no losses. Based on previous testing done by Huff [5] and Boller [16], a discharge coefficient of $C_D = 0.99$ was assumed for the current research.

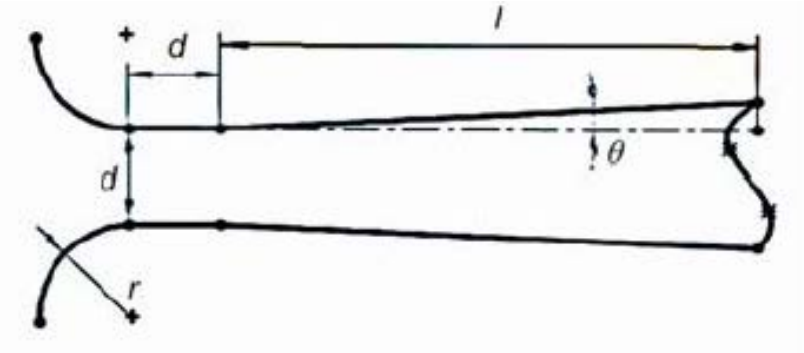

Figure 24. Cross-sectional view of sonic nozzle [24].

The mass flux was used as the flow condition parameter by assuming that the bulk flow of the reactants was due to the air mass flow rate. Mass flux ($\dot{m}''$) was calculated by Huff [5] as a function of the mass flow rate ($\dot{m}$) and the inlet detonation chamber area (A_c) immediately aft of the throat at a radial distance of r_t from the centerline (C_L) so that,

$$\dot{m}'' = \frac{\dot{m}}{A_{c,r_t}} \tag{6}$$

where,

$$A_{c,r_t} = 2\pi r_t h_{c,r_t}. \tag{7}$$

In Equation 7, A_{c,r_t} and h_{c,r_t} represent the chamber area and the channel height immediately aft of the throat at r_t, respectively.

2.4.2 Pressure Measurement Techniques

Historical pressure measurement techniques of RDEs include infinite tube pressure (ITP) measurements, capillary tube average pressure (CTAP) measurements, and Kiel stagnation pressure probes. ITPs and CTAPs have been implemented due to their ruggedness when exposed to the high-pressure/high-temperature environment of the detonation chamber within an RDE [25].

CTAPs, shown in Figure 25, can measure a time-average pressure signal. They consist of a long narrow tube connecting an RDE to a pressure transducer. The high length-to-diameter ratio provides high attenuation of the transient pressure changes typical in an RDE by allowing the viscous losses within the tube to attenuate the pressure waves. This process allows for little noise and can protect the transducer from the large heat transfer inherent in an RDE, but because of the attenuation, it does not provide a time-accurate signal [25].

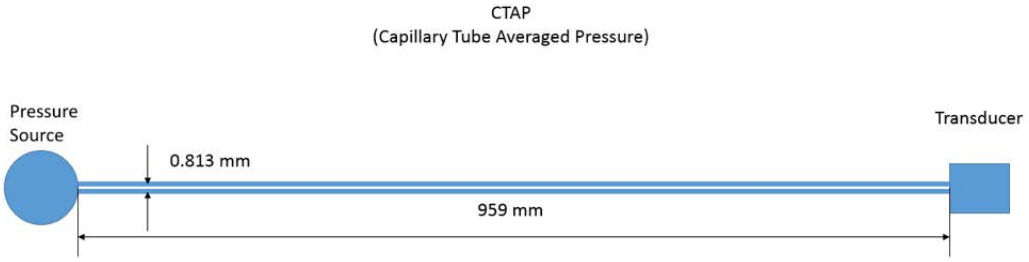

Figure 25. Schematic of CTAP [25].

ITPs, shown in Figure 26, can measure transient pressure signals, albeit attenuated. Similar to CTAPs, they feature a long tube and also help protect the transducer to the extreme environments of an RDE. Shown in the figure, the tube is considered infinitely long compared to the distance from the pressure source and from the transducer. The pressure transducer is able to measure when the pressure wave enters the tube as it propagates down the tube to the open end. The transducer is positioned

closer to the pressure source to measure the RDEs pressure rather than ambient pressure. The configuration allows for shock reflections to travel down the tube rather than affect the transducer [25].

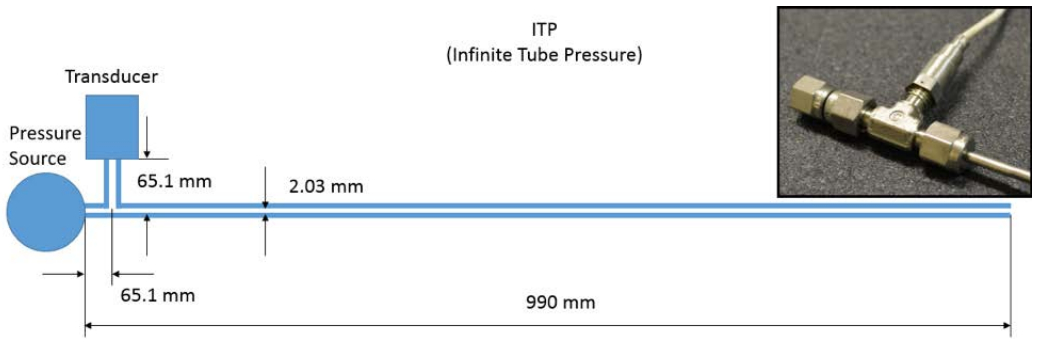

Figure 26. Schematic of ITP [25].

Kiel probes, a variant of a Pitot probe shown in Figure 27, measure stagnation pressure and are protected by a shroud so that they are less sensitive to angles of attack [26]. This is useful since the flow direction within an RDE can be variable. The shroud measures stagnation pressure over a 90-degree field of view with less than 10% error. Since the probes are exposed directly to the RDE, they were only used at the ejector in the cooler section of the rig [25].

The study by Stevens et al. to determine the response of different pressure probes in an RDE used a sealed detonation tube with five sensors tested simultaneously on the same steel insert containing: (1) CTAP, (2) ITP, (3) Kiel probe, (4) static pressure transducer, and (5) piezo-electric static pressure transducer. While the experimental method is important to understanding the mechanics of the shock tube in producing a detonation wave to measure, this review will not cover that method and further details can be found in the study by Stevens et al [25].

The static pressure transducer contained the most accurate pressure signal in both time-accuracy and magnitude and can be used to compare with the other pressure methods. While this sensor provides the most information, it is not considered for

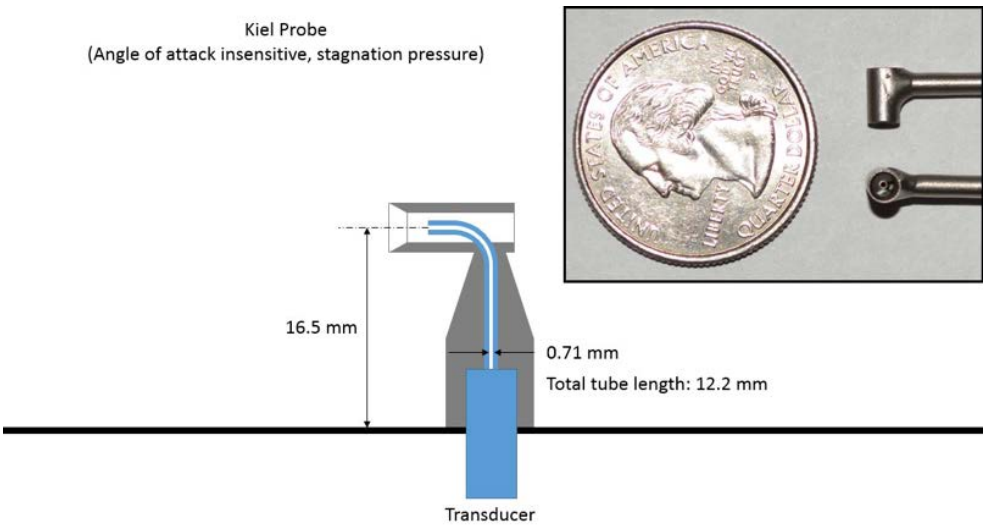

Figure 27. Schematic of Kiel probe [25].

other RDE use since it would not withstand exposure to the high temperatures within the RDE. The CTAP provided accurate pressure magnitude but did not capture the transient responses to the pressure except for spikes when the detonation wave passed the sensor caused by physical vibrations. For this study by Stevens et al., the ITP followed the static pressure transducer the closest but experienced resonance issues past the initial pressure spike [25].

Therefore, when examining the pressure within the detonation chamber of the RRDE, the CTAPs can be used to determine the magnitude of the pressure at various locations to determine the possible location of the detonation wave. The ITPs can be used in the detonation chamber to determine the wavespeed, number of waves, and wave direction if multiple ITPs are used at the same radial distance along the channel plate and their angular offsets are known. Boller used this method, specifically employing two ITPs set 45° apart to determine the wave direction, wavespeed, and the number of waves. Wave direction was determined based on which ITP provided a pressure spike first. Wavespeed could be also calculated using the frequency observed by the ITPs as well as the radial location of detonation wave. However,

this measurement has uncertainty since the RRDE experienced detonation waves at various radial locations depending on the number of waves and the flow conditions [5]. The number of waves was determined using a cross-correlation between the two pressure signals obtained by the ITPs. If the cross-correlation provided a 45° offset, one wave was present. Two wave corresponded to a 90° offset, while 135° suggested three waves [16].

A four wave condition would provide a 180° offset due to the 45° offset of the ITPs. However, Boller assumed that a four wave condition would not be present based on previous operation of the RRDE examined using high-speed imaging with a clear detonation channel [16]. In general, it was determined that a 180° offset in the two ITP signals was due to an acoustic mode, or an operating mode between an absolute deflagration and detonation. However, the cause of this offset was unknown. This acoustic mode was confirmed by examining the trends of the pressure wave signal, shown in Figure 28, with a rounded signal suggesting the acoustic mode and the detonative mode featuring sharp peaks and drop-offs corresponding to the rotating detonation wave.

2.4.3 Temperature Measurement Techniques

As discussed in Section 2.3.1, the temperature leaving the combustor and through NGVs is important to characterize to determine the efficiency of a combustor and a turbines expected performance or possible failure points. To determine the temperatures necessary to calculate performance characteristics like pattern factor, thin-filament pyrometry (TFP) can be used as an indirect method to measure the temperature. Probe techniques such as thermocouples or high-fidelity optical-thermometers are not suitable to high-temperature flow fields [27]. Thermocouples are located to only provide temperature data in one spatial location, and while they do have a high

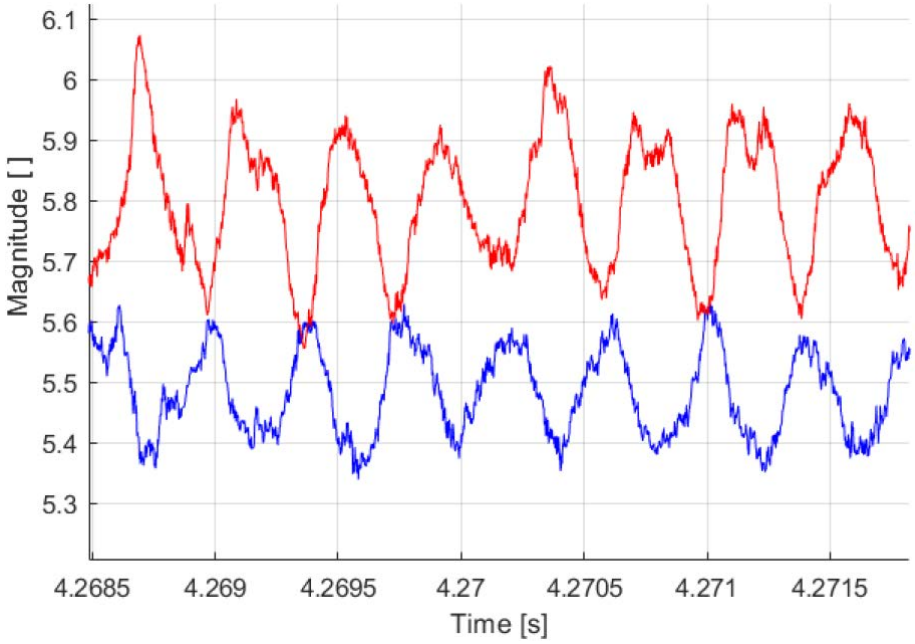

(a)

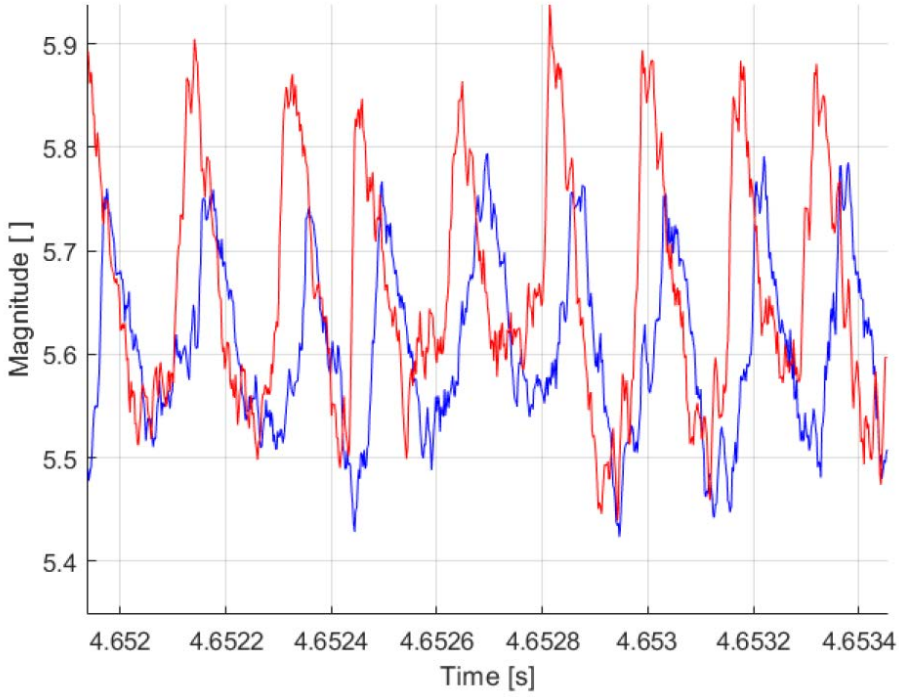

(b)

Figure 28. Sample signal from two ITPs on RRDE detonation chamber showing (a) acoustic mode and (b) detonation (two wave) mode.

response rate, they can be affected by perturbations in the flow field and are likely to melt or break within an RDE's environment.

TFP uses the graybody emission of a thin, Silicon Carbide (SiC) filament to measure the temperature distribution in a high-temperature flow field, such as from combustion. It is of note that TFP cannot be used with soot-creating flames. Specifically, the filament in TFP is ultrafine β-SiC with excess carbon and is available commercially. The diameter of the thin filament was originally 15 micrometers when it was first implemented, leading to a high response rate to the filament's environment. Its thermal conductivity is around $10\frac{kcal}{m-h^{\circ}C}$ at room temperature. The response for ambient conditions was experimentally measured to be 750 Hz. However, this frequency could have been limited by the existing equipment at the time of publication rather than the capability of the thin-filament. The filaments provide a high response to the temperature changes within its environment due to its small size. In addition, the wires thermal conductivity is around 40 times lower than platinum-rhodium wire. A lower thermal conductivity provides less conduction along the wire so that the emission of the wire only represents the temperature of the flow field right where it interfaces with it; therefore, a higher resolution is established [28].

When considering radiation measurements like TFP, the emissivity of the wire is needed, which is normally a function of the temperature, angle, and wavelength. However, the emissivity of SiC specifically has been shown to be a weak function of temperature, wavelength, and angle, with Figure 29 demonstrating the typical temperature change versus intensity. It can be noted that at the higher temperature range probable in RDEs, the intensity is relatively linear with temperature. To use TFP, the relative change in emissivity as a function of temperature, rather than the real value of emissivity, is more important. This is true based on the filaments calibration with a fluid of a known temperature. The study by Volimpoc et al.

notes that TFP is typically calibrated in either a hydrogen-air diffusion flame or a propane-air premixed flame. Temperature uncertainty existed due to the limited dynamic range of the digitization system and was larger at lower temperatures. Due to radiation losses, the filament may not have the same temperature of the surrounding fluid. An energy balance can be used to consider the radiation losses of the filament relating the radiation lost equal to the convective heat transfer between the gas and the filament [28].

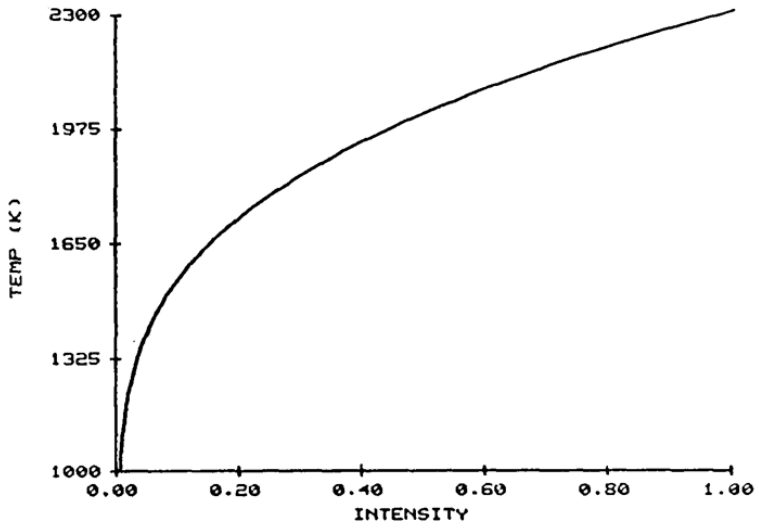

Figure 29. Sample calibration curve for TFP of temperature given emissivity [28].

The TFP process has been outlined further in a study by Innovative Scientific Solution, Inc. led by Dr. Larry Goss that was conducted with the Air Force Research Laboratory (AFRL) [29]. The TFP method can be observed using the intensity-ratio method or the two-color approach. The study, provided to AFRL, utilized the intensity-ratio method where the filament is given through Plancks law with the following equation:

$$I_R = \frac{\epsilon I_b(\lambda, T)}{\epsilon I_b(\lambda, T_0)} = e^{\frac{C_2}{\lambda}\left(\frac{1}{T_0} - \frac{1}{T}\right)} \tag{8}$$

where I_R is the intensity-ratio, I_b is the spectral radiance, ϵ is the emissivity, λ is

the wavelength, T is the temperature of the filament, T_0 is the calibration reference temperature, and C_2 is Planck's second constant [29].

The reference temperature can be obtained through a calibrated burner such as a Hencken or premixed flat flame, or through a calibrated pyrometer. In general, a pyrometer can refer to any measurement equipment that uses remote-sensing to determine the temperature of a surface. In the study by Goss, the calibrated pyrometer method was used, and the calibration occurred using the same flow and environmental conditions as what was expected during the experiment to reduce uncertainty from the radiation correction factor present in low-speed calibration flames. The color temperature of the filament was also measured at a fixed condition during the tests so that the color temperature could be corrected for the emissivity to establish the reference conditions [29].

The simple energy balance to solve for the gas temperature can be given as follows:

$$T_g = T_f + \frac{\epsilon\sigma(T_f^4 - T_\infty^4)}{h} \tag{9}$$

where T_g is the gas temperature, T_f is the filament temperature, T_∞ is the ambient temperature, ϵ is the emissivity, σ is the Stefan-Boltzmann constant, and h is the convective heat transfer coefficient [29].

The conductive heat transfer can be ignored in the energy balance due to the low thermal conductivity of the SiC ceramic filament. However, for a combustion rig, the energy balance becomes more complex to account for the hot, radiating walls. A subsequent heat transfer model was used for this study to provide radiation corrections for the gas temperature from 1000 K to 2000 K [29]. The radiation correction factor increased from ∼5 K at lower temperatures to ∼100 K for the higher gas temperatures. This is still smaller than the high correction factor, upwards of 300 K, at the higher gas temperatures for a low-speed calibration burner. Using the

results and methodology outlined by Goss, found in more detail in the interim report produced, the TFP method can be implemented for the RRDE, discussed further in Section 3.3.3 [29].

III. Experimental Method

To accomplish the research objectives of detonation confinement for the stand-alone combustor and bleed air turbine (BAT) configurations, an existing RRDE was modified and used. The RRDE used was previously tested by Huff [5] and Boller [16] and was distinguished by its constant area detonation chamber geometry. During both studies, two configurations were examined: the stand-alone combustor configuration and the bleed air turbine (BAT) configuration. This current research uses the same configurations but employs a constant height detonation chamber geometry to examine detonation confinement.

The facility used for all testing is detailed in Section 3.1 in addition to the previously tested RRDE design, distinguished by its constant area geometry. The general outline of the current equipment and test procedures is also given in this section. The stand-alone combustor configuration is described in Section 3.2, along with the flowfield visualization setup used for that configuration and the measurement techniques used. The BAT configuration is detailed in Section 3.3 and includes the design of the unique components needed for that configuration, as well as the implementation of thin-filament pyrometry (TFP) to characterize the temperature profile of the RRDE into the radial-inflow turbine.

3.1 Facility and Previously Tested Equipment

The present research makes use of an existing RRDE that was modified to achieve the detonation confinement goals. The RRDE was tested at the Detonation Engine Research Facility at Wright-Patterson Air Force Base. This facility, as well as the test procedures, is detailed in Section 3.1.1. The previously tested RRDE, distinguished by its constant area detonation chamber, is detailed in Section 3.1.2 so that

the fundamental characteristics which were used in the current configuration can be appreciated.

3.1.1 Detonation Engine Research Facility and Setup

All testing was accomplished at the Detonation Engine Research Facility (DERF) at Wright-Patterson Air Force Base, Ohio. The facility was able to provide safe operation of the RRDE for use with air and hydrogen, though other fuels are able to be tested. Furthermore, an existing configuration was used to measure mass flows of air and hydrogen, control when each reactant flow was initialized and cut off, fire the pre-detonation to initiate operation, and collect measurements using a Data Acquisition (DAQ) system.

Huff [5] detailed the full configuration of the facility and will be summarized here. Figure 30 provides a diagram of the necessary components of the facility to operate the RRDE. High pressure air was used as the oxidizer for the current research, while hydrogen was used as the fuel. Both were supplied from high pressure sources located outside the facility that were brought in using pipes with a variety of safety valves. The reactants were brought to a working pressure up to final valves controlled from a control room outside the main bay of the test facility. Nitrogen was used as the inert working fluid to regulate and actuate the valves in the system and was supplied by both high pressure and low pressure bottles within the test bay. These valves provided the last stop before the reactant flow traveled through the sonic nozzles and manifolds into the RRDE.

A Laboratory Virtual Instrument Engineering Workbench (LabVIEW) program provided control of the valves from the control room. Downstream of the air and hydrogen valves were sonic nozzles given in Table 1 with a diagram given in Figure 31a. Two sonic nozzles are given for the fuel line since the smaller $0.089''$ sonic nozzle

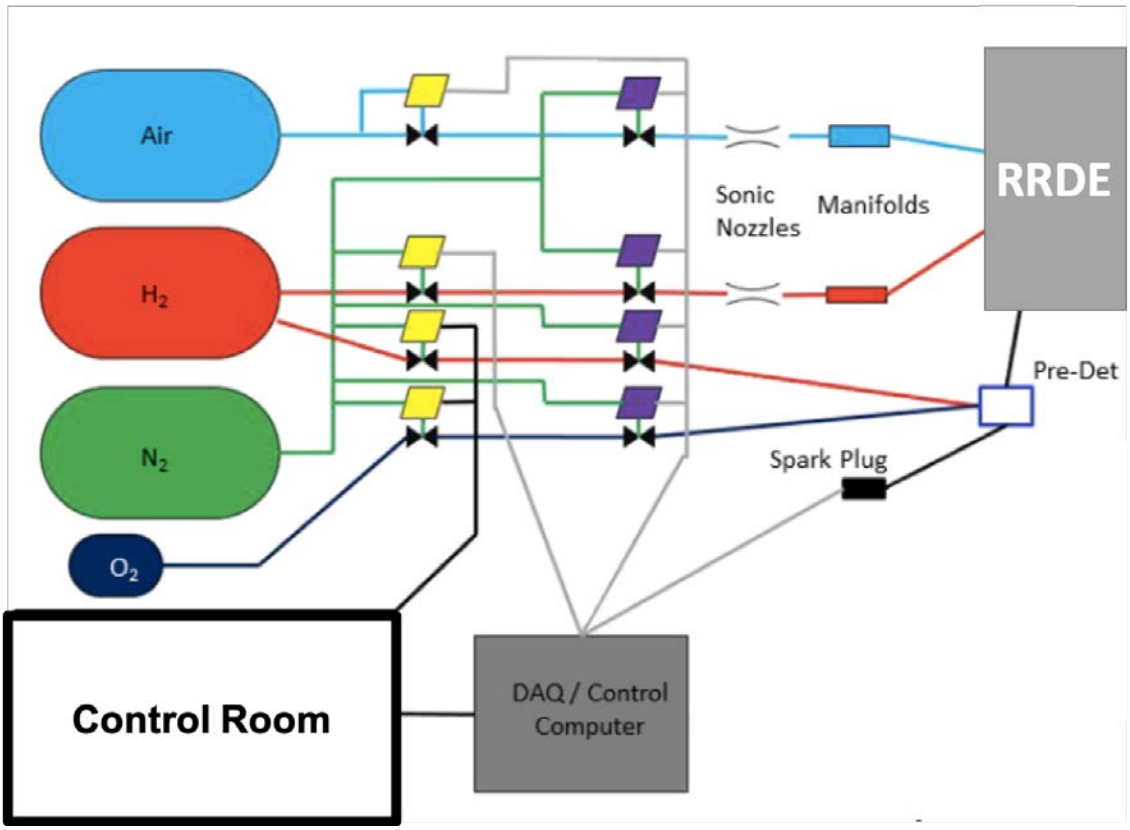

Figure 30. Test facility setup, adapted from Boller [16] and Huff et al. [30].

was replaced with a $0.125''$ sonic nozzle so that higher fuel flow rates could be used for larger channel heights and mass fluxes. These were used to provide a choke point upstream of the device and measure the reactant flow rates into the device. This was done using Equation 5 discussed in Section 2.4.1. In addition to the properties of the sonic nozzles, the thermodynamic properties of the flow were needed to calculate the flow rate. Therefore, pressure transducers provided the pressures upstream and downstream of the sonic nozzles, and were PX429-2.5KA5V and PX429-2.5KG5V Omega transducers with a range of 0-17200 kPa (0-2500 psia) and an uncertainty of ±14 kPa (±2.0 psia). In addition, K-type thermocouples with an uncertainty of $\pm 0.0075T$ were used downstream of the sonic nozzles to provide the temperature. The location of these measurements relative to the sonic nozzle are given in Figure

31b and 31c. While the transducers and thermocouples provided static pressure and temperature values, respectively, Boller [16] showed through 1D isentropic flow theory that these measurements are essentially the same as the total pressure and temperature values needed for Equation 5 due to low Mach numbers on either side of the sonic nozzles.

Table 1. FlowMaxx sonic nozzles used to monitor mass flow rates.

Flow Type	**Model**	**Diameter, mm (in)**	**Serial #**	Uncertainty
Air	SN32-SA-0395	10.033 (0.395)	980-1	±1%
Fuel	SN16-SA-089	2.251 (0.089)	922-2	±1%
Fuel	SN16-SA-125	3.175 (0.125)	930-2	±1%

Once the reactant flow passed through the sonic nozzles, the air and fuel were distributed through ten and twelve flex lines, respectively, from a manifold to the RRDE. Shown in Figure 32, the ten air flex lines were distributed evenly on the outside radius of the device, while the twelve fuel flex lines were distributed on the back of the RRDE. The flow path of the reactants within the RRDE is detailed in Section 3.1.2 through the discussion of the RRDE hardware.

To attempt to initiate a detonation once the reactant flow was within the device, a pre-detonator (pre-det) was used. The pre-det operated by creating a deflagration-to-detonation transition (DDT) event to carry the initial detonation into the RRDE. The pre-det contained a four-way connector for hydrogen, oxygen, a spark plug, and outflow to the RRDE. The hydrogen was brought from the same pressure source as the fuel, but through a different line at a lower pressure. The oxygen was brought from a bottle within the test facility. These two flows were controlled by injectors operated by the same LabVIEW program discussed earlier. The spark plug combusted the mixture in the pre-det, and this deflagration propagated through a machined screw obstructing the flow that provided the DDT for the detonation to enter the device. The pre-det could be fired without the RRDE's reactant flow to confirm that the

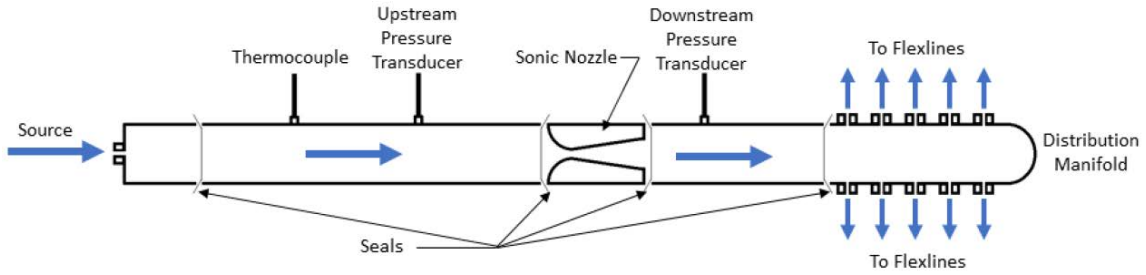

(a)

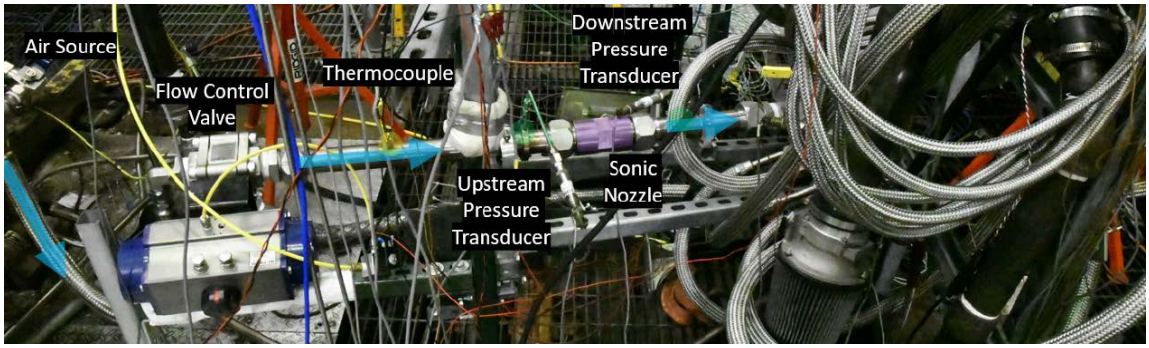

(b)

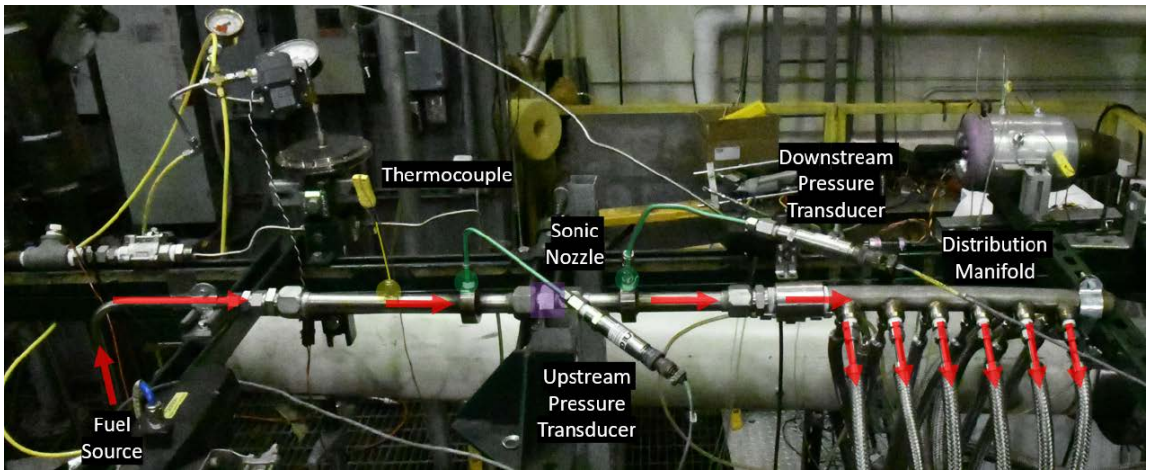

(c)

Figure 31. Diagram of (a) sonic nozzle used for the (b) air and (c) fuel measurement sections [16].

pre-det operated properly. This was done before a series of tests, and the pre-det was also initiated multiple times before a single test during cold ambient conditions when a low testing duty cycle was observed.

Testing the RRDE, regardless of whether in the stand-alone combustor or bleed

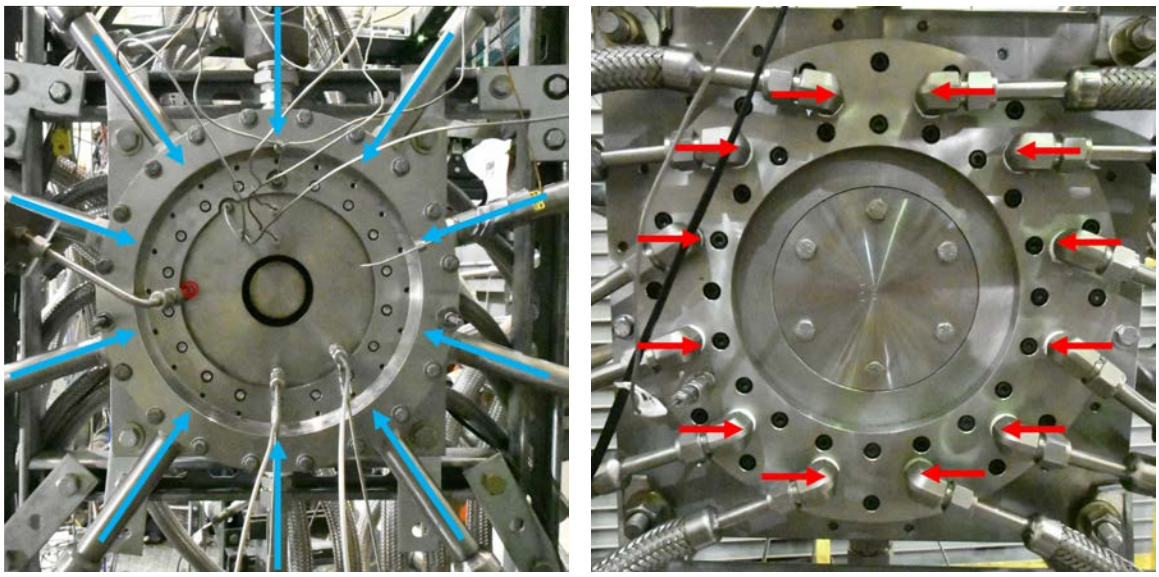

(a) (b)

Figure 32. RRDE with (a) ten air flex lines (blue arrows), pre-det (red dot), and (b) twelve fuel flex lines (red arrows) into the device.

air turbine configuration, followed a generic sequence of events to ensure safety and maintain consistent testing procedures for each condition. From the control room, the mass flow rates of the air and fuel were set for each reactant to obtain the desired mass flux and equivalence ratio. To set the flow rates, the valves were initiated from the LabVIEW program which also measured the flow rate and confirmed that the flow was choked based on the pressure and temperature measurements at the sonic nozzles and by applying Equation 5. Based on the flow rate outputs, the valves were adjusted til the desired conditions were met. Due to the uncertainty of the measurement devices, mass flow rates and equivalence ratios within two significant digits were assumed to be within the tolerance to provide data for a desired test condition.

Once the flow conditions were confirmed, an automated sequence was initiated. Figure 58 provides an example pressure trace within the RRDE that indicates the different steps of the testing sequence. While this example pressure data is for the stand-alone combustor configuration, it demonstrates the typical procedures used for

all configurations. First, after ambient conditions were recorded for 1.0 seconds, the air flow was initiated for 2.0 seconds so enough time was given to provide choked flow. After the 2.0 seconds, the fuel valve was opened and allowed to flow for 1.0 seconds. Less time was given due to the smaller mass flow rate and to conserve fuel, but the given time was enough for choked flow and to reach the desired equivalence ratio. Next, the pre-det was initiated, and this was considered the start of detonative operation. The iniation of the pre-det was also used, depending on the configuration, as a trigger for high-speed data collection. The pre-det trigger indirectly initiated the start of high-speed pressure measurements, which was set to record data 0.1 seconds before ignition using ITPs, whose fundamentals are given in Section 2.4 and implementation is discussed later in Section 3.1.2. The trigger was also used during flowfield visualization with the high-speed camera and is discussed further in Section 3.2.3.

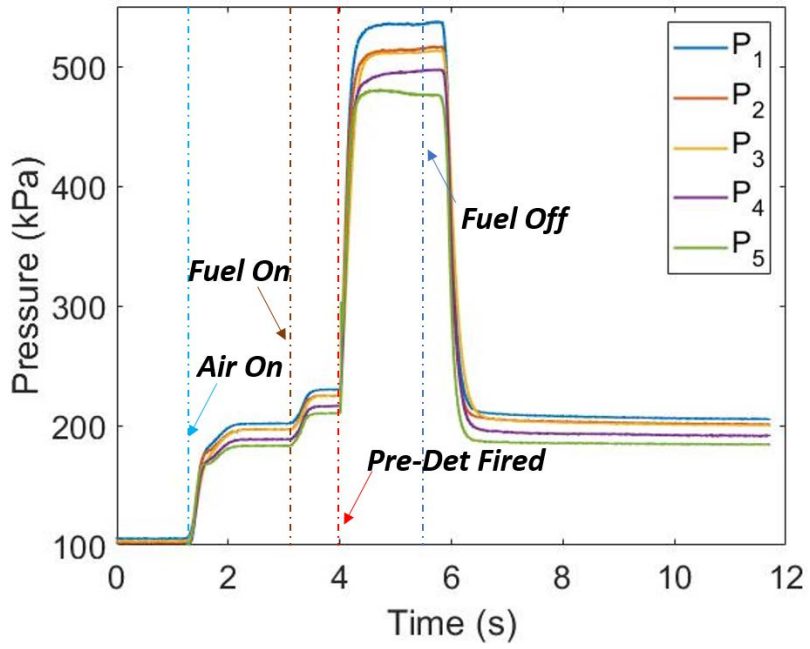

Figure 33. Sample pressure measurement from a test in stand-alone combustor configuration.

After ignition, the RRDE was set to run for 1.5 seconds. This amount of time was determined to provide an adequate view of the detonative modes within the RRDE, as well as to achieve steady state operation. In some cases, the operation time was extended to 2.5 seconds to determine if the operating mode at the end of test was the final operating mode for the device since mode shifts occurred for some test conditions. These mode shifts are discussed further in Section 3.2.2. Allowing the RRDE to run for longer than 2.5 seconds was not done to protect the sensitive ITP pressure transducers that were within close proximity to the detonative event, as well as to prevent plastic deformation of the RRDE hardware since it was not protected from thermal stress through a cooling mechanism.

To turn off operation, the fuel flow was closed off after the operation time had concluded, and air flow was left on for 6.0 more seconds to clear out remaining detonated products, possible soot, and cool off the device. Nominally, two minutes were allocated between tests to cool off the RRDE, as monitored through a thermocouple measuring the surface temperature of the RRDE. This cool-down period between tests was complimented by providing 30-60 seconds of cold air flow to provide forced convection to the hardware.

3.1.2 Constant Area Geometry Radial Rotating Detonation Engine

Since the RRDE used by Huff [3] and Boller [6] was modified for the current research, it is important to understand the fundamentals of its operation as originally developed. This previously tested RRDE maintained a constant area for the flow field as it travelled radially inward. Most of the components that were used for the current constant area geometry were also used for the constant height geometry, with the exception of the channel plate. Therefore, this section discusses the function of the components of the main chassis that remains constant between the two geometries

and configurations.

Figure 34 shows the exploded view of the stand-alone combustor configuration within the Computational Aided Design (CAD) software, demonstrating the layout of the main components. In addition, Figure 35 provides an example cross-section of the constant area RRDE fully assembled, showing the flow paths of the air and fuel into the plenum and the location of the throat before the reactants enter the detonation chamber. The top plate provided the chassis for the throat and channel subassembly, and it sealed the detonation chamber. The throat ring created the plenum for the reactants and was shimmed to set the throat area (A_t) of reactants into the detonation chamber. The channel plate created the geometry of the detonation chamber and was also shimmed to set the effective channel height (h_c) within the detonation chamber. A channel plate with a linearly increasing channel height as the radial distance from the centerline (C_L) decreased led to a constant detonation chamber area (A_c), while a flat channel plate as was used for the current research led to a constant height, decreasing A_c.

The air distribution ring provided uniform air flow into plenum with 55 0.375″ diameter holes. The spacer ring accepted the initial air flow with ten high pressure lines from the manifold described in Section 3.1.1 and positioned the throat ring relative to base plate. The fuel ring provided uniform fuel flow into plenum with 120 small diameter holes. The base plate made up the chassis for the RRDE to hold all the components and assemblies and was mounted to the thrust stand located in the test facility. The fuel mounting ring accepted the initial fuel flow with twelve high pressure lines from the manifold described in Section 3.1.1. The nozzle shown provided the aerodynamic surface to turn the flow from the initial radial direction to axial and simulated the blockage area (A_n) of a turbine.

In addition to the channel height set by the channel plate, the throat area ratio

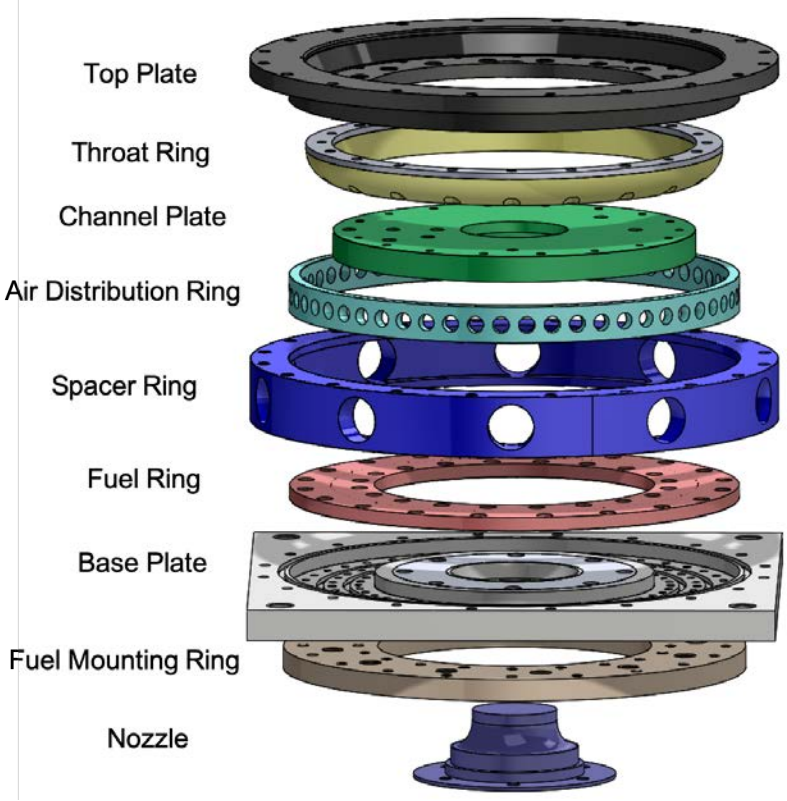

Figure 34. Exploded view of main components within RRDE assembly.

(AR_t) and nozzle area ratio (AR_n) were also used to characterize the configuration of the RRDE. The throat area ratio was determined by the ratio of the throat area to the initial detonation chamber area calculated at the radial location (r_t) given in Figure 35. Since both of these areas are calculated at the same radial location, the ratio is a function of distance between the throat and base plate (h_t) to the channel plate and base plate (h_c). The nozzle area ratio was calculated as the ratio between the effective flow area before it was turned by the nozzle to the exit plate area given as A_n in Figure 35. For the constant area geometry, effective flow area before the nozzle is the same as the inlet area of the detonation chamber, while these two areas are different for the constant height geometry. This area ratio was also considered the blockage area ratio since it determines the amount of area restriction as the flow was turned and exhausted.

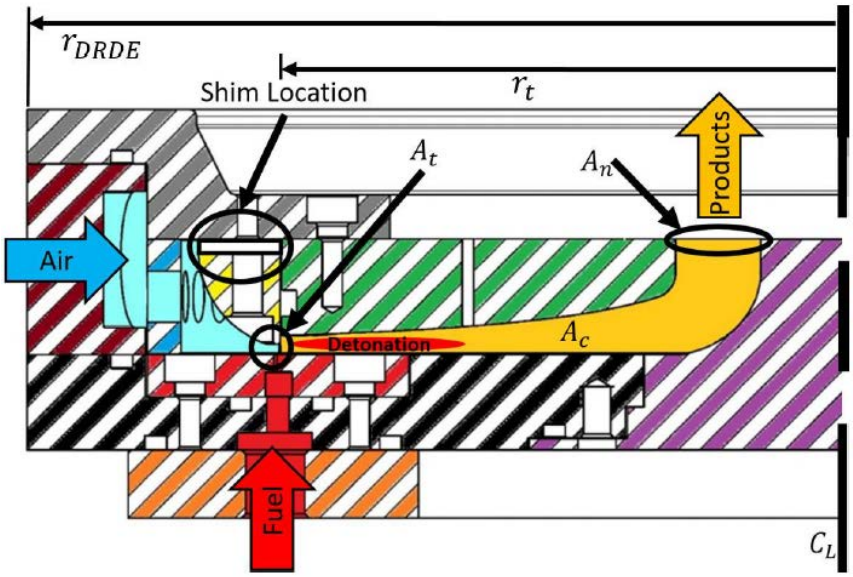

Figure 35. Cross-section view of the constant area RRDE in stand-alone combustor configuration from Huff [5].

Two configurations existed for the RRDE, shown in Figure 36 as the stand-alone combustor and bleed air turbine (BAT) configurations. The stand-alone combustor configuration, discussed in Section 3.2, had no integration with turbomachinery and only the characteristics of the RRDE alone were considered. Testing in this configuration allows for the characterization of the RRDE without interference from turbomachinery and its associated hardware. A larger area is available for access to support a larger array of pressure measurements to locate the detonation wave, characterize the pressure loss, and quantify the detonation mode. To simplify the turning of the flow, the nozzles were used in place of the turbine.

However, the stand-alone combustor configuration does not replicate the exact conditions of the BAT configuration, discussed in Section 3.3. The detonation chamber of the BAT configuration is larger to incorporate the guide vanes, whose inclusion in the RRDE signified the BAT configuration. In addition, the guide vanes dictated the chamber height at the radial location before the flow enters the turbine. In pre-

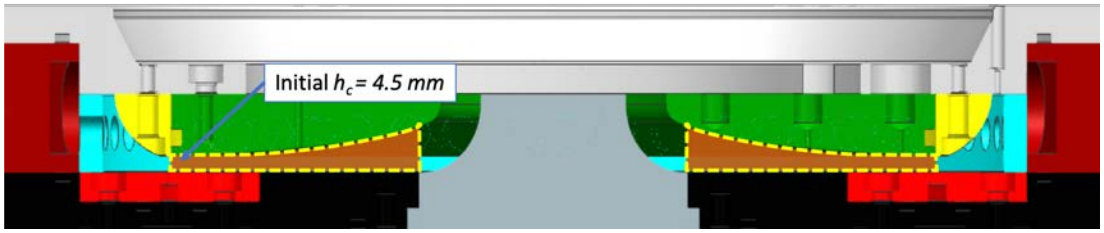

(a)

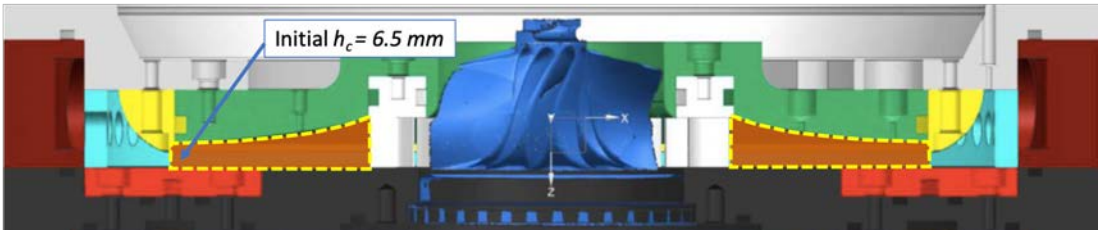

(b)

Figure 36. Comparison of constant area geometry channels in (a) stand-alone combustor configuration and (b) BAT configuration.

vious studies conducted to characterize the RRDE by Huff [3] and Boller [6], this geometric constraint led to different detonation channel heights between the two configurations in order to maintain the constant area, given in Figure 36. While the channel height varied between 3.5, 4.0, and 4.5 mm for the stand-alone combustor configuration, the channel height for the BAT configuration was extended to approximately 6.5 mm. This was dictated by the guide vanes' height, with the curvature of the turbine channel plate from the guide vanes to the outer radius leading to the 6.5 mm channel height.

The stand-alone combustor configuration for the constant area geometry provided large operability for equivalence ratios between 0.5 - 1.0 and mass fluxes between $50\frac{kg}{m^2s}$ and $200\frac{kg}{m^2s}$ [5]. However, this operability decreased with the turbine integration with the constant area geometry, with a detonative mode only occurring at a mass flux of $75\frac{kg}{m^2s}$ at an equivalence ratio of 0.6. While the reason of the limited operability was not discovered, the difference in geometries could be a factor [4].

If the combustor mode configuration could isolate the detonation event in the area

outboard of the guide vanes and turbine integration, the operation of this configuration could relate closer to the BAT configuration. Despite detonation confinement, the changing area and influence of the turbomachinery could still affect the detonative mode. However, the configurations are more likely to relate if confinement occurs in a constricting area detonation chamber away from the turbine.

3.1.3 Constant Height Geometry Radial Rotating Detonation Engine

The constant height geometry was developed to obtain detonation confinement with a decreasing A_c as the flow travels radially inward, unlike the constant area geometry that was shown in Section 3.1.2 to describe the general layout of the RRDE. Figure 37 shows the difference in the detonation chamber between the constant height and constant area geometries while maintaining same flow paths, throat inlet, and exit area. Figure 37 represents the stand-alone combustor configurations for both geometries since this cross-section best demonstrates the difference between the two geometries. The current RRDE, shown in Figure 37a, featured a constant channel height by maintaining parallel plates to define the detonation chamber. Previous work by Huff et al. [3] and Boller et al. [6] have characterized an RRDE with a constant area detonation channel, given in Figure 37b, by shaping the channel plate to increase the channel height as the radial distance decreases. The constant height geometry created an effective flow area that decreased by almost 65% from the detonation chamber inlet til the flow was turned by the nozzle for the stand-alone combustor configuration. This configuration is detailed in Section 3.2. The constant height geometry BAT configuration created an effective flow area that decreased by 30.9% from the detonation chamber inlet. However, to accommodate the guide vanes, the flow area increased, with the percent increase dependent on the initial channel height. The BAT configuration is discussed in Section 3.3.

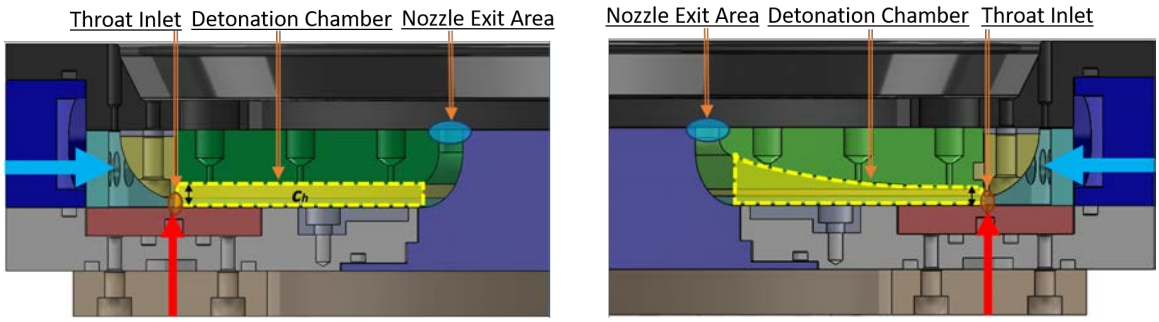

(a) (b)

Figure 37. Comparison of (a) constant height geometry and (b) constant area geometry in the assembly.

3.2 Stand-Alone Combustor Configuration

The first configuration to attempt detonation confinement with a constant height geometry was the stand-alone combustor configuration. The configuration, shown with its components in an exploded view in Figure 34 and whose cross-section is given in Figure 37a, was used to test the RRDE operating without any turbomachinery such as guide vanes to introduce swirl downstream of the detonation event.

For this research, two flat plates were designed, of stainless steel and polycarbonate, to test the constant height, stand-alone combustor configuration. The stainless steel plate was designed and tested first due to its ability to be instrumented along the detonation chamber and its durability through a variety of test conditions. The polycarbonate provided high-speed visualization of the flowfield within the detonation chamber. The testing procedures between the steel and clear channel plate remained the same, with the steel channel plate having the ability to increase the running time from 1.5 seconds to 2.5 seconds.

First, the stainless steel plate was designed to test the constant height configuration. The design was based on the success of the channel plate designed by Huff [5] for his investigation of the constant area RRDE. The CAD view of the channel plate with a cross-section is given in Figure 38. The constant height was maintained until

the flow met the nozzle, as seen in Figure 37a. At this radial location, a radial curve was used to turn the flow with the nozzle from the radial direction to its axial outlet. Since multiple nozzles previously designed by Huff [5] were to be tested, the radial curve was not set to match a specific nozzle. The radius was set to turn the flow with minimal losses while providing a 6 mm vertical straight edge before the exhaust that was also included in all the nozzles. To maintain compatibility with existing hardware, the outer radius was set to 10.48 cm, the inner radius was set to 3.1 cm, and the thickness of the channel plate was set to 1.5 cm.

With the geometry set based on the constant height required within the detonation chamber, the channel plate was also designed to accommodate ports for measurements. Unlike the clear channel plate, the stainless steel plate provided the robustness to withstand the detonation waves and contained access ports at seven locations that provided pressure data within the detonation chamber to characterize the detonation wave. Five of these ports provided the amplitude of the static pressure at various radial locations of the detonation chamber and is discussed in Section 3.2.1. The other two ports provided the frequency of the detonation wave and is discussed in Section 3.2.2. In addition to the pressure ports, a through hole was included to provide a location to weld a $1/4''$ tube to connect the pre-detonator device to the channel plate to provide the initial detonation event into the detonation chamber.

The three variables that were tested to determine the operability of the constant height geometry was the channel height (h_c), throat area ratio (AR_t), and nozzle area ratio (AR_n). The thickness of the channel plate created a channel height of $h_c = 6.5$ mm, with the ability to be shimmed to smaller channel heights of 4.5, 5.0, and 5.5 mm. The throat ring was also shimmed to create different throat heights (h_t) and throat area ratios. The nozzle area ratio was modified by using various existing nozzles. For this study, the effect of the blockage on the performance was examined.

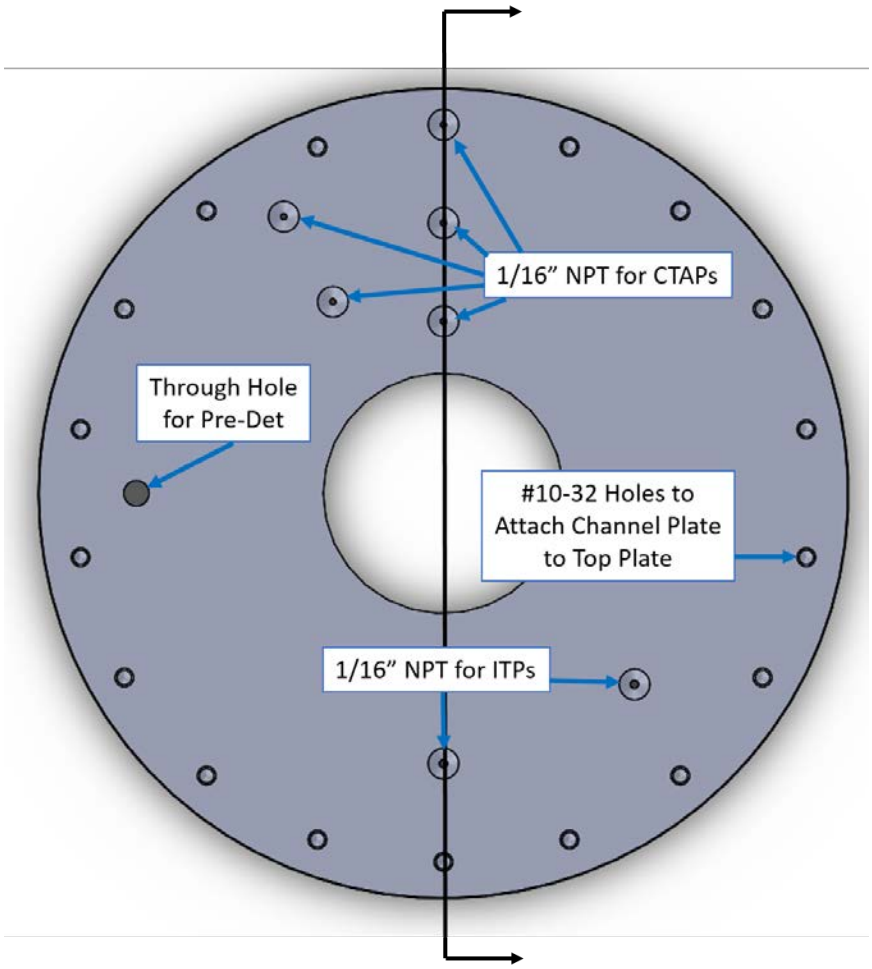

Figure 38. Design of steel flat channel plate with (a) top view and (b) cross-section with relevant features highlighted.

3.2.1 Pressure Amplitude Techniques and Analysis

Measuring the thermodynamic properties within the detonation chamber of the RRDE is important in characterizing the detonation and quantifying the performance

of the device. The temperature within the detonation chamber was attempted using Thin-Filament Pyrometry, as detailed in Section 2.4.3 and discussed further in Section 3.3.3 as it was used with the bleed air turbine configuration. The pressure in the chamber was measured using the techniques detailed in Section 2.4.2. This included the use of Capillary Tube Averaged Pressure (CTAP) devices to measure the static pressure amplitude attenuated from the detonation chamber and the use of Infinite Tube Pressure (ITP) devices to measure the frequency response of the detonation wave. Figure 39 demonstrates the location of the CTAPs as $P_1 - P_5$ and the ITPs as F_1 and F_2 on the channel plate of the stand-alone combustor.

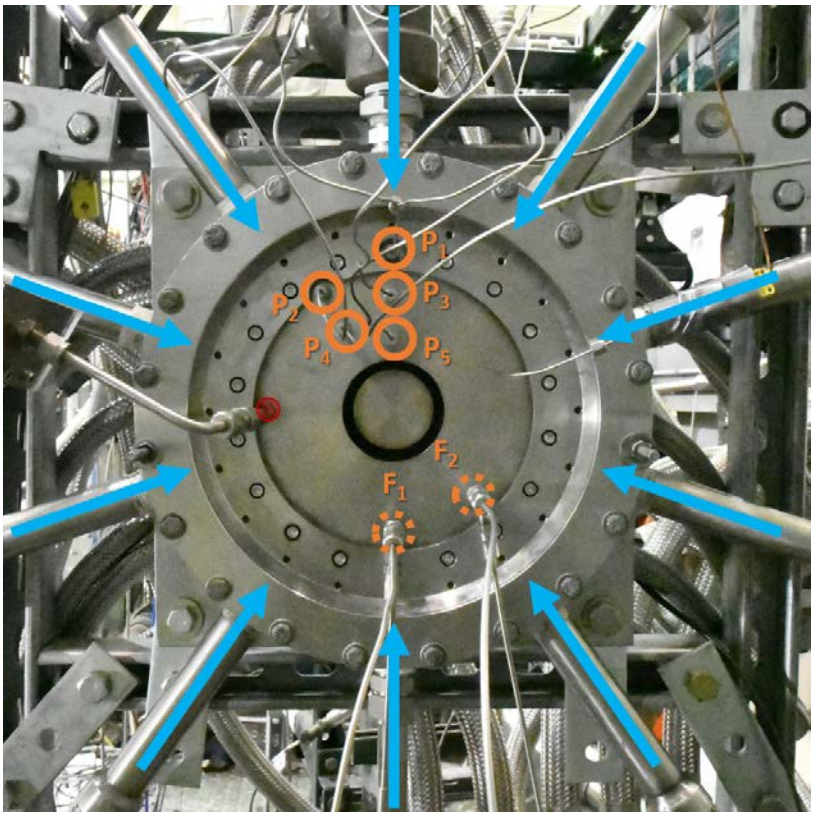

Figure 39. Front of RRDE in stand-alone configuration showing pressure port locations, with $P_1 - P_5$ showing CTAPs and F_1 and F_2 showing ITPs.

The CTAPs functioned by attenuating the high frequency pressure signals generated by the detonation wave through a tube between the chamber and the transducer.

For each of the CTAPs, an Omega PX429-250A5V transducer was used with a range of 0-1700 ±1.4 kPa (0-250 ±0.2 psia). For all configurations, a CTAP was used to measure the plenum pressure (P_{plenum}) just upstream of r_t through the top plate. On the stand-alone combustor, five CTAPs were used on the detonation chamber at radial locations of $P_1 = 9.5$ cm, $P_2 = 8.3$ cm, $P_3 = 7.0$ cm, $P_4 = 5.7$ cm, and $P_5 = 4.4$ cm from the centerline, where P represents the static pressure value obtained from the CTAPs. These locations matched the positions of the CTAPs employed by Huff [5] so that performance characteristics could be compared.

On the channel plate, $1/16''$ NPT to $1/16''$ Swagelok fittings were used. Between the channel plate and the transducers, $1/16''$ tubing was used. The relatively small diameter was used to attenuate the unsteadiness of the pressure signal due to the detonation wave. However, a quick response was needed to ensure that the pressure increase during operation was measured within the limited testing time. Therefore, shorter tubes of around 40 cm of length were used.

The pressure measurements were used to locate the detonation wave and measure performance of the stand-alone combustor. The highest pressure trace of the five CTAPs approximately located the detonation wave since the detonation would produce the highest pressure region. To compare the constant height geometry's performance with the previously tested constant area geometry, the pressure loss through the device was measured. While the primary goal for an RDE is as a pressure-gain device, currently there are losses affiliated with the throat area restriction invoked to provide ideal mixing of the reactants and set a choke point before the flow enters the detonation chamber. In addition, an RDE is also affected by the amount of back pressure that occurs into the plenum from the detonation. Initially, the pressure loss (dP_{inj}) was calculated and was based on the difference between the P_{plenum} and the pressure farthest from the throat, P_5, near the nozzle. This is given in Equation 10

and was consistent with Huff's definition [5]. The pressure measurement at P_5 was selected since it measures the static pressure past the combustion event and accounts for the expansion and losses inherent in the channel.

$$dP_{inj} = \frac{P_{plenum} - P_5}{P_{plenum}} \tag{10}$$

However, despite the use of Equation 10 in the initial characterization of the RRDE [5], the negligible Mach value in the plenum provides a stagnation value for P_{plenum}. Therefore, dP_{inj} does not provide a fully accurate pressure loss due to the stagnation to static pressure values comparison. Further research of pressure-gain combustors (PGC) has led to the development of techniques to derive an equivalent, steady, and uniform gas pressure that helps provide a comparison of PGCs to other propulsive devices [31]. This technique, developed by Kaemming and Paxson [31], proposed the use of an Equivalent Available Pressure (EAP) that represents the flow's stagnation pressure and available pressure through a nozzle or a turbine. For the RRDE in stand-alone combustor configuration, the EAP is considered at Station 5 as the radial location just upstream of the flow being turned by the nozzle and is given in Equation 11.

$$EAP = P_{t5} = P_5(1 + \frac{\gamma - 1}{2}M^2)^{\frac{\gamma}{\gamma-1}} \tag{11}$$

To determine the EAP, the ratio of specific heats (γ) and Mach number (M) must be estimated. The value for γ was determined through the use of CEA [32] and varied between 1.17 and 1.24 depending on the equivalence ratio. While γ is also a function of the inlet thermodynamic conditions, the values were within 0.004 for a given equivalence ratio across different mass fluxes that affected the initial pressure. The Mach number was estimated by assuming the choked point within the RRDE.

For most of the test conditions where the nozzle used provided converging flow, the flow was assumed choked at the exit plane of the nozzle. In some cases where the area diverged through the nozzle with $AR_n > 1$, the flow was assumed choked just upstream of the nozzle. Using this assumption with isentropic flow relationships, the Mach number at P_5 was estimated using compressible area ratio ($\frac{A}{A^\star}$) equation given in Equation 12.

$$\frac{A}{A^\star} = (\frac{\gamma+1}{2})^{-\frac{\gamma+1}{2(\gamma-1)}} \frac{(1+\frac{\gamma-1}{2}M^2)^{\frac{\gamma+1}{2(\gamma-1)}}}{M} \tag{12}$$

The area at the sonic condition where the Mach number is 1.0 is denoted by $A^\star$, which was usually the exit area, and A is the area at the location of interest. For the stand-alone combustor configuration, A was determined in the detonation chamber at P_5 as:

$$A = 2\pi r_5 h_c \tag{13}$$

where $r_5 = 4.4cm$ and h_c is the channel height tested. Knowing the compressible area ratio ($\frac{A}{A^\star}$) and γ, Equation 12 can be used to solve for the Mach number for use in Equation 11. The subsonic solution for M was used since the area upstream of the choked condition would be subsonic, and the isentropic flow calculator provided by NASA was used.

The uncertainty of EAP was determined by the assumptions for γ and M. Using CEA for γ assumed an ideal detonation event for the given equivalence ratio which was different from the effective equivalence ratio during operation as the back pressure from the detonation event feeds into the air and fuel plenums separately. Furthermore, γ downstream of the detonative event would also be different. For the calculations, a conservative error for the calculated value of γ of ± 0.04 was used based on the results provided through the NASA developed CEA, or Chemical Equilibrium

with Applications, program. Solving for M used this same assumed value for γ and assumed that the flow was choked at the smallest area within the RRDE. However, it was possible that the Mach number was subsonic at the exit, especially at lower flow rates and larger channel heights. Assuming the Mach number at $A^\star$ was within 10% of the sonic condition assumption, the uncertainty can be calculated by substituting the maximum error provided for γ and $A^\star$ for each condition.

For the calculation of pressure loss using Equations 10 and 11, the values for P_{plenum} and P_5 were obtained as the last recorded value during operation. It is important to consider that these values were obtained from CTAPs. Therefore, due to the attenuation of the pressure from the tubing, uncertainty exists from the transient differences between the two measurements. However, the uncertainty was not quantified since the exact differences between the actual plenum and channel pressures and the CTAP measurements were not investigated.

3.2.2 Pressure Frequency Techniques and Analysis

While the CTAPs provided the pressure amplitudes, they could not provide a transient response due to the attenuation from the tubing. To measure the high-speeds of the detonation wave, ITPs were used. Two ITPs were used, shown as F_1 and F_2 in Figure 39, that were 45° apart at the same radial location. Another Swagelok fitting was used from the $1/16''$ NPT ports to the T fitting that connected the pressure signal from the detonation chamber to the transducer and tubing. Two Kulite ETL-4-GTS-190-1000A transducers were used with a pressure range of 0-6900 kPa (0-1000 psia) and a bandwidth of 50 Hz-150 kHz. These were selected due to their relatively high temperature rating of 773 K while still providing a high frequency sampling rate. Since the magnitude of the pressure was not examined from the signal, the error of the pressure values was not examined. The transducers were connected to

an amplifier that were regulated to provide 10 V, which were both processed through the DAQ with a sampling frequency set to 50 kHz.

The signal generated from the ITPs were processed using MATLAB to measure the dominant frequency. This was done using a fast Fourier transform (FFT) that showed the power spectrum for the signal. A sample test run is given in Figure 40, with the CTAP pressure trends given in Figure 40a and the FFT taken during the high frequency window given in Figure 40b. For this test, multiple frequencies appeared. Based on the previous visualization studies conducted by Boller et al. [6] of what modes correlated to what frequency, it was concluded that one wave modes operated between 2.0-3.0 kHz, with two waves between 4.0-5.0 kHz and three waves between 5.0-6.0 kHz. Within these ranges for a given wave mode, higher frequencies were observed for higher equivalence ratios and lower channel heights. However, using just the FFT plot could not provide the wave mode and the mode transitions over time, which occurred often during tests that had increasing pressure during operation as shown in Figure 40a. Therefore, other signal diagnostic tools were implemented to monitor the mode changes over time.

In conjunction with the FFT, a spectrogram was used to show the dominant

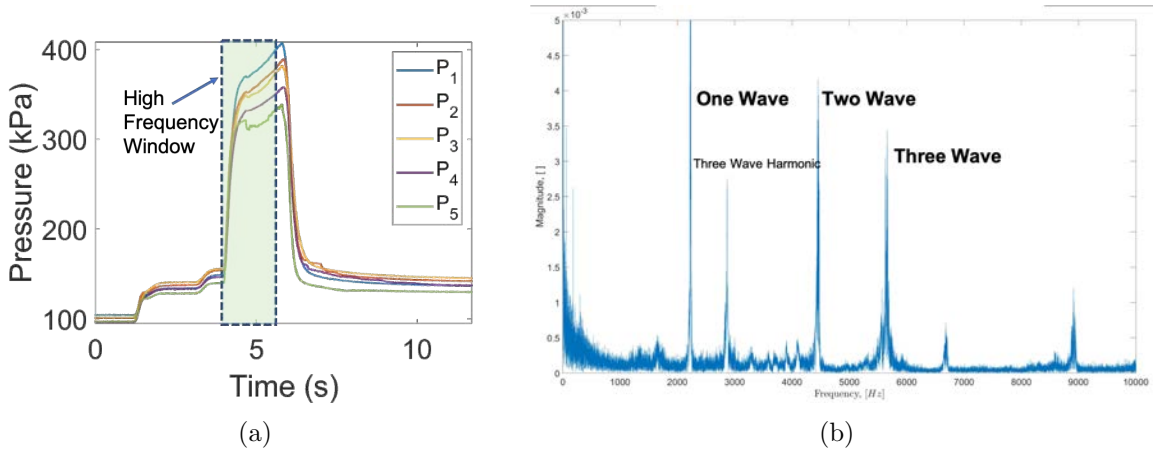

(a) (b)

Figure 40. Sample test with (a) CTAP plot with high frequency window and (b) FFT plot measured with ITPs during window.

frequency of the signal over time. The same pressure signal processed in Figure 40 is given as a spectrogram in Figure 41a. The same wave modes were shown, with a transition from the one wave mode to the three wave mode at the end of the run. To further validate the number of waves at a given frequency, a cross-correlation was done between the two ITPs. The cross-correlation techniques were developed and explained by Boller [16] to determine wave modes and provided the phase difference between the two F_1 and F_2 signals to confirm wave numbers and determine direction. Since F_1 and F_2 were 45° apart, one wave modes operated at a 45° phase shift, with two waves at 90° and three waves at 135°. These correlations are given in Figure 41b and were accomplished by assuming the frequency bands for each wave mode so that both signals were analyzed over the correct frequency. For example, for a suggested one wave mode through the spectrogram, the signals were analyzed between 2.0 kHz and 3.0 kHz to confirm a phase shift of 45° between the two signals. For a suggested three wave mode, the signals were analyzed between 5.0-6.0 kHz to confirm a 135° phase shift. To generate Figure 41b, the results from the three different correlations were combined by omitting zero correlation points that occurred after the wave mode transitioned.

3.2.3 Flowfield Visualization of Stand-Alone Combustor

To examine the flowfield within the detonation chamber, a polycarbonate channel plates was manufactured, shown installed in Figure 42. The polycarbonate channel plate had the same function as the steel channel plate, with the same ability to be shimmed to set the desired channel height. The radial location, number of waves, and wave direction were determined at a variety of test conditions using this clear plate. The initial selection of polycarbonate as the material was based on the research and results detailed by Boller [16]. While the polycarbonate experienced operation-

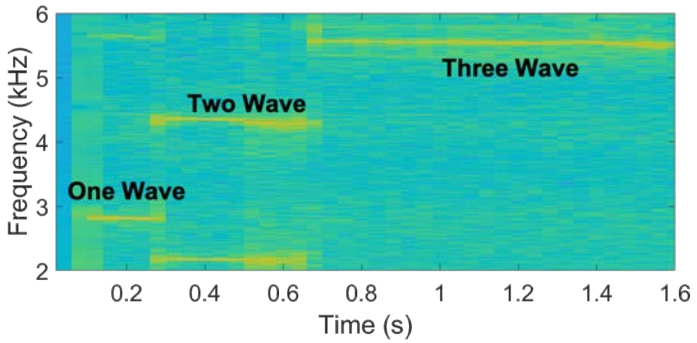

(a)

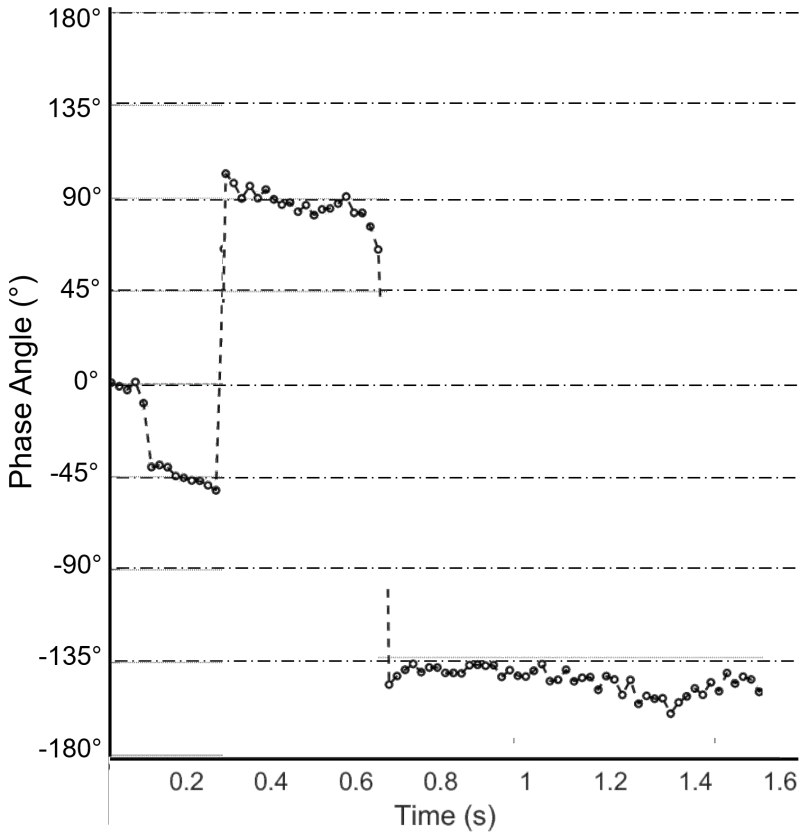

(b)

Figure 41. Sample test with (a) spectrogram and (b) cross-correlation between the two ITPs.

altering burning and melting due to the high thermal loads given by the detonations, the materials low cost was the primary factor in its selection. Furthermore, the polycarbonate plate could be tapped to accept the same fasteners of the steel channel plate without concern of fracture despite the high vibration environment.

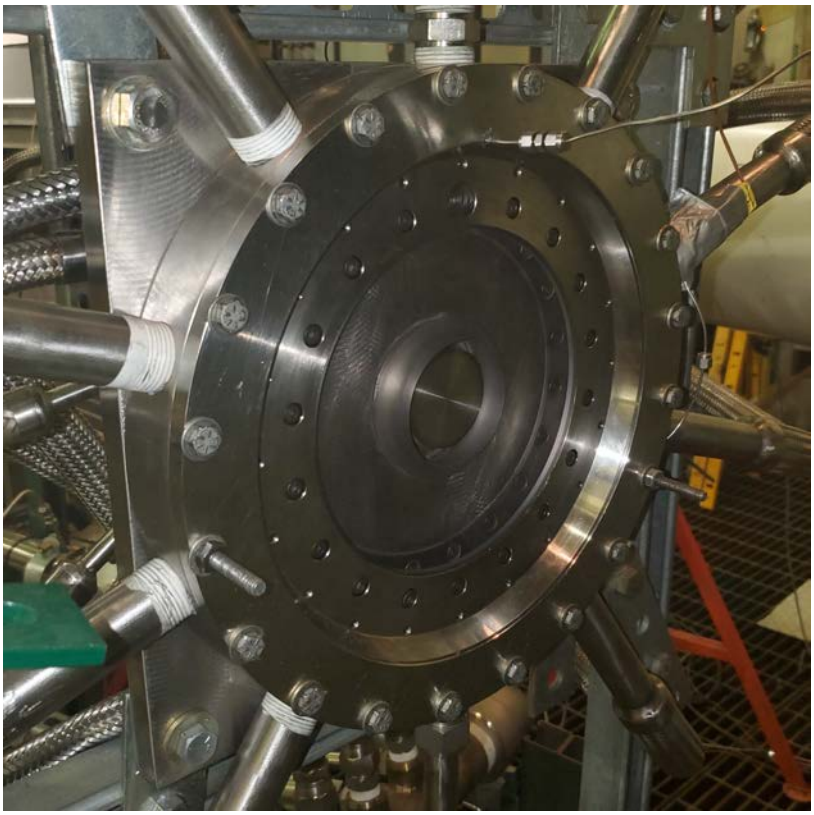

Figure 42. RRDE in stand-alone configuration with polycarbonate channel plate.

Figures 43a and 43b provide the view of the previous polycarbonate channel plate before and after operation, respectively, used by Boller to examine the constant area flowfield. Similarly, Figures 43c and 43d show the flat polycarbonate channel plate. Before operation, the constant height plate allowed for greater optical clarity since the top and bottom faces of the plate were parallel and were not machined unlike the constant area plate which was shaped to a specified profile. While the constant area plate was semi-transparent due to its machining imperfections, the plates thin size and the detonation waves close proximity to the polycarbonate allowed sufficient light exposure to measure the flowfield characteristics. The constant height plate was machined to be more than two times as thick as the constant area plate to increase the plates robustness during operation.

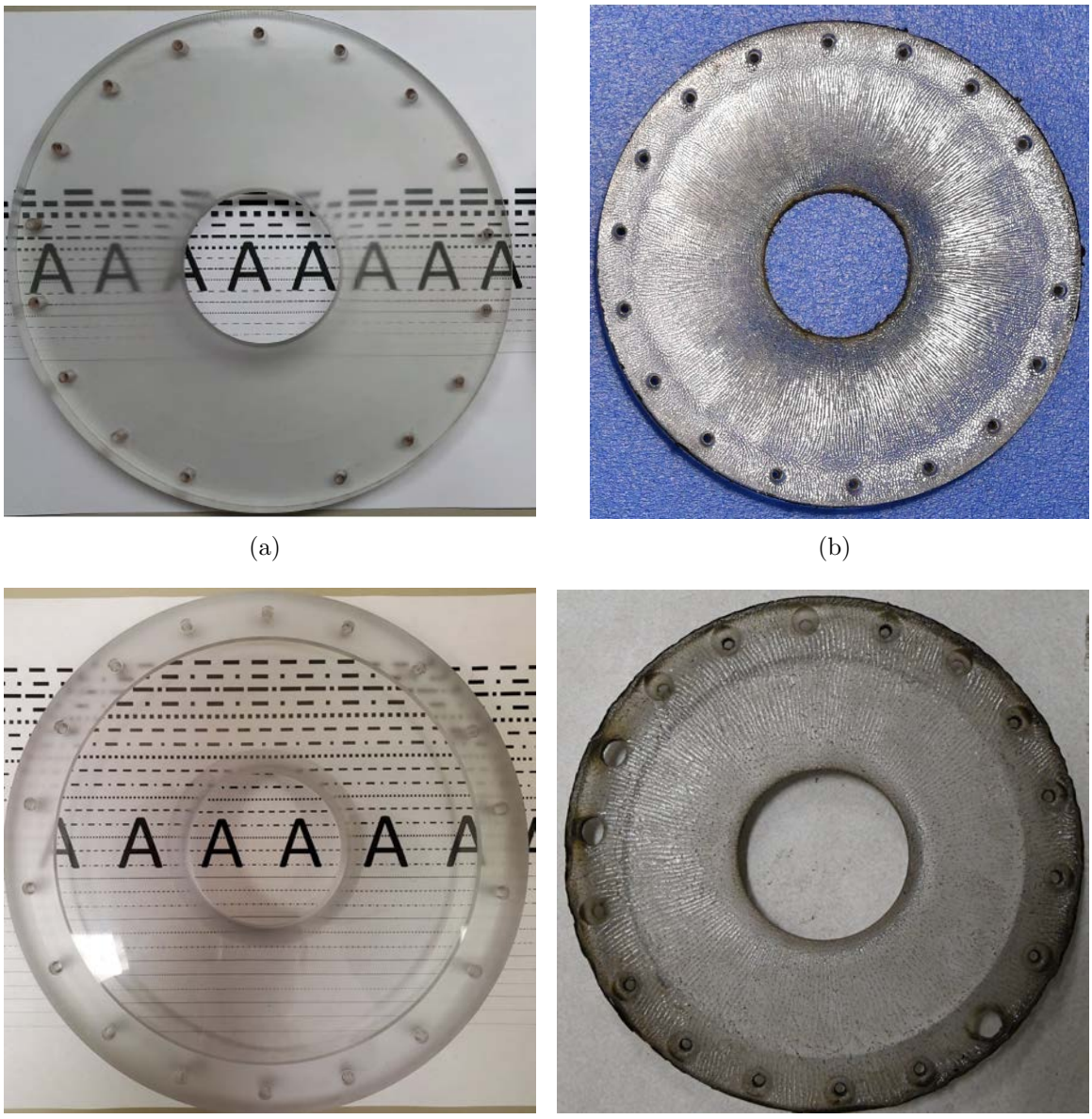

(a) (b)

(c) (d)

Figure 43. Comparison of the polycarbonate channel plate used in the constant area geometry (a) before and (b) after operation [16], and the channel plate used in the constant height geometry (a) before and (b) after operation.

After testing, both polycarbonate channel plates experienced burning that altered their optical clarity and their physical dimensions. The constant area geometry made use of multiple polycarbonate plate, with the largest increase from its initial channel height of $h_c = 4.5$ mm leading to approximately $h_c = 9.9$ mm [6]. The constant

height geometry had an initial channel height of $h_c = 6.5$ mm that increased to approximately $h_c = 13.7$ mm after the final test. The increasing channel height increased the uncertainty of the input mass flux since the exact channel height variation during tests was not known.

For flowfield visualization through the clear channel plate, a Phantom v711 high-speed camera was used. To avoid direct contact with the heat from the exhaust, the camera looked into the RRDE using a mirror. A diagram of this setup is given in Figure 44a with the view of the device from the camera's point of view shown in Figure 44b. The Phantom operated with a resolution of 384x384 pixels. With this relatively lower resolution, a high frame rate of 40,988 frames per second (fps) could be maintained. At this resolution and frame rate, the exposure was adjusted to 0.9 μs to attempt to capture the detonation wave's illumination while limiting the exposure from capturing secondary burning. The DAQ was connected as the trigger source for the Phantom camera and was also the same trigger source for the pre-det. Therefore, the camera was able to capture the flowfield within the detonation chamber from pre-ignition through the fuel shut off process.

To maintain optical access into the detonation chamber, the pressure measurements made along the channel plate detailed in Sections 3.2.1 and 3.2.2 were not included. However, the plenum pressure was still measured through the top plate. In addition, an ITP was installed in the pressure port located into the fuel plenum. While the pressure increases were not as large as seen in the ITPs used in the channel plate and only one ITP was used that prevented the use of cross-correlations, the ITP installed into the fuel plenum still provided the detonation frequency. This was due to the detonation wave's pressure influence on the reactant's plenum, and it was assumed that the pressure fluctuations seen in the fuel plenum pressure signal was equivalent in frequency to the detonation wave. This assumption was confirmed by

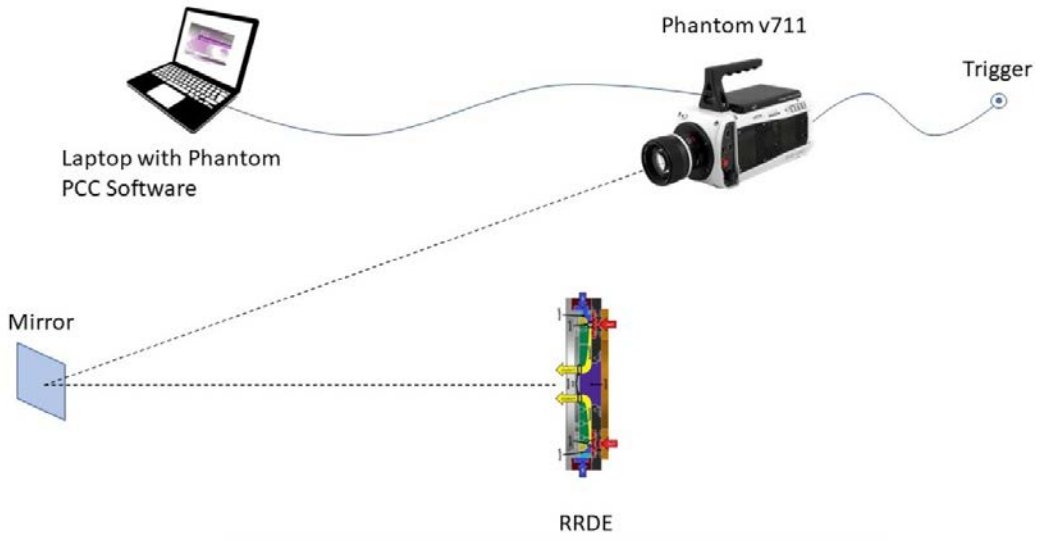

(a)

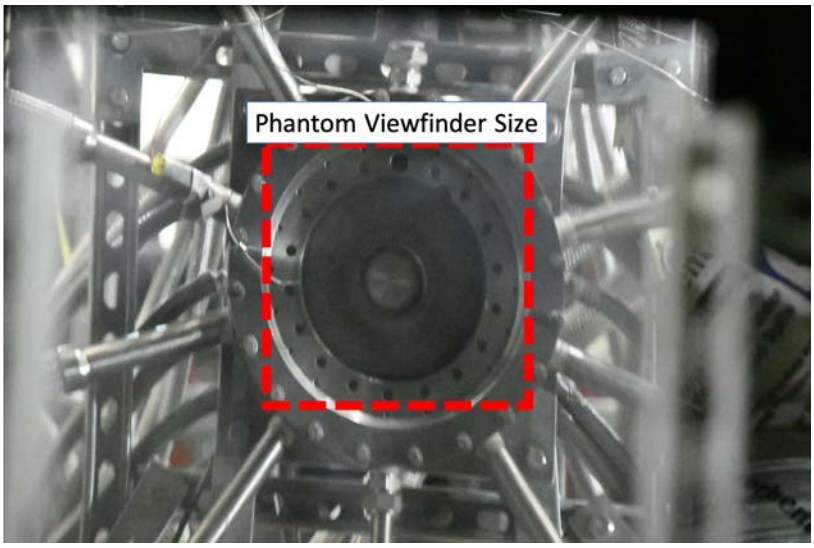

(b)

Figure 44. High-speed visualization setup with (a) Phantom camera setup and (b) view of RRDE from the camera.

comparing the frequency obtained through an FFT at a time to the frequency observed by counting the number of revolutions for a set amount of time through the high-speed camera.

3.3 Bleed Air Turbine Configuration

The second configuration tested is called the bleed air turbine (BAT) configuration, derived from previous testing of the RRDE with an automotive turbocharger to measure specific power and thermal/turbine efficiency. The configuration, shown in an exploded view in Figure 45, was considered to use bleed air since the compressor was not feeding the air flow into the RRDE. The main chassis of the RRDE used during the stand-alone combustor configuration remained unchanged in the BAT configuration. This included the fuel mounting ring, base plate, fuel ring, spacer ring, and air distribution ring. In addition, the throat ring and top plate were the same. The inclusion of the guide vanes and turbine channel plate, which consisted of the outer channel plate, transition channel piece, and quartz disk, were the distinguishing features of the BAT configuration. The development of the guide vanes using computational fluid dynamics and velocity triangles is given in Section 3.3.1 and the design of the turbine channel plates are detailed in Section 3.3.2. The introduction of either of these components were considered part of the BAT configuration, even if there was no turbine installed. This was to evaluate the performance of the detonation chamber with the turbine channel plate with and without the turbine. Without the turbine, a nozzle was used to simulate the turning of the flow and blockage experienced as the flow passes through the guide vanes.

3.3.1 Computational Fluid Dynamic Analysis of Guide Vanes

In order to integrate a potential radial-inflow turbine to test the BAT configuration, guide vanes were necessary. Though the detonation wave travelled cyclically around the annulus, the opposing forces produced by the oblique and trailing expansion shocks resulted in a primarily radial flow. This was confirmed in an optically clear annular RDE tested by Andrus [33] who concluded that an RDE operates as a

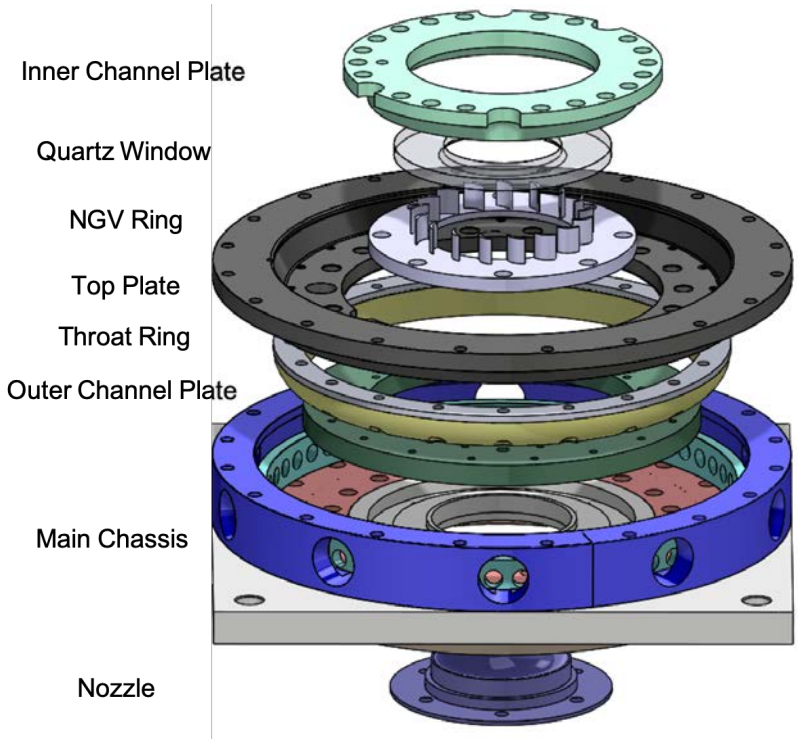

Figure 45. Exploded view of main components within RRDE in BAT configuration.

low-swirl combustor as the flow travels from the detonation event to the exit plane. Due to the lack of swirl, guide vanes can be used as a tool to turn the flow before it enters the turbine so that it can operate efficiently, as described in Section 2.3.1. A computational fluid dynamic (CFD) analysis was conducted to design a set of guide vanes for a selected radial-inflow turbine.

A radial-inflow turbine (RIT) was desired to increase the compactness of the RRDE as a Bleed Air turbine (BAT) device, as discussed in Section 2.3.2. The RIT selected by Huff [5] in his original study was part of the Garrett GTX3582R turbocharger, shown in Figure 46 along side its compressor and turbine maps. The second generation of this model was considered for this research and had a slightly different compressor operating map but with the same dimensions that were used to design the first, constant area geometry RRDE. This turbocharger provided a commercial off-the-shelf solution that allowed for a high mass flow rate in a relatively

small size, balancing higher performance with the desired compactness. The compressor map given in Figure 46b provides the surge line, choked flow conditions, and design conditions to achieve maximum efficiency. The choked condition for the turbine, indicated in Figure 46c at the point where the corrected mass flow rate does not increase with increasing pressure ratio, occurs at a pressure ratio of over 2.5. Using these maps and results while operating the stand-alone combustor configuration, the guide vanes were designed to achieve speed above 100 kRPM since the RRDE has detonative operability at corrected air flow rates and pressure ratios within this region for the constant height geometry and in previous BAT configuration testing as shown by Huff et al. [4]. While a higher efficiency would be observed around 100 kRPM, the RRDE required higher overall mass flow rates than the RIT. Therefore, the realistic design goal included higher rotational speeds reaching 130 kRPM.

Previously, three guide vanes were designed with the use of TurbAero. The turbine design program was developed based on the aerodynamic principals and analysis tools described by Aungier [20] and discussed in Section 2.3.1. To design the guide vanes, input conditions were required which were estimated based on the NASA CEA program. This computational tool was used to provide Chapman-Jouguet detonation parameters by calculating chemical equilibrium product concentrations and their associated thermodynamic properties, for hydrogen and air. Using these reactants at an equivalence ratio of $\Phi = 1.0$ provided a burned gas temperature of 2965 K, assuming input conditions of 300 K and 137 kPa based on previous data from stand-alone combustor tests at 75 $\frac{kg}{m^2 s}$. However, these thermodynamic properties are assumed to relax to a certain magnitude due to the expansion from the detonation event in the combustor section. Furthermore, the physical phenomena experienced by the experimental RRDE, such as incomplete combustion and secondary burning [16], leads to temperature and pressure values lower than the outputs from CEA. The burned gas

(a)

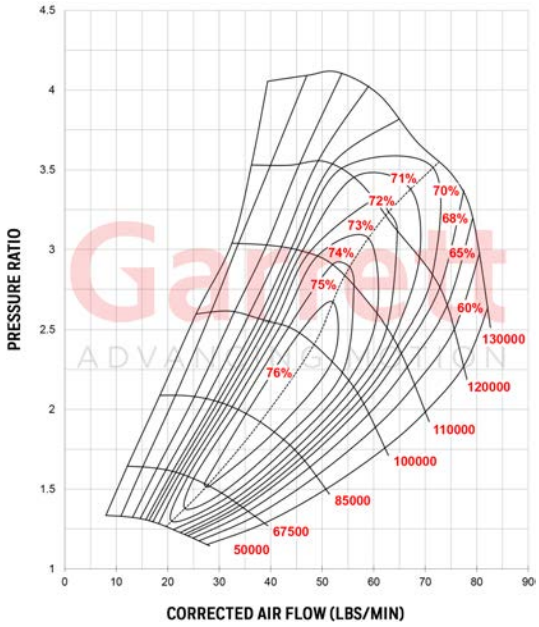

(b)

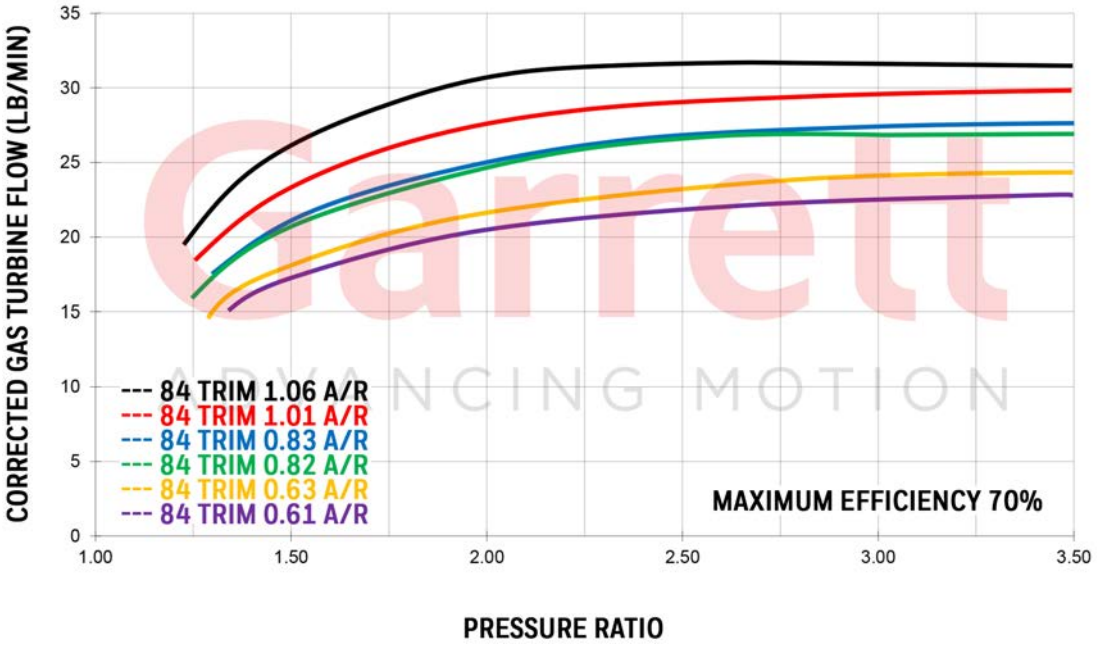

(c)

Figure 46. Garrett GTX3582R Gen II Turbocharger selected for design of RRDE in BAT configuration with (a) disassembled turbine [5], (b) compressor map, and (c) turbine map. Operating maps of GTX3582R Gen II retrieved from manufacturer website 08 November 2019 [34].

temperature was assumed to be 1400 K to match the design conditions used by Huff [5].

These three guide vanes were tested by Huff [5] with varying exit flow angles given in Figure 23 in Section 2.3.2. Of the three guide vanes tested, the 32° turning angle vane set led to the highest specific power from the turbine. However, all three guide vanes did not match the design turbine tip speed at three flow cases of 50 $\frac{kg}{m^2 s}$, 75 $\frac{kg}{m^2 s}$, and 100 $\frac{kg}{m^2 s}$, suggesting that the turbine was not receiving the necessary flow angle [5]. Furthermore, when examining the turbines operating map by Huff et al. [4], the tested points provide a choke point at a critical pressure ratio of 1.83, over 10% less than its design operating map provided by the manufacturer [4] given in Figure 46c. It was recommended in that study that the effects of the guide vane geometry, solidity, and angle be examined to attempt to match expected turbine performance.

Therefore, another set of guide vanes were designed for the design condition of 130 kRPM with a mass flux of 75 $\frac{kg}{m^2 s}$ by examining the desired flow angle necessary for the rotor of the selected RIT. Using the velocity triangles provided in Section 2.3.1, the necessary flow angle was calculated by the following equation:

$$\alpha = \arctan(\frac{U}{C_x} + \tan(\beta)), \tag{14}$$

where α is the flow angle relative to the tangent line, U is the rotor tip speed, β is the inlet blade angle, and C_x is the absolute meridional velocity, which is equivalent to the radial velocity for the RIT. The blade angle was examined to be zero so that the flow angle was only a function of the rotor tip speed and the meridional velocity. The rotor tip velocity (U) was calculated to be approximately 460 m/s based on the inducer radius of the turbine $r_{turb} = 34$ mm and the design operating rotational speed

of the turbine $\omega = 130$ kRPM $= 13,614$ rad/s, so that

$$U = \omega r_{turb}. \tag{15}$$

Because the meridional velocity is not a function of the rotors geometry and could not be accurately calculated using continuity at given mass fluxes, the guide vanes, and the resulting flow velocities and angles, were iteratively designed based on a computational fluid dynamics (CFD) analysis. The goal of using CFD was to converge the measured metal angles of the vanes to match the calculated flow angle using Equation 14. Therefore, only a non-reactive study was conducted. While the effects of the detonation wave past the combustor section and possibly into the guide vanes were not examined, the CFD analysis was able to provide a guide vane geometry solution with high-confidence of determining whether the velocity conditions were matched to the rotor.

Pointwise was used to develop a 2D unstructured mesh for a set of guide vanes, with an example mesh shown in Figure 47. The 2D approximation was used since the channel plate and base plate are parallel through the guide vanes and into the turbine. Furthermore, since the detonation wave was not modelled, the expansion of the product gases through the transition piece from the combustor section was not taken into account. The upstream boundary condition was set as a mass flow inlet with the downstream boundary condition set as a pressure outlet. The domain was determined to provide sufficient fully developed flow away from the near-wall boundary conditions of the airfoils.

ANSYS Fluent was implemented to examine the flowfield of the generated meshes. The pressure-based solver was used, and the Spalart-Allmaras turbulence model was used due to its robustness for aerodynamic flows, simplicity as a one-equation model, and ability to implement an Enhanced Wall Treatment for y+ insensitivity [35].

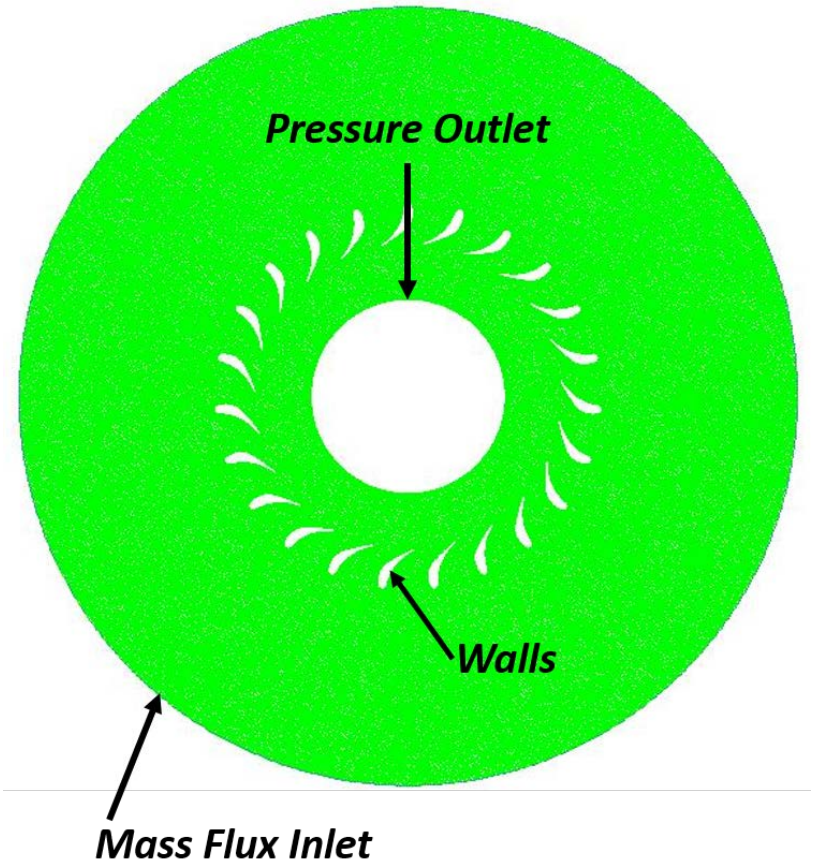

Figure 47. Unstructured 2D Mesh used for CFD analysis of guide vanes with boundary conditions labeled.

Heated air was used, with the initial temperature set to 1400 K to match the results found when designing the initial guide vanes used in the constant area geometry BAT. This temperature was updated to 1700 K after the results from the TFP were analyzed, though the CFD analysis remained relatively the same. The initial mass flux condition was set to $75\frac{kg}{m^2 s}$ due to the previous geometrys success for detonative operation while in BAT configuration for the mass flux. For each case, 5,000 iterations were run to ensure a time-averaged result.

A series of 17 different designs and cases were completed. Figure 48 provides example outputs analyzed through ANSYS Fluent. First, the angle of the flow,

relative to its centerline at a radial distance of $r_{turb} = 3.1$ cm, was measured to check whether it matched the metal turning angle which was measured from the suction side. The relative locations for these measurements are given in Figure 48a, though the absolute values were obtained from each case's raw data. If the flow did not turn fully to match the metal angle, the camber/airfoil was modified or the solidity was increased. With the increase in solidity, the Mach number was examined to ensure the flow would not exceed sonic conditions between the vanes, shown in Figure 48b. Once the solidity for a given airfoil was set, the meridional, or radial, velocity was measured at the turbine inducer radial distance of 3.1 cm.

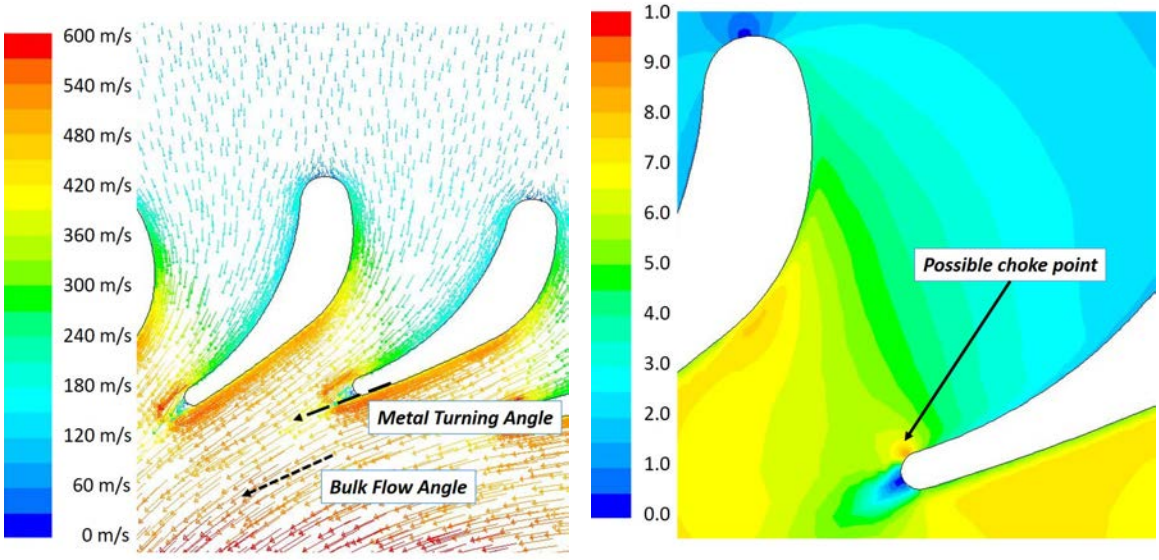

(a) (b)

Figure 48. Sample CFD results from ANSYS Fluent showing (a) velocity vectors and (b) Mach number contour for ideal gas at 1700 K.

Figure 49 shows the final design of the two guide vanes used for the BAT configuration testing. The guide vanes featured 23 and 29 blades that provided metal angles of 67° to achieve a similar flow angle. Based on the CFD simulations, the 23 and 29 blades provided flow angles of 56° and 59°, respectively. This was assumed to be within acceptable limits without increasing the vane count to choke the flow

at the guide vane exit. These designs provided meridional velocities between 490-530 m/s which matched the design condition of operating the RIT above 100 kRPM at approximately 130 and 150 kRPM for the 23 and 29 vane rings, respectively. The outer diameter of the blades matching the tip of the leading edges was set to 10.16 cm, with the inner diameter, coincident to the trailing edges, was 7.62 cm. The guide vanes' height of 13.9 mm matched the previously designed vane sets since this was constrained by the rotor's initial height. In contrast to the previous design, the guide vanes were manufactured to be attached to the base plate, rather than the channel plate, so that the guide vanes could be installed at the back end opposite the exhaust end, proving optical access to the passages between the guide vanes for thin-filament pyromtery (TFP). Furthermore, small 0.5 mm diameter holes were burned into nine vanes to install thin filaments for TFP and are detailed in the TFP experimental setup described in Section 3.3.3.

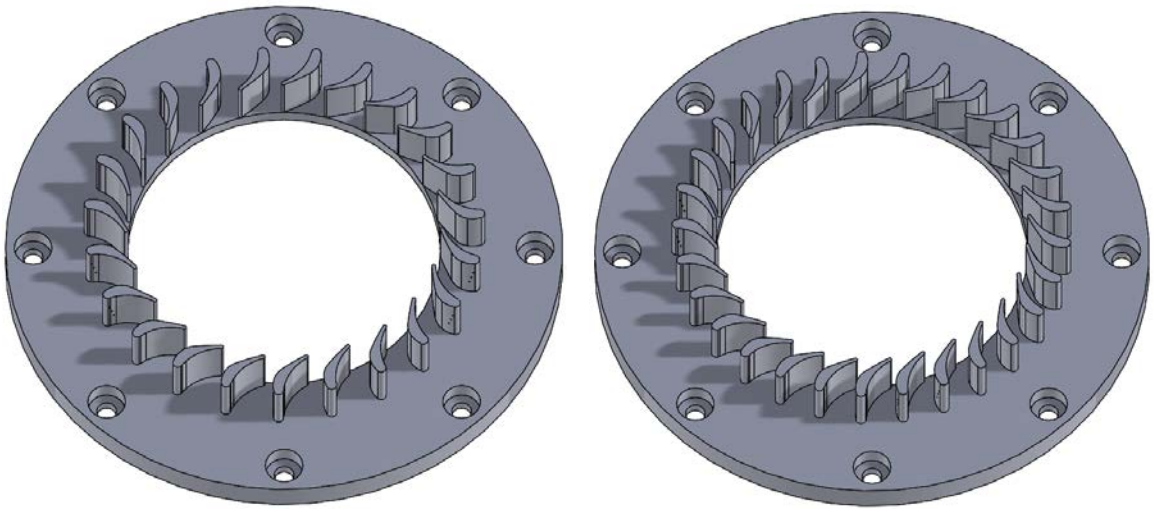

(a) (b)

Figure 49. Guide vane rings featuring (a) 23 and (29) blades with metal angles of 67°.

3.3.2 Turbine Channel Plate Design

The turbine channel plates were designed to accommodate the guide vanes while maintaining detonation confinement. To do so, a modular channel plate design was implemented, shown in Figure 50. Design considerations included allowing for a combustion section that would enable detonation confinement, transition sections designed to avoid separation while the channel height expanded to match the guide vane height, implementation of pressure instrumentation, optical access to the guide vanes, and ease of access to the guide vanes during testing. These design objectives will be discussed further throughout the section as the individual components are detailed. The final design consisted of one outer channel plate, three transition channel pieces, and one quartz disk. The design allowed for the testing of three channel heights of 10 mm, 6.5 mm, and 4.5 mm. The upper channel height limit was constrained as the thinnest channel plate able to be manufactured while still allowing for pressure instrumentation. The smallest channel height was set to match the smallest channel height tested in the combustor-only configuration. All three channel heights still required a transition from the combustion section to the guide vanes since a channel plate allowing for a 13.9 mm channel height would be too thin to test in this modular configuration.

An outer channel plate, shown in Figure 51, was used that featured a flat surface with the ability to be shimmed to the three desired channel heights of 10 mm, 6.5 mm, and 4.5 mm. The outer diameter was set by the top plate constraint and matched the combustor-only configuration's channel plate with an outer diameter of 20.96 cm. The outer set of tapped holes matched those of the combustor-only channel plate as well so that it could be attached to the top plate. The inner diameter of the outer plate was determined by the location of the detonation wave during testing in the stand-alone combustor configuration. It was set at 14.48 cm to attempt the same

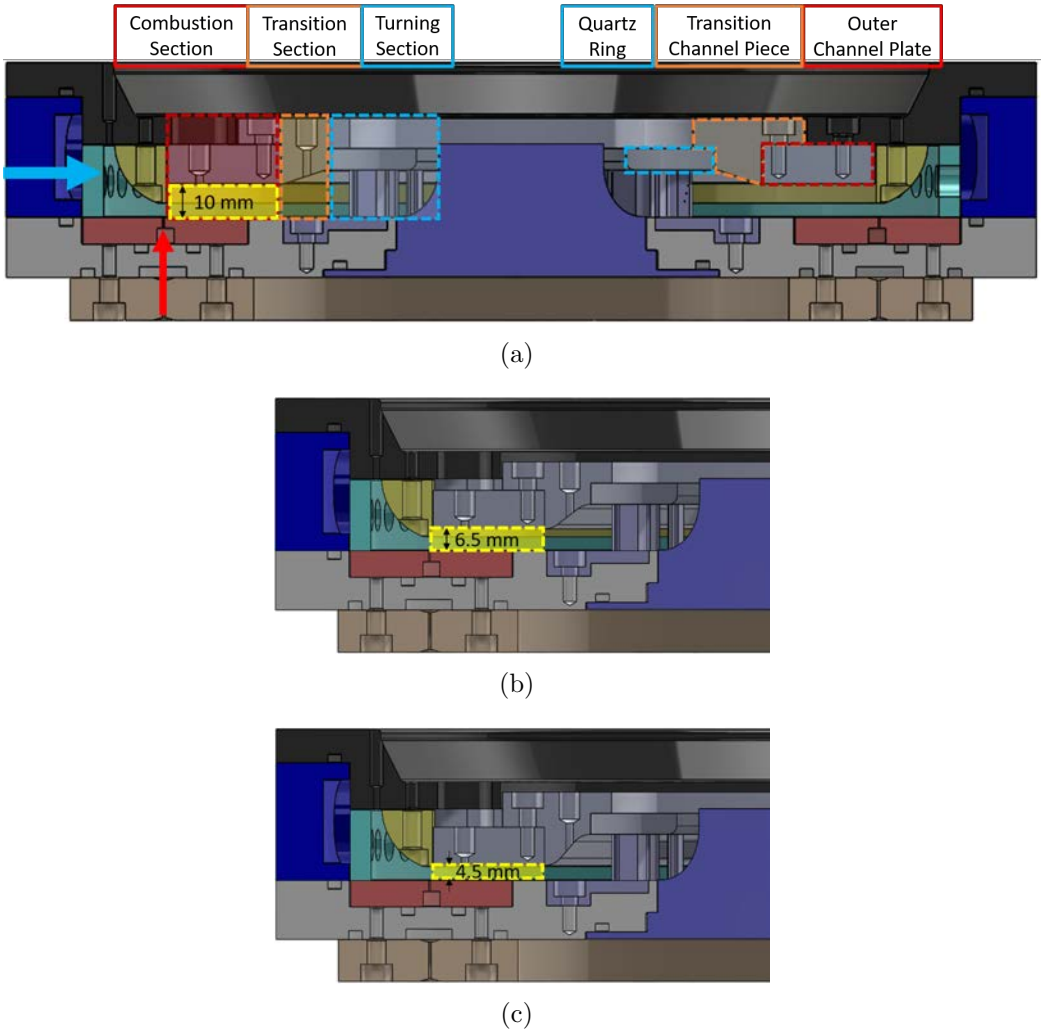

Figure 50. Cross-section view of RRDE in BAT configuration showcasing the combustor, transition, and turning sections and three components of turbine channel plate creating (a) 10 mm, (b) 6.5 mm, and (c) 4.5 mm channel heights.

confinement seen during the stand-alone combustor configuration around the 10.1 cm radial location but large enough to not have a strong expansion from the end of the detonation chamber to the leading edges of the guide vanes that would lead to separation. Furthermore, the inner diameter allowed enough spacing for the inner set of tapped holes where the transition channel pieces attached. Four $1/16''$ NPT were used to allow for two CTAP measurements set at the same first two CTAP locations in the combustor-only configuration, and it provided two ITP measurements that were 45° apart. The radial location of the two ITP ports, set 9.5 cm from the centerline to

match P_1, were farther outboard than on the combustor-only configuration to allow space for the transition pieces. A through hole was also machined to provide a port for the pre-detonator tubing.

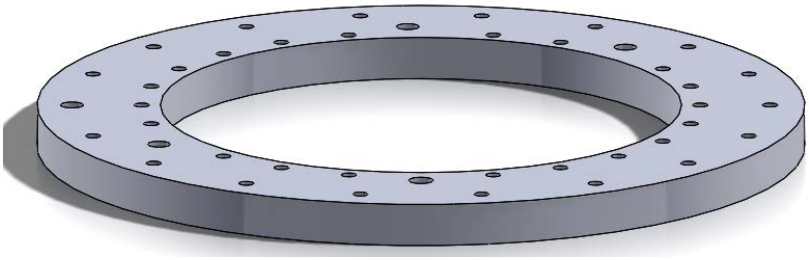

Figure 51. Outer channel plate used for the BAT configuration.

Three transition channel pieces, shown in Figure 52, were created to provide a transition from the smaller channel heights of the combustion section to the 13.9 mm channel height dictated by the guide vanes and the RIT. The slopes of the transition were held constant to maintain a constant change in area across the decreasing radial distance. The interfaces at the lower and upper sections were rounded with a radius selected based on ease of machining and to discourage immediate separation. On the lower contact section, the outer diameter was set by the 14.48 cm inner diameter of the outer channel plate. The step on the outer diameter allowed for enough space to use screws to attach to the outer plate while extending the contact section with the outer plate to avoid a high moment that could remove the transition piece during operation. The inner diameter was set by the desired optical view of the guide vanes whose leading edges were on a diameter of 10.16 cm. To provide enough of a step to securely hold a quartz piece, the inner diameter of the lower contact section was set to 11.43 cm. Four cut outs were created to provide space for the fitting of the two CTAP and two ITP ports on the outer channel plate. One $1/16''$ NPT tap was used to provide one CTAP measurement in the transition section of the channel.

The quartz disk, highlighted in the cross-section given in Figure 50 and shown

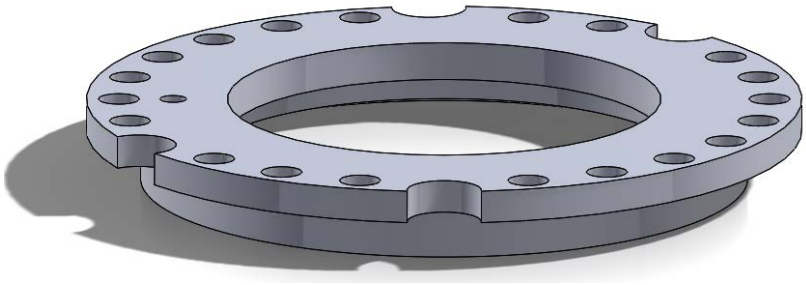

Figure 52. Transition channel piece used for the BAT configuration.

installed in Figure 53, was chosen to be quartz due to its optical clarity and resistance to heat compared to polycarbonate. It also met cost constraints since it was designed with no taps and limited curvature. Furthermore, there was less concern for the high vibrations since it was assumed the detonation wave would not be operating along the guide vanes. The outer diameter of 10.16 cm was set by the transition piece, while the inner diameter matched the inner diameter of the combustor-only channel plate at 6.22 cm. The quartz disk was constrained by the guide vanes and was also sealed to the inner transition piece with high-temperature room-temperature-vulcanizing (RTV) silicone, shown in Figure 53b. While the sealant was rated under the expected temperatures above 1000 K past the transition piece, the relatively short operation time of less than two seconds and two minute cool off period was assumed to allow functionality of limiting vibration of the quartz while providing a secondary constraint.

3.3.3 Thin-Filament Pyrometry Setup

Measuring the temperature of the flow, in conjunction to the pressures obtained through CTAPs and ITPS, can help characterize the flowfield with an RDE. Traditionally, thermocouples are used to measure the temperature, but probing measurement devices such as those create flow perturbations, provide temperature data at only one

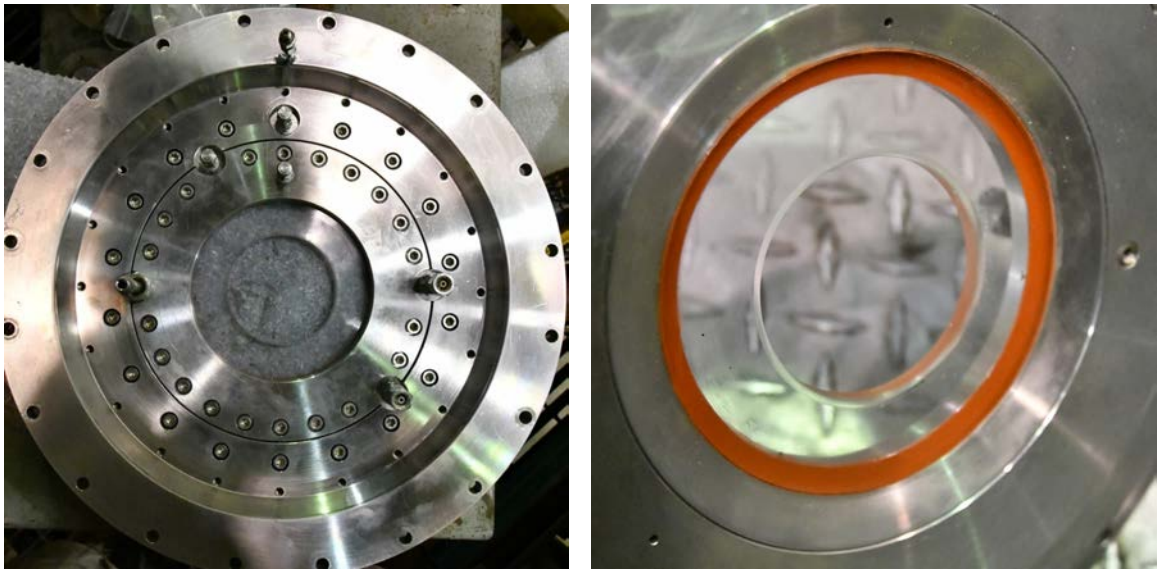

(a) (b)

Figure 53. Turbine channel plate (a) front view and (b) back view showing quartz disk sealed with high-temperature RTV sealant.

spatial location, and have limited survivability to extreme conditions such as those generated from the RRDE. Therefore, the thin-filament pyrometry (TFP) technique, as discussed in Section 2.4.3, was implemented as a non-intrusive technique to measure the temperature. TFP was attempted to provide temperature data at high rates. The current research did not attempt to measure the temperature in the combustion region due to concerns for the survivability of the filaments in close proximity to the detonation wave. However, TFP was implemented at the guide vanes to provide the temperature measurement of the product gases leaving the detonation chamber of the RRDE in BAT configuration.

The filaments used were nominally of 150 μm diameter and were made of β-SiC. This diameter filament was selected over the smaller 15 μm diameter filaments characterized by the initial TFP investigation by Vilimpoc et al. [28] to allow the filaments to not break until operation, such as during initial cold flow to the device and the initiation of the pre-detonator device. The larger diameter was also selected

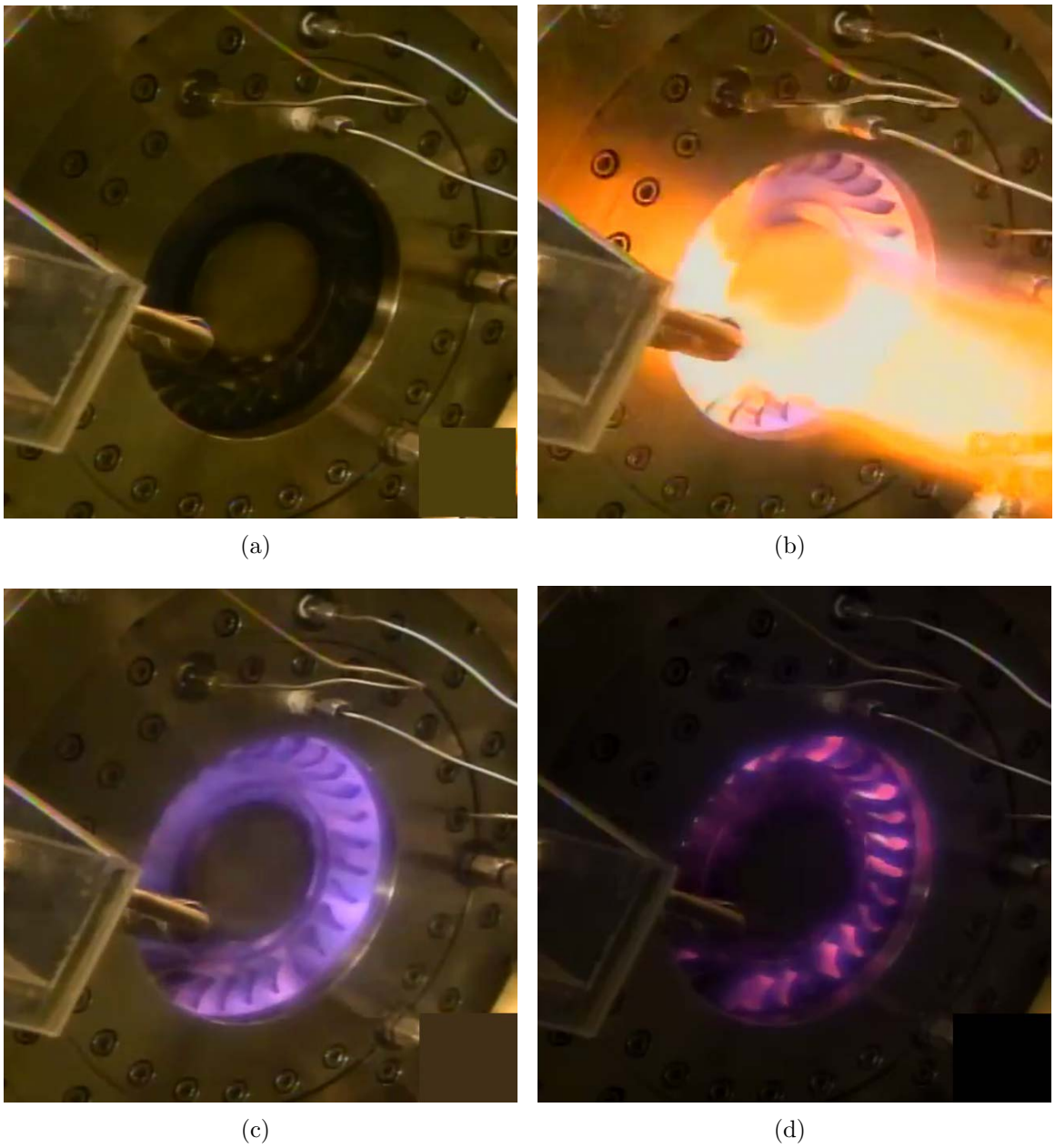

(a) (b)

(c) (d)

Figure 54. Operation of RRDE in BAT configuration during (a) cold flow, (b) initiation, (c) operation, and (d) shut-off.

to increase survivability during operation, though a larger filament was not used to maintain the nearly instantaneous response a thin filament would have to the temperature of the flow.

The guide vanes were selected as an ideal location to implement TFP since the

temperature of the flow at this location is important to know to characterize the performance of the turbine. Furthermore, the vanes provided an area to hold the filaments perpendicular to the flow and were designed to be easily removed so that the filaments could be replaced if they broke. The filaments installed in the guide vanes are shown in Figure 55. The guide vanes contained 600 μm diameter holes through the vanes that were drilled using electrical discharge machining so that the filaments could be placed through them. Each guide vane ring contained nine filament locations, with three filaments located between a single vane passage so that three different vane passages could be instrumented. While only one passage would be measured at a given time, instrumenting three different passages provided an opportunity to quickly measure a different passage if the filaments in one passage were to break. Furthermore, the larger diameter holes in the vanes allowed for multiple filaments to be used in one location if the survivability of the filaments needed to be improved. Initially, the filaments were adhered within the holes in the guide vanes using a high-temperature ceramic adhesive [36], shown in Figure 55a. However, after testing the filaments without the adhesive, the filaments were installed through the holes with using the adhesive, shown in Figure 55b, since its survivability was not affected.

To correlate the emissions from the filament to a temperature, a calibration of the equipment was performed. A tungsten bulb was selected for the calibration due to tungsten's known color temperature as a function of a given current and voltage. This relationship was confirmed using a MicroTherm optical pyrometer. After characterizing the tungsten bulb, it was setup up within the RRDE in BAT configuration at the same radial location of the guide vanes. Maintaining a similar location as the guide vanes, as well as installing the bulb behind the quartz disk, ensured that the calibration would measure the same losses as seen during testing.

The same high-speed camera and lens used for flowfield visualization in the stand-

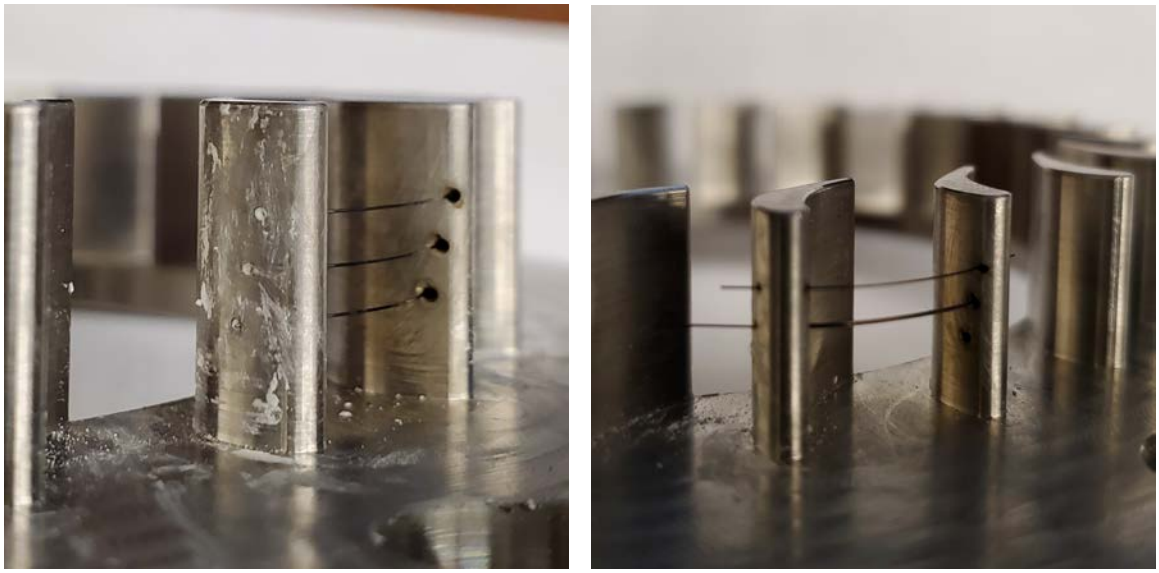

(a) (b)

Figure 55. Guide vanes with filaments attached (a) using ceramic adhesive and (b) without adhesives.

alone configuration was implemented for TFP in BAT configuration. The camera setup as used for the calibration is shown in Figure 56. The Phantom v711 was used with a focal length of 200 mm on the zoom lens to provide a close view into the vane passage, with a close focus adaptor so the filaments were in focus. The calibration, and subsequent testing, used the high-speeed camera with a resolution of 640x640 pixels, a frame rate of 22,000 frames per second, and a 0.5 μs exposure. The tungsten bulb was tested at twelve temperatures from 1713 K to 2194 K, with the calibration resulting in a linear relationship between the luminosity and the temperature within this range. Further calibration procedures are given in Appendix A. The final installation of the guide vanes into the device is shown in Figure 57 with the relative resolution used during testing represented by the focused image of the vanes.

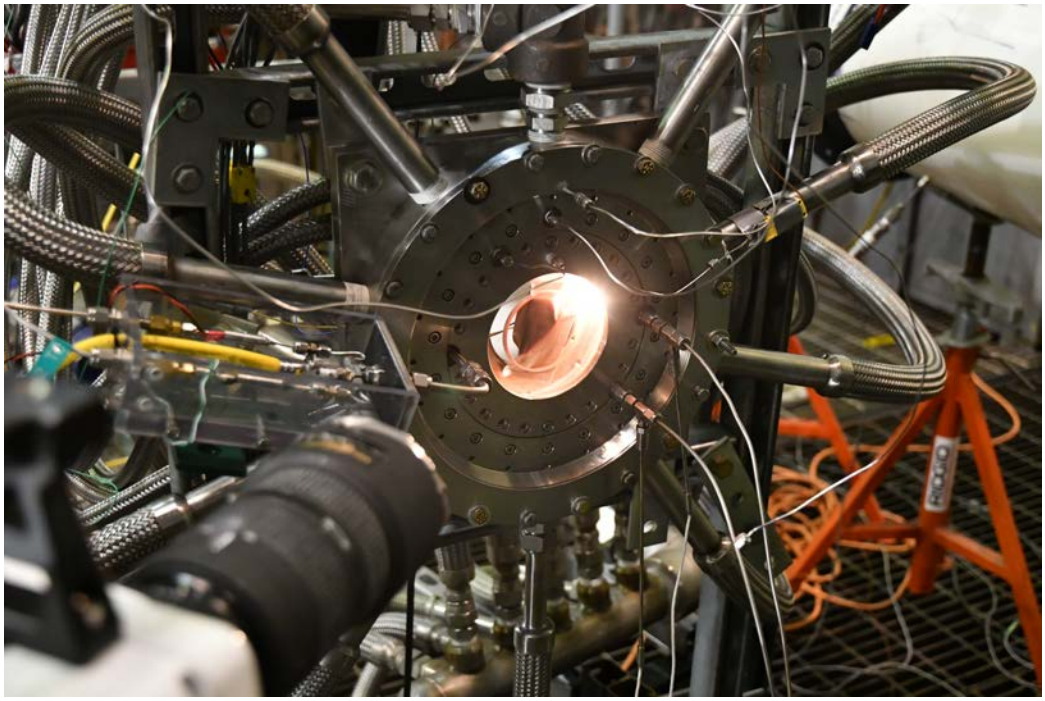

Figure 56. High-speed camera setup for calibration of TFP.

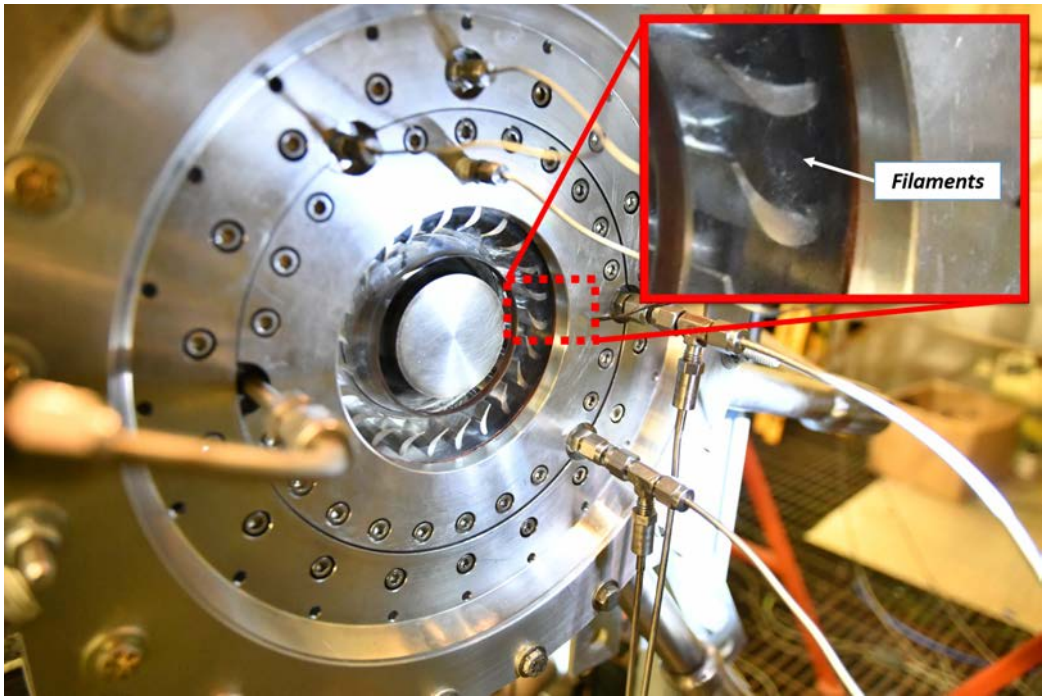

Figure 57. Guide vanes installed in RRDE from point-of-view of Phantom camera.

IV. Results and Discussion

To demonstrate the suitability of using a flat channel plate to provide detonation confinement and improve performance, the constant height geometry in the stand-alone combustor configuration was compared to the constant area geometry through operability and performance given in Section 4.1. Sections 4.2-4.4 provides a comparison of the different configurations of the constant height geometry to determine a channel height, throat area ratio, and nozzle area ratio that provided the highest performance as measured through the pressure of its device, as well as the most consistent operation. The modal operability observed through the polycarbonate channel plate is given in Section 4.5. Section 4.6 discusses the operability and performance of the constant height geometry RRDE in BAT configuration, with the inclusion of the guide vanes and analysis of TFP results to determine detonability of the RRDE with the guide vanes and the effects of detonation wave fluctuations on the temperature of the output flowfield.

The primary objective of the investigation was to confine the detonation wave outboard within the RRDE. Therefore, before analyzing the operability and performance, successful detonation confinement was examined for the constant height detonation chamber. To do so, the pressure amplitudes measured at the five pressure ports at CTAP 1 - CTAP 5, shown in Figure 39, were examined. An example of these pressure traces are given in Figure 58, reflecting the typical test procedures for the RRDE as well as the relative magnitude of each pressure measurement to each other. The highest pressure trace of the five locations approximately located the detonation wave since the detonation would produce the highest pressure region.

For successful detonations, most cases using the flat channel plate followed a similar trend given in Figure 58 in that CTAP 1 had the highest pressure value during operation, with some cases having CTAP 2 equivalent or higher than CTAP 1. How-

ever, no cases of the constant height geometry had its highest pressure measurement inboard of CTAP 3. Therefore, it was concluded that the detonation event was confined to the outer radial location over the range of flow conditions, channel heights, throat area ratios, and nozzle area ratios.

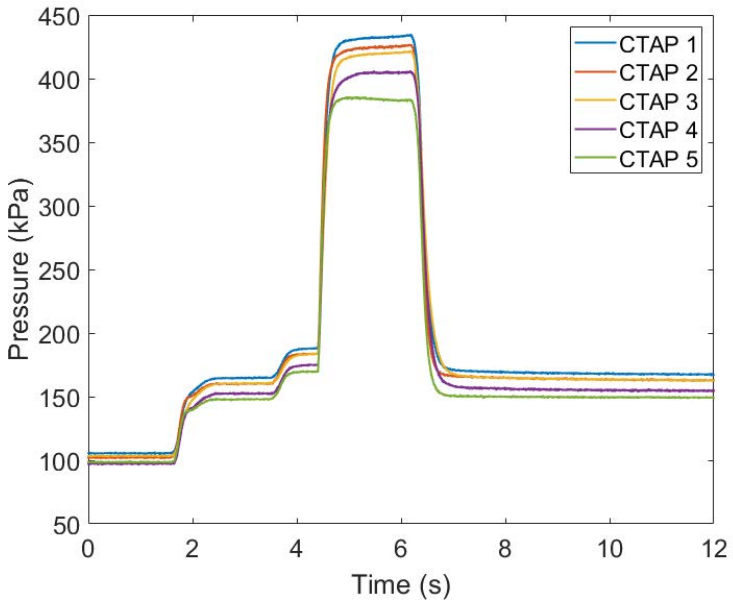

Figure 58. Sample CTAP measurements demonstrating confinement (h_c = 6.5 mm, $AR_t = 0.50$, $AR_n = 0.76$, $\dot{m}'' = 100\frac{kg}{m^2 s}$, $\Phi = 0.70$).

Across 253 constant height tests in the stand-alone combustor configuration, 89% of detonating tests ended with CTAP 1 having the highest pressure measurement before shut-off, with 11% of tests having a highest pressure measurement at CTAP 2 and no cases having a maximum value at CTAP 3 - CTAP 5. This was seen at varying channel heights, throat area ratios, and nozzle area ratios and at mass fluxes between $50\frac{kg}{m^2 s}$ and $200\frac{kg}{m^2 s}$ and equivalence ratios between 0.5 and 1.0. For the constant area geometry, the highest pressure measurement varied for different test conditions. Data was retrieved from Huff [5] for all cases of the constant area geometry at h_c = 4.5 mm that was tested at mass fluxes between $50\frac{kg}{m^2 s}$ and $200\frac{kg}{m^2 s}$ and equivalence ratios between 0.50 and 1.0. Nozzle area ratios of 0.5, 0.6, 0.8, and 1.0, as well as throat area

ratios of 0.2 and 0.4, were included. Based on this data of 275 tests, the maximum pressure measurement occurred at CTAP 1 for 6% of tests, with 19% at CTAP2 , 29% at CTAP 3, 11% at CTAP 4, and 34% at CTAP 5. Tests where CTAP 1 and CTAP 2 were the highest were at mass fluxes of $75\frac{kg}{m^2s}$ or less. At higher mass fluxes, the highest pressure measurement moved inboard, with $\dot{m}'' = 200\frac{kg}{m^2s}$ having a consistent maximum pressure at CTAP 5. Therefore, detonation confinement was confirmed for all constant height cases while the RRDE operated as a stand-alone combustor.

For the initial analysis for detonation confinement, it was assumed that a static pressure increase was indicative of a confined detonation wave. To increase the confidence in confinement, the total pressure was also examined by applying Equation 11 for all CTAPs and by assuming the ratio of specific heats and Mach number for a given test condition. The constant area RRDE's trends remained the same since the relative area at each CTAP location was the same. For larger channel heights of the constant height RRDE, the calculated total pressure at CTAP 1 remained the highest of the five pressure measurements. However, for 29 cases at $h_c = 4.5$ mm, the total pressure at CTAP 5 was 2±2% larger than CTAP 1. This was within the error of the CTAP measurements and total pressure calculations, but the difference demonstrated that the higher Mach numbers within the smallest channel height affected the distinction in the pressures throughout the detonation chamber created by the confined detonation wave. The level total pressures throughout the detonation chamber also suggest that the apparent three wave modes seen for $h_c = 4.5$ mm could be indicative of acoustic modes as well, as discussed in Section 4.1.1. These acoustic mode could also contribute to the similar total pressures in the chamber. However, it was assumed that the detonation wave was confined for all constant height cases based on the static pressure measurements.

4.1 Detonation Chamber Geometry Comparison

With detonation confinement confirmed using the flat channel plate, this study further examined the operability and performance of the constant height geometry RRDE as compared to the previously tested constant area geometry RRDE. For the constant area geometry, as tested by Huff et al. [3], results that were tested with $h_c = 4.5$ mm were used for the comparison since this was the most prevalently tested channel height. Since the channel height for the constant area was varied radially to maintain a constant area of 2993 mm^2, this 4.5 mm channel height was measured at the outermost radial location. Channel heights of $h_c = 4.5$ mm and $h_c = 5.5$ mm with the constant height geometry were used for the comparison.

Figure 59 shows the area variation for the stand-alone combustor for the constant area geometry tested previously, as well as the current research constant height geometry channel heights tested. The combustion section was considered the areas between 105 mm and 37 mm from the centerline where the flow travelled radially inward. While channel heights of 4.5 mm for the constant area and constant height geometries started at the same effective area of 2,990 mm^2 aft of the throat, the constant height geometry converged immediately as the flow traveled radially inboard, creating a 65% decrease in volume within the chamber from the outer radius of the channel plate to 37 mm from the centerline before the nozzle turned the flow. Due to the much smaller area created by the constant height 4.5 mm channel height, a larger channel height was desired to compare to the constant area geometry. It was determined that for the constant height geometry, the detonation propagated between 82-105 mm from the centerline between CTAPs 1 and 2. Therefore, when considering the area where the detonation occurred, a constant height of $h_c = 5.5$ mm, rather than $h_c = 4.5$ mm, provided a similar detonation area of 3,250$\pm$380 mm^2 to the constant area configuration with a channel height of 4.5 mm at the expected radial

location of the detonation. The turning section started at 37 mm from the centerline for all geometries when the flow met the nozzle and transitioned from the radial to axial direction.

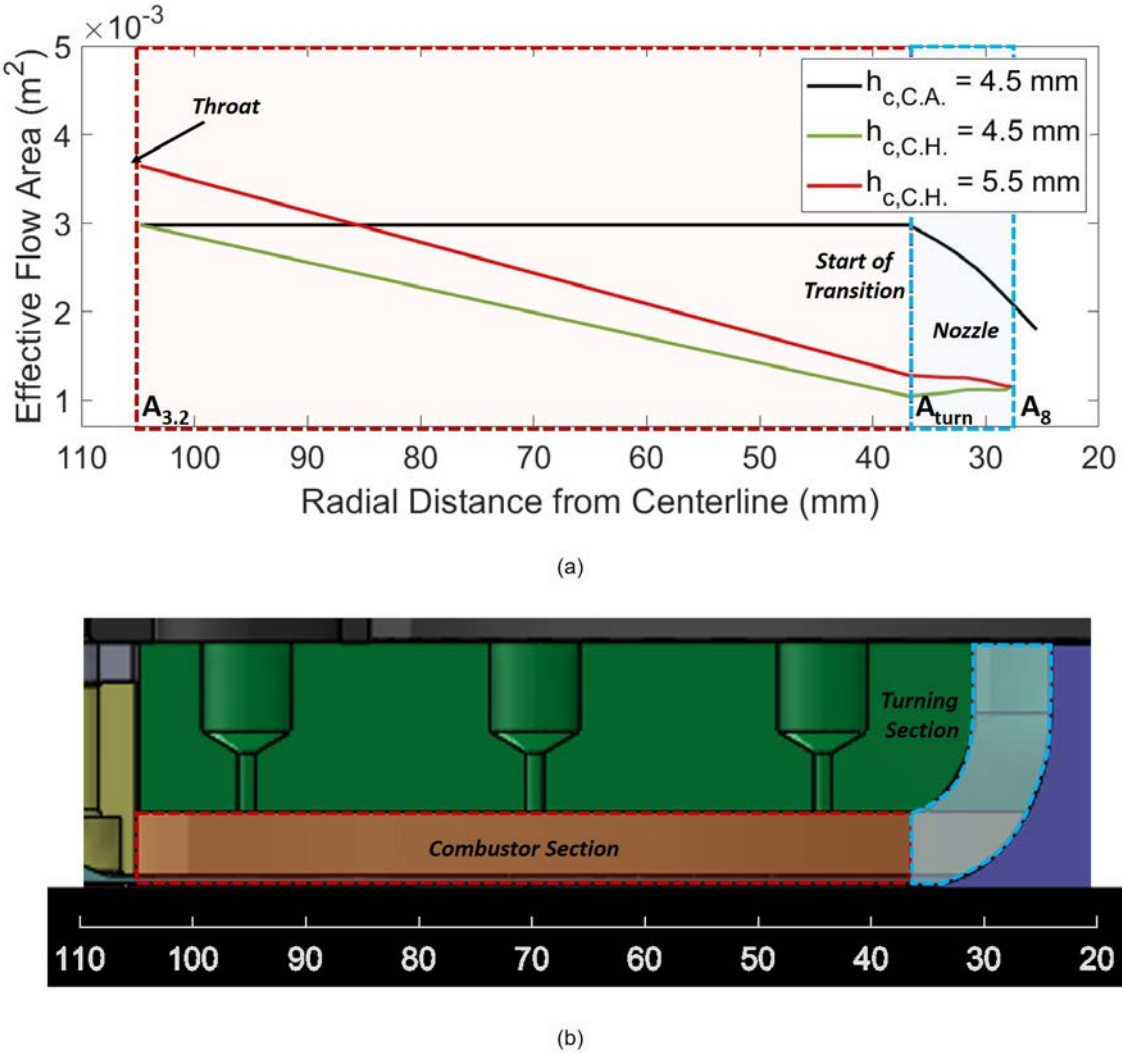

Figure 59. Effective area within detonation chamber for (a) constant area and constant height stand-alone combustor geometries with (b) sample cross-section of stand-alone combustor configuration.

For all tests in this comparison, a throat area ratio of $AR_t = 0.20$ and a converging nozzle were used. The nozzle area ratio for the constant area geometry was $AR_n = 0.60$. This set of data provided by Huff et al. [3] was selected since this nozzle area

ratio provided the high performance and was widely used for other investigations by Huff et al. [30] and Boller et al. [6]. For the constant height geometry, a different nozzle was used, with a exit diameter of 4.88 cm, to attempt a continuously converging area from the detonation chamber inlet to the exit. The nozzle was selected since it had the largest radius of the nozzles manufactured by Huff [30] when the constant area RRDE was initially investigated. The largest nozzle was necessary since the effective area decreases radially inward for the constant height geometry, as seen in Figure 59, and the nozzle used for the constant area geometry would not have provided an effective converging area.

While the same nozzle was used for the comparison of the constant height geometries in this section, that nozzle provided a different area variation for the different channel heights as the flow was turned from its initial radial inward direction to its exhaust. Despite being the largest nozzle available, the nozzle did not provide a converging section, as the flow turned, for the smallest constant channel height tested of $h_c = 4.5$ mm. The nozzle for $h_c = 4.5$ mm provided a nozzle area ratio, as defined by the ratio of the area before the flow turned to the effective area at the exit plane, of $AR_n = 1.1$. However, the area ratio from the inlet to outlet of the combustor provided overall convergence of $\frac{A_8}{A_{3.2}} = 0.39$. For this area ratio, A_8 represents the exit plane area and $A_{3.2}$ is the area immediately aft of the throat. While this overall area ratio can be used to compare to data of an axial RDE published by Kaemming et al. [31], who defined their area ratio this way, it does not take into consideration the area changes throughout the combustor that were inherent when implementing a flat channel plate in an RRDE. The larger channel height of $h_c = 5.5$ mm had a nozzle area ratio of $AR_n = 0.90$ and an overall area ratio of $\frac{A_8}{A_{3.2}} = 0.32$.

4.1.1 Wave Mode Comparison Between Geometries

The operating modes of the RRDE while in its constant height geometry in stand-alone combustor configuration was compared to the operating modes determined by Huff [5] for the constant area geometry RRDE using the pressure signals from the ITPs positioned 45° apart on the channel plate, as detailed in Section 2.4.2. In addition, a clear channel plate was also used to confirm trends at specific operating conditions. The implementation of this clear channel plate is detailed in Section 3.2.3 with the results from the flowfield visualization given in Section 4.5.

Figures 60-62 compares the number of waves, N_D, experienced by the constant area geometry and the constant height geometry at a throat area ratio of $AR_t = 0.20$. Figure 60 provides the wave modes for the constant area, $h_c = 4.5$ mm geometry, while Figures 61 and 62 provide the wave modes for the constant height, $h_c = 4.5$ mm and $h_c = 5.5$ mm geometries, respectively. The test cases that do not provide data for the constant height geometry was not due to an inability to detonate but rather the inability for the device to receive enough hydrogen at higher equivalence ratios for higher mass fluxes due to facility flow restrictions and the sonic nozzle used.

Huff [5] found that the transition regimes from a one wave operating mode to a two wave mode for the constant area geometry, given in Figure 60, occurred as either the equivalence ratio decreased or as the mass flux increased. At equivalence ratios greater than 0.7, the device operated in a one wave mode. However, two waves existed at $\Phi = 0.7$ or lower, with three waves occurring at higher mass fluxes. At mass fluxes of $\dot{m}'' = 150\ \frac{kg}{m^2 s}$ or greater, the constant area geometry also operated in a higher wave mode.

For the constant height geometry, the same trend occurred, shown in Figures 61 and 62, but with higher wave mode numbers. The constant area geometry experienced three wave modes only at higher mass fluxes in select equivalence ratios while the

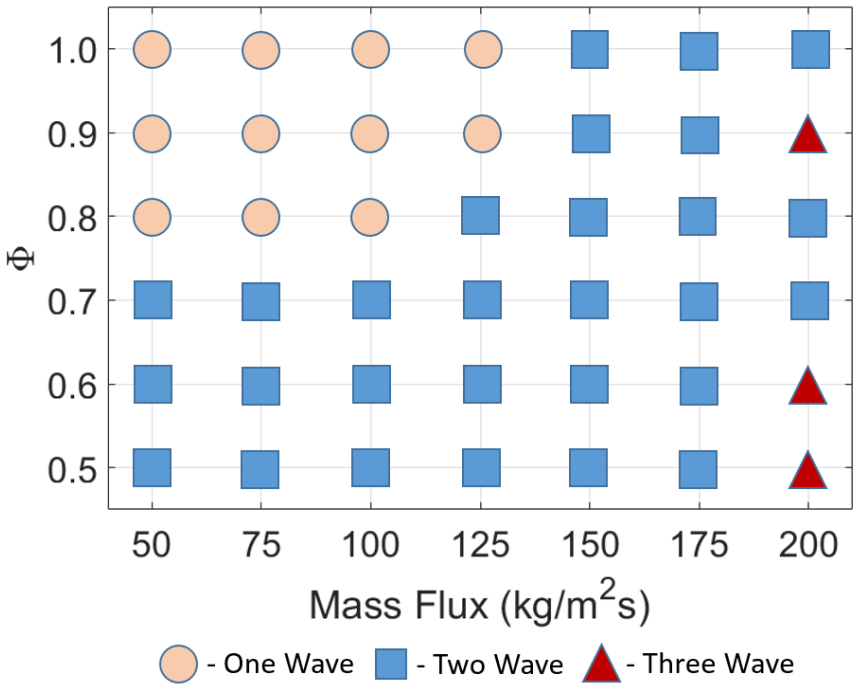

Figure 60. Number of waves, N_D, for constant area $h_c = 4.5$ mm [5] RRDE.

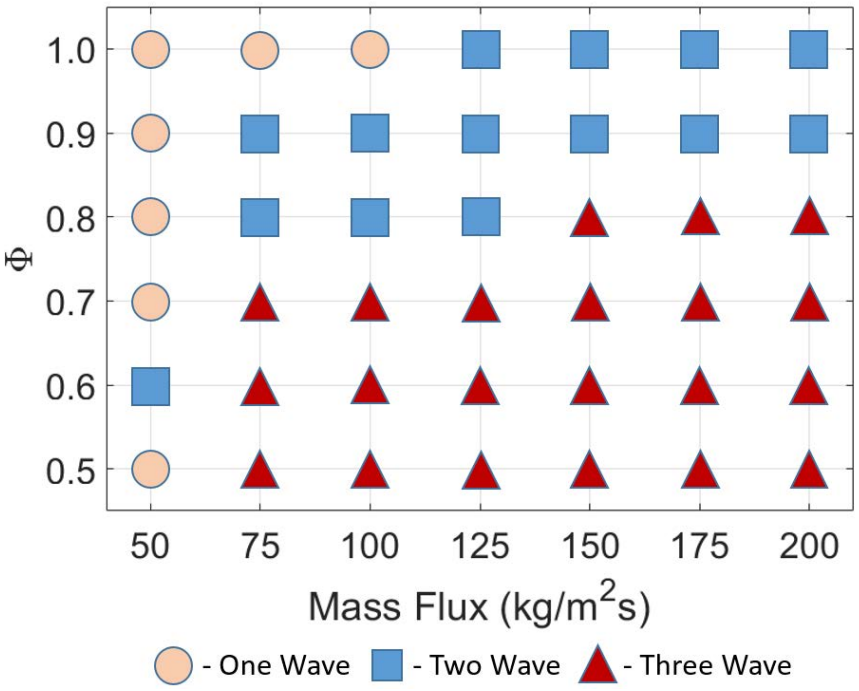

Figure 61. Number of waves, N_D, for constant height $h_c = 4.5$ mm RRDE.

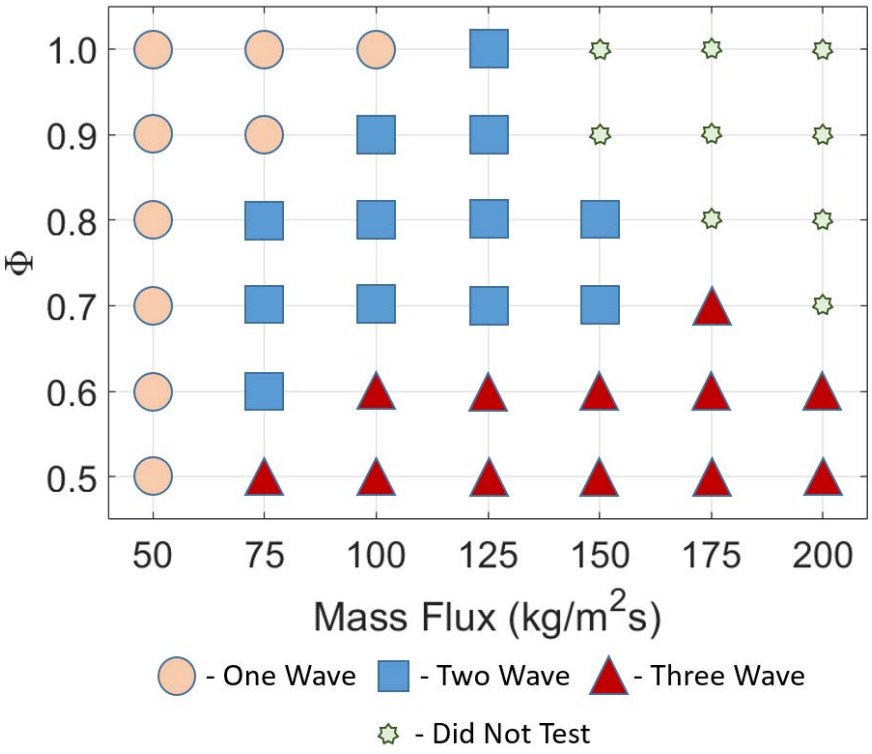

Figure 62. Number of waves, N_D, for constant height $h_c = 5.5$ mm RRDE.

constant height geometry operated at three wave modes at mass fluxes as low as $\dot{m}'' = 75\frac{kg}{m^2 s}$. While there were less test conditions leading to three wave modes for the constant height $h_c = 5.5$ mm configuration, the larger detonation chamber, as compared to the smaller constant channel height configuration, still had more cases for three wave modes than the constant area geometry. However, at $\dot{m}'' = 50\frac{kg}{m^2 s}$, the constant height $h_c = 5.5$ mm only experienced one wave modes unlike the other two configurations. The same trends across the equivalence ratios and mass fluxes existed for all configurations as more waves were likely as either the equivalence ratio decreased or the mass flux increased.

Boller et al. [6] saw that a higher wave mode promoted a detonation wave operating in the outer radial location for the constant area geometry. Despite the variety of operating modes, the constant height geometry saw detonation confinement across

all test conditions confirmed by the higher pressure traces for the outermost pressure transducer. To maintain the confinement, the RRDE transitioned to wave modes that allowed this confinement.

With the channel height constrained, the wave mode was a function of the equivalence ratio and the pressure within the detonation chamber. For the RRDE, when the equivalence ratio decreased, the number of waves increased. This trend is contrary to axial RDE tests and expectations of a smaller cell size (and greater possibility of more waves) as the equivalence ratio approaches stoichiometric conditions [37]. Huff [5] suggested that for the constant area geometry, an increase in the number of waves was a result of a lower wavespeed due to lower equivalence ratios and radially outboard waves.

However, with detonation confinement seen in the constant height geometry, wavespeed was assumed to have negligible change with equivalence ratio. Therefore, this trend could suggest that the frequencies observed above the one wave mode condition could be transitions to an unstable acoustic mode close to the assumed three wave mode. Ideally, flowfield visualization using a clear channel plate would provide insight into these trends, but complications as discussed in Section 4.5 prevented confirmation for the current research. Further flowfield visualization investigations are required to provide higher certainty of the two and three wave modes and confirm the trends across equivalence ratio.

The pressure within the detonation chamber also affected the wave mode. This pressure in the chamber was determined primarily by the mass flux, as well as the pressure increase that occurred during operation. Higher mass fluxes led to higher pressures aft of the detonation's radial location and created an environment to further confine the detonation event. This can be seen by the higher wave mode trend as mass flux increased for a given equivalence ratio in Figures 60-62.

Furthermore, the increase in pressure during operation for some cases also led to higher pressures aft of the detonation's location that led to a wave mode increase during operation. For most cases, the three wave mode occurred during unsteady operation. The device was determined to be at an unsteady or steady-state condition depending on the change in the plenum pressure with time during operation. ITP results from a 4.5 mm test at $\dot{m}'' = 100\frac{kg}{m^2 s}$ and $\Phi = 0.8$ is given in Figure 63a, which accompanies the CTAP measurements given in Figure 63b. The pressures both within the plenum and detonation chamber continuously increased until a mode shift or operation ended. The continuously rising pressures and unsteadiness were most likely due to the shorter fill heights for each detonation wave. While a given detonation wave has a slower velocity as the wave number increases, the higher frequency of the detonation does not allow enough time for a full fill height. The lower refresh rate and higher frequency back pressures the plenum continuously as it attempts to reach its steady state condition before shut-off.

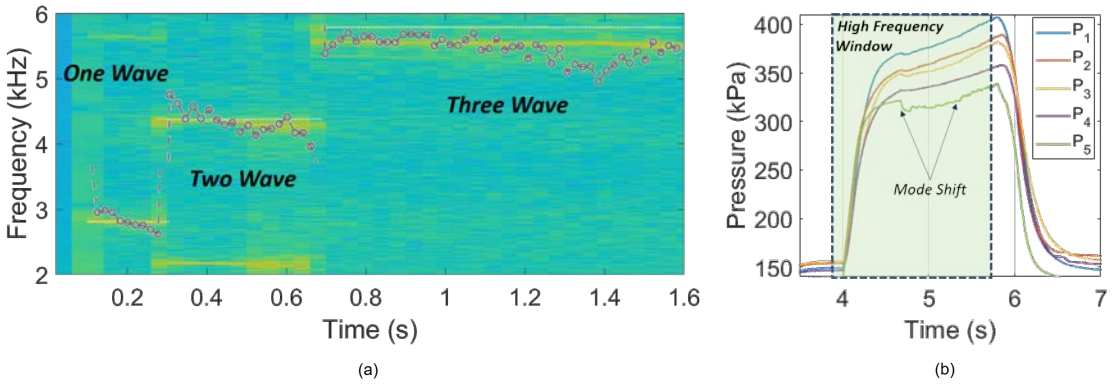

Figure 63. Example (a) spectrogram with cross-correlation relative values from ITPs showing changing wave modes and (b) CTAP increase during test run for $h_c = 4.5$ mm at $\dot{m}'' = 100\frac{kg}{m^2 s}$ and $\Phi = 0.8$.

Since it was shown that detonation confinement occurred for all cases of the constant height geometry, this confinement was independent of the wave number in contrast to the constant area geometry. Therefore, when configuring the constant height

geometry, it is more beneficial to operate at lower wave modes due to the unsteadiness and potential acoustic modes at the assumed three wave mode. Between the 4.5 mm and 5.5 mm channel heights, the larger channel height provided less three wave modes. This provided motivation to explore a larger channel height of 6.5 mm to attempt consistent one wave modes, which will be given in Section 4.2.

4.1.2 Pressure Performance Comparison Between Geometries

In this section, the pressure performance is provided to characterize the potential for pressure-gain for a given configuration. The values for P_{plenum} and P_5 for the calculations were obtained as the final measurements before fuel shut-off and is consistent with the analysis from AIAA 2020-0200 [38]. As discussed in Section 3.2.1, it is important to note the uncertainty provided in the CTAP measurements which influenced the calculated pressure difference, ΔP, between the plenum and the area closest to the nozzle. While this uncertainty was not quantified for this investigation, the method remained consistent across all test conditions to provide comparable, rather than absolute, values.

Table 2 provides the change in normalized pressure from P_{plenum} to P_5 as defined by dP_{inj} through Equation 10. Similarly to the wave mode comparisons conducted between the two geometries, the constant area geometry with a channel height of 4.5 mm and the constant height geometries with channel heights of 4.5 and 5.5 mm were examined. In general, the pressure loss as defined by dP_{inj} was lower for the constant height geometry. This could be explained by the confinement and the lack of an expansion fan upstream of the detonation wave that could allow a greater pressure loss. However, a two wave mode in the constant area geometry, seen located radial outboard by Boller et al. [6], would have led to a lower pressure loss with this assumption, which is not the case. Huff [5] observed an independence between

the operating mode and the pressure loss for the constant area geometry. Instead, he noted that a lower pressure loss occurred at lower mass fluxes and equivalence ratios. Another factor for a lower pressure loss for the constant height detonation chamber was the converging detonation chamber area since the effective area of the flow decreased as the flow traveled radially inward. This constriction at the inner radial locations, which also led to the detonation confinement, could have led to a greater P_5 value and a lower pressure loss.

Table 2. Comparison of pressure loss, dP_{inj}, between constant area $h_c = 4.5$ mm (C.A. 4.5) and constant height $h_c = 4.5$ mm and $h_c = 5.5$ mm (C.H. 4.5/C.H. 5.5) geometries of RRDE.

Φ \ $\dot{m}''$	50 kg/m^{2}s			75 kg/m^{2}s			100 kg/m^{2}s			125 kg/m^{2}s			150 kg/m^{2}s			175 kg/m^{2}s			200 kg/m^{2}s		
	C.A. 4.5	C.H. 4.5	C.H. 5.5	C.A. 4.5	C.H. 4.5	C.H. 5.5	C.A. 4.5	C.H. 4.5	C.H. 5.5	C.A. 4.5	C.H. 4.5	C.H. 5.5	C.A. 4.5	C.H. 4.5	C.H. 5.5	C.A. 4.5	C.H. 4.5	C.H. 5.5	C.A. 4.5	C.H. 4.5	C.H. 5.5
0.5	0.19	0.20	0.16	0.25	0.27	0.20	0.28	0.27	0.19	0.27	0.26	0.19	0.30	0.27	0.19	0.30	0.27	0.19	0.30	0.24	0.18
0.6	0.21	0.22	0.17	0.27	0.26	0.20	0.30	0.30	0.20	0.29	0.29	0.20	0.33	0.26	0.16	0.33	0.27	0.18	0.31	0.25	0.18
0.7	0.22	0.22	0.20	0.29	0.26	0.20	0.33	0.27	0.18	0.34	0.27	0.18	0.35	0.25	0.18	0.34	0.25	0.18	0.33	0.24	-
0.8	0.20	0.26	0.17	0.32	0.25	0.18	0.34	0.25	0.19	0.35	0.25	0.19	0.34	0.24	0.17	0.34	0.25	-	0.37	0.24	-
0.9	0.27	0.26	0.20	0.36	0.25	0.20	0.31	0.26	0.20	0.31	0.25	0.20	0.36	0.26	-	0.35	0.25	-	0.34	0.24	-
1.0	0.23	0.26	0.23	0.31	0.27	0.21	0.39	0.26	0.22	0.40	0.25	0.20	0.41	0.25	-	0.41	0.25	-	0.41	0.24	-

While the average pressure loss of all tests for the constant height geometry was lower than the average of pressure losses given from the constant area geometry, the consistency of the pressure loss for the constant height geometry is more noteworthy. While Huff [5] showed a dependence on equivalence ratio and mass flux on the pressure loss for the constant area geometry, the constant height geometry did not have the same trend. The standard deviation of the pressure loss, based on the achieved pressure values for all tests, was 0.018 for the constant height and 0.059 for the constant area. This showed less variation from the average pressure loss of $dP_{inj} = 0.26$ for the constant height geometry independent of the equivalence ratio or mass flux. When considering the wave mode operation and its confinement, as well as the lower pressure loss with low deviation, the constant height RRDE demonstrated a more predictable, higher performance operation over a variety of flow conditions

when compared to the constant area geometry.

To account for the total pressures within the detonation chamber, rather than the static pressures provided by the CTAP measurements, the Equivalent Available Pressures, or EAP, were considered by implementing Equation 11 and the assumptions given in Section 3.2.1. In addition, the static pressure values obtained through the plenum CTAP was assumed to provided stagnation pressures. This provided different pressure loss values when considering these total values and are given in Appendix B.

4.2 Configuring the Channel Height of the Stand-Alone Combustor

With the constant height geometry providing a greater performance compared to the constant area, the constant height geometry was further tested to determine the highest performance configuration. While Huff [3] explored channel heights of $h_c = 4.5$ mm and lower for the constant area geometry RRDE to improve its detonability, larger channel heights were examined for the constant height geometry RRDE to match the BAT configuration that required a higher channel height for guide vanes. These larger channel heights were possible due to the decreased detonation chamber volume compared to the constant area geometry, despite a larger channel height. In addition to varying the channel heights between 4.5, 5.5, and 6.5 mm, the throat restriction was varied for the larger channel height to determine the largest throat possible while still maintaining operability since it was assumed that the larger throat would lead to a lower pressure loss. Furthermore, the nozzles were varied to determine the effect of the blockage on the operability and performance of the constant height RRDE.

First, three channel heights of 4.5, 5.5, and 6.5 mm were examined by maintaining the throat area ratio at $AR_t = 0.20$ and using the same nozzle, with a diameter of 4.88 cm at the exit, for each test. Figure 64 provides the areas within the three channel heights tested. While the nozzle provided different area ratios for different

channel heights, the blockage of this nozzle was more similar to the turbine used in the BAT configuration. In addition, since the turbine would provide constant blockage, regardless of the channel height, the same blockage for different channel heights was desired over a constant nozzle area ratio. The nozzle provided area ratios of $AR_n = 1.1$ and $\frac{A_8}{A_{3.2}} = 0.39$ for $h_c = 4.5$ mm, $AR_n = 0.90$ and $\frac{A_8}{A_{3.2}} = 0.32$ for $h_c = 5.5$ mm, and $AR_n = 0.76$ and $\frac{A_8}{A_{3.2}} = 0.27$ for $h_c = 6.5$ mm.

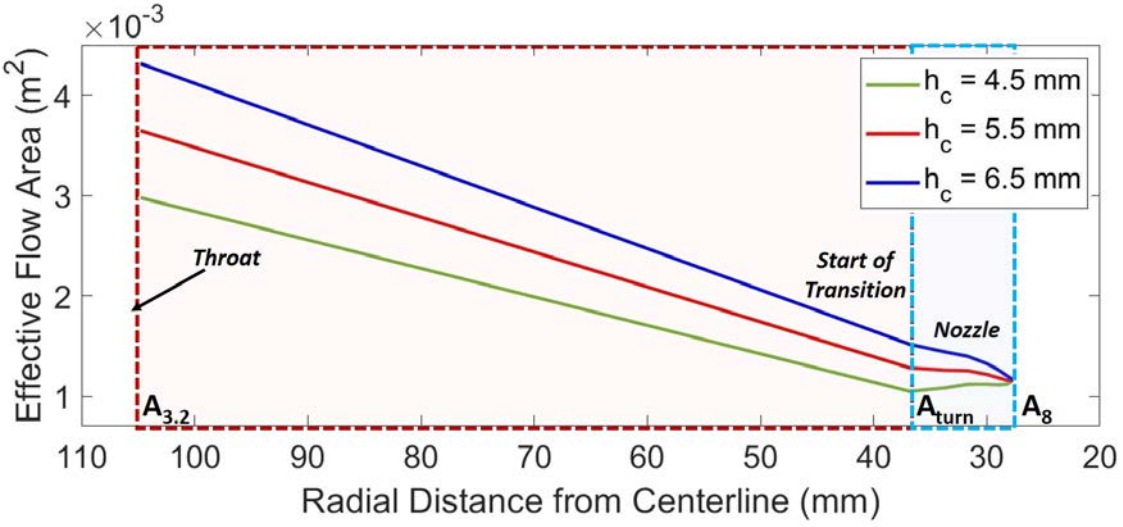

(a)

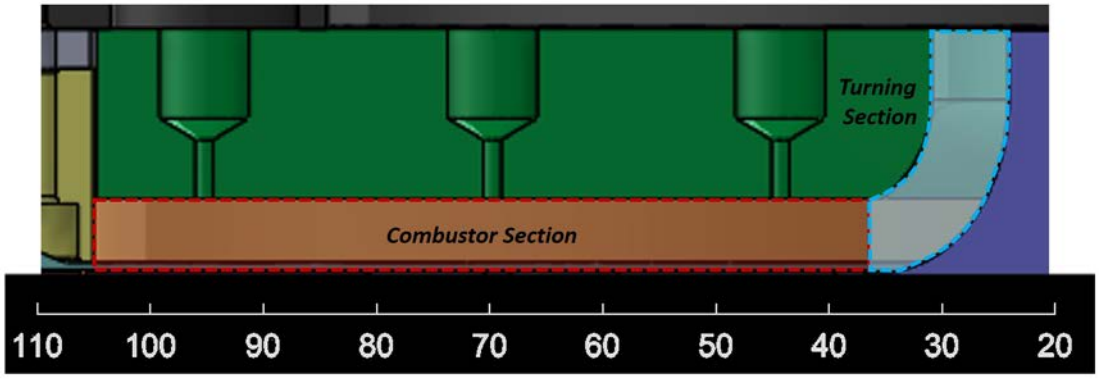

(b)

Figure 64. Effective area within detonation chamber for (a) different channel heights of stand-alone combustor configuration with (b) sample cross-section of stand-alone combustor configuration..

While $h_c = 4.5$ mm experienced a variety of operating modes, given in Figure 65, the 6.5 mm channel height mainly operated at one wave mode conditions during the 1.5 second run time. At higher mass fluxes of $\dot{m}'' = 150\ \frac{kg}{m^2 s}$ and greater, the 6.5 mm channel height configuration did operate at two wave modes since the flow rate was large enough to pressurize the larger detonation chamber to provide a greater wave number mode. This suggests that a larger channel height could provide a more consistent wave mode.

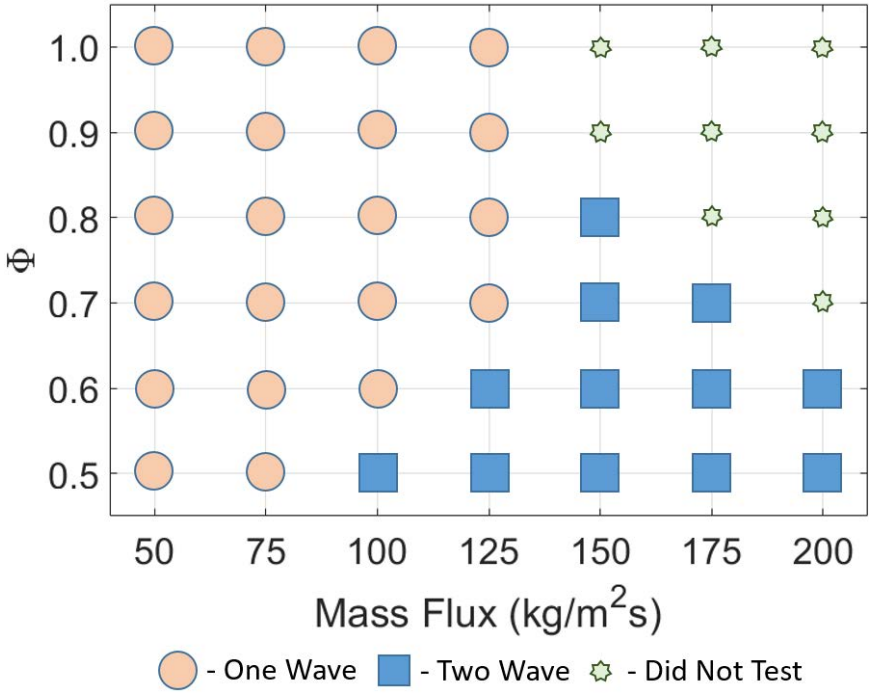

Figure 65. Number of waves, N_D, for constant height $h_c = 6.5$ mm RRDE.

This consistency was also confirmed by each channel height's CTAP measurements. Figure 66 provides typical pressure profiles for P_{plenum} and P_5 for the three channel heights at a throat area ratio of $AR_t = 0.20$. The smallest channel height of 4.5 mm had chamber pressure measurements that noticeably increased during most test conditions, leading to the variety of operating modes seen for this channel height. This increase was mirrored in the plenum, suggesting that the device had not reached

steady state, which would also affect the operating modes. All three channel heights experienced increases in the plenum during operation, suggesting that the smaller throat for each geometry restricted the plenums ability to reach a steady value. The response of the plenum, after the detonation was initiated, increased (i.e. greater coupling between the detonation chamber and plenum) when the throat height was increased for a given channel height, as discussed in Section 4.3.

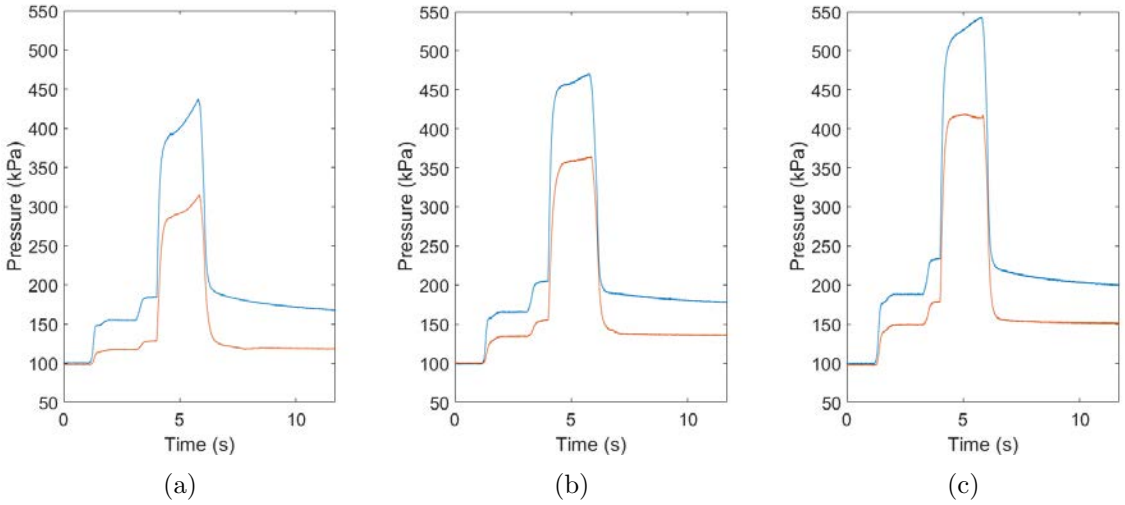

Figure 66. Transient pressure response of P_{plenum} and P_5 at $\dot{m}'' = 100 \frac{kg}{m^2 s}$ and $\Phi = 1.0$ for (a) $h_c = 4.5$ mm, (b) $h_c = 5.5$ mm, and (c) $h_c = 6.5$ mm.

In addition to the consistency given by the larger channel height, the two larger channel heights of 5.5 mm and 6.5 mm also provided lower pressure differences from P_{plenum} to P_5 than the 4.5 mm constant channel height. However, when P_5 was adjusted to EAP and the pressure loss was examined, given in Appendix B, channel heights of 4.5 and 6.5 mm were seen to have similar pressure losses, with $h_c = 5.5$ mm having the lowest pressure loss. The smallest channel height may have experienced larger pressure losses due to the divergence that occurred with the nozzle used. The larger pressure losses for $h_c = 6.5$ mm suggest that a larger channel height, while providing consistency in operating mode, suffers from a lower Mach value that lowers the total pressure despite having a lower static pressure drop from the plenum.

Multiple wave modes can benefit the RRDE with potential turbine integration since as the frequency of the waves increases with more waves, the detonation is less likely to affect the turbine's operation. This can be quantified through further studies to determine whether pressure fluctuations downstream of the detonation radial location are low enough to provide steady operation to a turbine. However, the lower operating mode experienced by the larger channel height also led to the lower pressure loss. A single wave allowed for a longer refill rate compared to the multiple wave modes, providing a more complete detonation event and a greater pressure increase. Furthermore, multiple waves would have their own expansion that would lower the pressure downstream of the detonation event, where a one wave mode would only have the expansion fan from its single shock. Therefore, if a single wave could operate at the outer radial location of the RRDE, this would be preferred since it would allow a lower pressure loss while maintaining confinement away from integrated turbomachinery at the center of the RRDE. This was achieved at $h_c = 6.5$ mm at lower mass fluxes and equivalence ratios. The confinement would provide less interference closer to the turbine, lowering the need to have multiple waves that would provide a steadier flow into the turbine. A larger channel height would allow a confined single wave mode and should be explored for future implementation with a radial-inflow turbine.

4.3 Configuring the Throat of the Stand-Alone Combustor

For most of the tests, the throat was set at a throat area ratio of $AR_t = 0.20$ relative to the channel height. This throat area ratio was determined to be a high operability condition based on previous testing of the RRDE by Huff et al. [3]. A smaller throat height allows proper mixing of the reactants before entering the detonation chamber and attempts to prevent backpressure into the plenum during

operation. However, invoking a throat in a device provides a source of pressure loss which is ineffectual to the goal of providing pressure-gain combustion. Therefore, configuring the throat for the constant height RRDE and examining its effect on operability and performance was desirable.

Since the throat area ratio was constant for the data given in Sections 4.2 and 4.1 and not the actual throat height, h_t, which increased with larger channel heights, the pressure loss was examined to determine whether it was a function of h_t or AR_t. To do so, the pressure loss was examined by maintaining the throat height constant at $h_t = 0.89$ mm for channel heights of 4.5 and 5.0 mm, resulting in throat area ratios of $AR_t = 0.20$ and $AR_t = 0.18$, respectively. This is tabulated in Appendix B. For the constant throat area, the pressure loss increased as the channel height increased. For example, at $\dot{m}'' = 75 \frac{kg}{m^2 s}$, the pressure loss increased between 20%-50% depending on the equivalence ratio, with no correlation between the equivalence ratio for a given mass flux and the pressure loss or pressure difference between the two geometries. The increase in pressure loss as the channel height increased with constant h_t was due to the greater expansion for the same throat area into the detonation chamber. Therefore, for the same throat area ratio, given in Section 4.2, larger channel heights with larger throats allowed for a lower pressure loss. However, future configurations of an RRDE would need to determine the optimal channel height for a given RRDE to provide a large h_t while maintaining a channel height that still provides acceleration to increase the total pressure aft of the detonation. Between the channel heights of $h_c = 4.5$ mm and $h_c = 5.0$ mm for this comparison, the operability remained the same, with similar number of one, two, and three wave modes following the same trend of increasing wave number with lower equivalence ratios and higher mass fluxes.

Using the higher area nozzle of $AR_n = 0.76$, the effect of opening the throat for the 6.5 mm channel height was examined. Despite the pressure rise during operation,

focused regions on ITP data shown in Figure 67 provide sinusoidal pressure changes characteristic of acoustic modes rather than full detonative modes with sharp pressure rises followed by a relaxation as the detonation wave passes by. Therefore, it can be assumed that opening the throat promotes these acoustic modes over detonative modes. Operability for the device was reduced to larger mass fluxes for the larger throat. The device did not detonate at lower equivalence ratios until the mass flux was increased to $\dot{m}'' = 150\frac{kg}{m^2 s}$. This was also expected since the larger h_t allowed greater backpressure into the plenum and reactant flow feeds, lowering the refresh rate of the reactants until the detonation event could no longer propagate for non-detonative cases. It can be assumed that during detonative operation, while there wasn't enough back pressure to prevent the device from operating, there was enough to limit fuel flow so that the local equivalence ratio in the detonation chamber was lower than expected to result in acoustic modes. Therefore, while a larger throat could decrease the pressure loss experienced by the system, a larger throat could change the wave modes seen for the same channel height at a more constrictive throat.

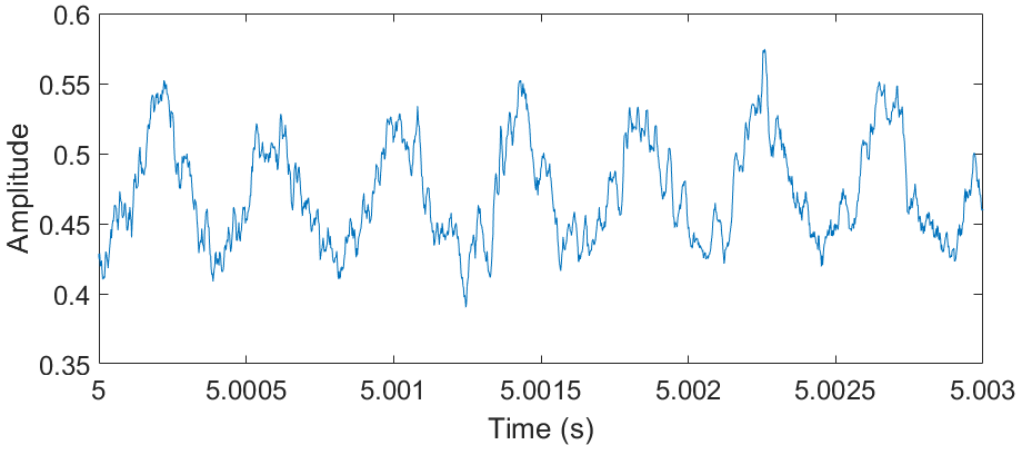

Figure 67. Sample ITP transient signal for $AR_t = 0.50$ at $h_c = 6.5$ mm.

The pressure loss decreased as throat area ratio increased from $AR_t = 0.20$ ($h_t =$ 1.3 mm) to $AR_t = 0.50$ ($h_t = 3.3$ mm). This is given in Appendix B. Both geometries

had the same standard deviation of 0.016, demonstrating that the pressure loss did not vary significantly across the test conditions for a given geometry. Of note between the two throat area ratios was the difference in the CTAP measurement distribution from the plenum through the channel. For example, at $\dot{m}'' = 100\frac{kg}{m^2 s}$ and $\Phi = 0.80$, the smaller throat area ratio of 0.20 resulted in $P_{plenum} = 500$ kPa, $P_1 = 480$ kPa, $P_2 = 470$ kPa, $P_3 = 450$ kPa, $P_4 = 440$ kPa, and $P_5 = 400$ kPa. The larger area ratio of $AR_t = 0.50$ had $P_{plenum} = 460$ kPa, $P_1 = 460$ kPa, $P_2 = 450$ kPa, $P_3 = 440$ kPa, $P_4 = 430$ kPa, and $P_5 = 410$ kPa. The plenum pressure dropped 9% and initial pressures in the channel at CTAP 1 and 2 dropped 5% from $AR_t = 0.20$ to $AR_t = 0.50$. Despite these pressure drops, the exit pressure at CTAP 5 increased by 3%. With P_{plenum}, P_1, and P_2 decreasing and the other CTAP measurements increasing, the pressure change throughout the channel was more uniform for $AR_t = 0.50$. In addition, the higher decrease in the plenum pressure compared to the smaller increase at P_5 contributed to the lower pressure loss for $AR_t = 0.50$. This trend was seen for all 17 detonated test conditions, with a decrease in P_{plenum} from $AR_t = 0.20$ to $AR_t = 0.50$ of $11\% \pm 1.7\%$, $5\% \pm 1.2\%$ for P_1, $5\% \pm 2.0\%$ for P_2, $3\% \pm 1.7\%$ for P_3, $3\% \pm 1.8\%$ for P_4, and $0\% \pm 1.8\%$ for P_5. The decrease in the plenum pressures also affected the fuel plenum created by the fuel mounting ring and the base plate, with a 6.8% decrease in the maximum pressure measured from the CTAP in the fuel plenum from $AR_t = 0.20$ to $AR_t = 0.50$ at $\dot{m}'' = 100\frac{kg}{m^2 s}$ and $\Phi = 0.80$.

While the pressure change from the plenum to the end of the detonation chamber was quantified, Table 3 provides the percent pressure change from plenum (P_{plenum}) to CTAP 1 aft of the throat (P_1). Increasing the throat while maintaining the same channel height also resulted in a greater coupling between the plenum and initial pressure in the channel given by CTAP 1. This could be a result of the relatively large throat or the acoustic modes. For example, at $\dot{m}'' = 100\frac{kg}{m^2 s}$ and $\Phi = 0.80$,

the pressure reduced 3.4% P_{plenum} to P_1 at $AR_t = 0.20$ while the pressured reduced only 0.7% at $AR_t = 0.50$. In some cases, noted by negative values in Table 3, the measured values for P_1 were greater than the measured values for P_{plenum}, but this phenomenon of $P_1 > P_{plenum}$ was negligible due to the $\pm 1.4kPa$ uncertainty of each CTAP measurement. In addition, at the larger h_t, the plenum did not experience the same rise during operation as it did at $AR_t = 0.20$. This could be due to the lack of a rotating detonation wave in conjunction with a larger throat that allowed for a faster plenum recovery after the initial detonation.

Table 3. Comparison of static pressure loss across throat from P_{plenum} to P_1 at $h_c = 6.5$ mm with throat area ratios of $AR_t = 0.20$ and $AR_t = 0.50$ for the constant height RRDE. $(*)$ denotes a non-detonating condition

AR_t	0.2	0.5	0.2	0.5	0.2	0.5	0.2	0.5
$\dot{m}''$ / Φ	75 kg/m^{2}s		100 kg/m^{2}s		125 kg/m^{2}s		150 kg/m^{2}s	
0.5	6.2%	*	6.9%	*	6.3%	*	7.0%	0.6%
0.6	4.4%	*	6.9%	*	6.6%	0.3%	6.0%	1.0%
0.7	4.9%	*	3.4%	0.1%	6.7%	0.2%	6.7%	0.9%
0.8	5.3%	0.6%	4.9%	0.7%	6.6%	0.8%	6.6%	1.4%
0.9	6.0%	*	5.5%	-0.3%	6.5%	0.0%	6.8%	-0.1%
1.0	7.7%	0.5%	7.4%	-0.5%	6.4%	-0.2%	8.7%	0.5%

4.4 Configuring the Nozzle of the Stand-Alone Combustor

Detonation confinement occurred due to the converging area created in the detonation chamber that promoted the detonation to propagate at the outer radius at the largest effective area. However, the effect of the blockage created by the nozzle was not examined as the largest nozzle available was primarily used to test a fully converging flow area. CFD results by Kaemming et al. [31] showed that for a given throat restriction, pressure gain performance increased by increasing the blockage, or

decreasing $\frac{A_8}{A_{3.2}}$. Without the nozzle, the flat channel plate created an area ratio between the area immediately aft of the throat to the area before the flow was turned by the nozzle of 0.35. This area ratio was independent of the channel height, throat, and nozzle since with a flat channel plate, the area ratio was only a function of the radial distance from the centerline. Fotia et al. [39] examined the use of an aerospike nozzle, compared to bluff bodies, that provided converging-diverging exhaust flow for an axial RDE and found that this area variation created a performance increase with respect to specific thrust. This converging-diverging nozzle flow was explored by utilizing the constant height RRDE's converging combustion chamber, independent of the nozzle, with various smaller nozzles to determine whether a large converging section followed by divergent turning, locating the choked condition within the detonation chamber before turning, affected performance.

Figure 68a provides the area variation through the stand-alone combustor for various nozzles at $h_c = 6.5$ mm through the full detonation chamber, with Figure 68b providing a closer view of the area changes while turning for the different nozzles. The area through the nozzle was determined by assuming the bulk flow traveled normal to both the nozzle and channel plate's curvatures. The difference in the final radial distances from centerline in Figure 68b was due to the different radii of the nozzle, with a smaller nozzle providing flow closer to the centerline than a bigger nozzle. The four nozzles selected, given Table 4, provided fully converging areas, a relatively constant area, and a diverging turning area. The largest stand-alone combustor channel height of $h_c = 6.5$ mm was chosen for the testing and in calculating the ratios given in Table 4. This large channel height provided an opportunity to examine multiple AR_n values through existing nozzles. Smaller channel heights of 5.5 and 4.5 mm only had one previously manufactured nozzle that provided full convergence and were not tested in this nozzle parameter study. The throat area ratio was set at $AR_t = 0.20$.

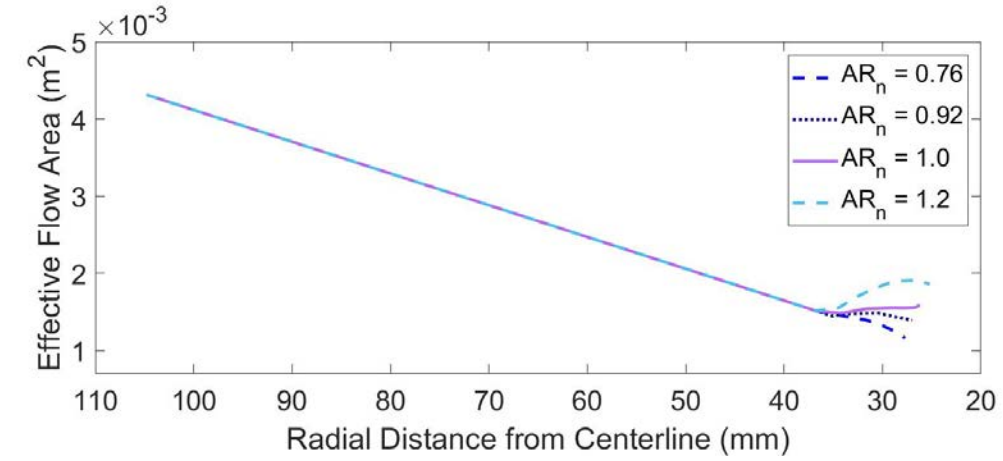

(a)

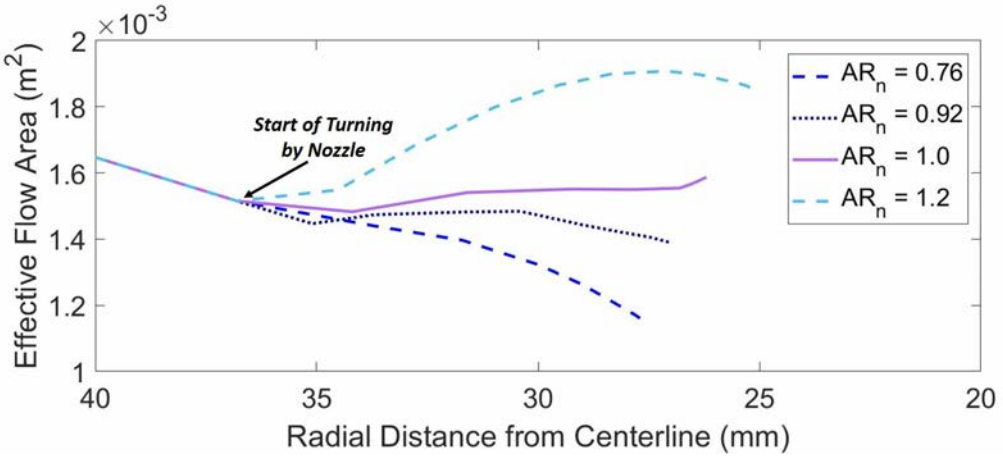

(b)

Figure 68. Effective area for different nozzles (a) within full detonation chamber and (b) focused region through nozzle turning section for the constant height $h_c = 6.5$ mm.

Table 4. Nozzle dimension and area ratios for $h_c = 6.5$ mm testing.

Nozzle #	r_n, mm	AR_n	$\frac{A_8}{A_{3.2}}$
A	24.4	0.76	0.27
B	22.8	0.92	0.32
C	21.4	1.1	0.37
D	19.3	1.2	0.43

The nozzle variation study was conducted at a mass flux of $100\frac{kg}{m^2 s}$ at an equivalence ratio of 0.7. Ideally, the modal operability between the different nozzles could also be examined. However, this testing was conducted after modifications were made

to the base plate for the BAT configuration, and it was observed that these modifications transitioned the operating mode to unsteady three wave modes while detonating. The modifications to the base plate due to the guide vanes are detailed in Section 3.3 with its possible implication on the modal operability discussed in Section 4.8.

Instead of comparing the modal operability, the steadiness of the device, as determined through the relative change of the CTAP measurements during operation, was examined. Figure 69 provides the CTAP measurements of the plenum, CTAP 1, and CTAP 5 for the four nozzles. Three tests were conducted for each nozzle at the same test condition of $\dot{m}'' = 100\frac{kg}{m^2 s}$ and $\Phi = 0.7$ and showed repeatable results. Nozzles A and B provided a converging area while turning the flow. These converging geometries had the choked condition at the exit plane and had the most stable operation, with plenum pressures changing 2.9% and 4.3% during operation for Nozzles A and B, respectively, and are given in Table 5.

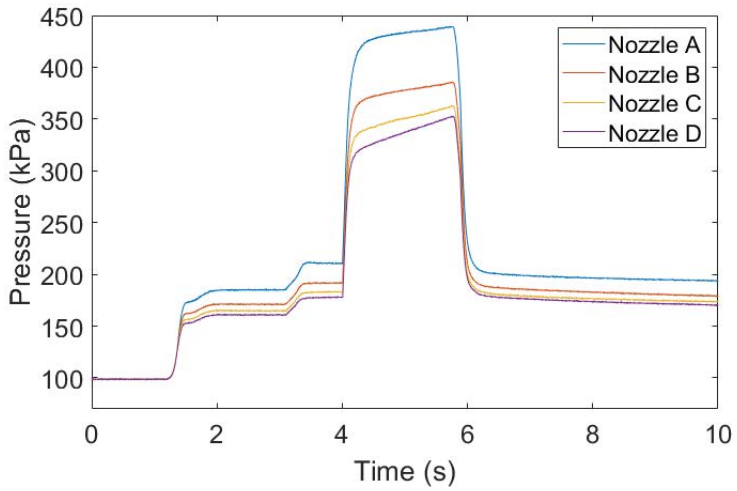

Figure 69. CTAP measurements for the four nozzles given in Table 4 for $h_c = 6.5$ mm at $\dot{m}'' = 100\frac{kg}{m^2 s}$, $\Phi = 0.7$.

As the detonation chamber geometry was modified to feature a diverging turning section with the implementation of Nozzles C and D, the device was seen to operate with more unsteadiness. The plenum pressure changed 8.4% and 11.0% during op-

eration for Nozzles C and D, respectively, and are given in Table 5. This increasing pressure was also seen for the 4.5 mm constant channel height geometry which also featured a diverging turning section. In addition, this smaller channel height also had increasing pressures during operation as seen Figures 63 and 66. It was assumed that this unsteadiness was caused by the small throat invoked to maintain the same throat area ratio at smaller channel heights. However, this nozzle variation study suggests that the diverging turning section aft of the combustor section influences the steadiness of the detonation chamber and plenum during operation.

The performance based on the pressure loss through the device was also examined for the different nozzles. This was calculated as both a static pressure comparison using Equation 10 and considering EAP through Equation 11, and they are given in Table 5. The pressure loss increased as the nozzle restriction was relaxed, showing that not only is a converging nozzle ideal, but that a greater area change results in a greater performance. Therefore, it is suggested that the choked condition exist at the exit plane for the constant height RRDE to maintain a constantly decreasing effective area throughout the device. This condition increases stability and improves operability towards potential pressure-gain.

Table 5. Pressure performance for the four nozzles given in Table 4 for $h_c = 6.5$ mm at $\dot{m}'' = 100 \frac{kg}{m^2 s}$, $\Phi = 0.7$.

Nozzle #	dP_{inj}	P_{loss}	**Change in Plenum**
A	0.15	0.06	2.9%
B	0.23	0.10	4.3%
C	0.28	0.12	8.4%
D	0.29	0.13	11.0%

4.5 Flowfield Visualization of Stand-Alone Combustor

The CTAPs through the channel plate were used to confirm detonation confinement in the detonation chamber to the outer radial location. However, flowfield

visualization of the detonation chamber using a clear channel plate was attempted to confirm this trend. Furthermore, while the ITPs on the channel plate were used to confirm the wave modes for a given test, high-speed visualization was performed to confirm the trends suggested by the high-frequency pressure measurements. Polycarbonate was used as the clear channel plate to examine the flowfield and locate the detonation wave within the detonation chamber. The setup, as given in Section 3.2.3 and Figure 42, was modeled after results given by Boller et al. [6]. However, while the polycarbonate channel plate was tested to compliment the wave mode results given by the stainless steel plate, the high uncertainty created by the ablation of the material during testing did not allow for full correlation between the high-speed visualization and pressure measurement results for a desired test condition. In addition, the limited view of the detonation chamber prevented visual confirmation of a confined detonation wave.

4.5.1 Ablation of Polycarbonate Channel Plate

Initially, polycarbonate was selected for use as the clear channel plate despite the survivability drawbacks associated with the material seen by Boller et al. [6]. The ablation of the polycarbonate, shown in Figure 70 affected multiple variables. This includes the effective area during testing, the potential chemistry change of the reactants due to the melted polycarbonate, and the changing physical environment associated with the melted polycarbonate on the hardware that occurred during testing. Boller [16] discusses these effects as it pertained to his study as well.

The largest quantifiable change that occurred while testing with the polycarbonate channel plate was the increase of the channel height throughout the combustor as the material ablated during testing. Table 6 provides the change in the channel height for the ten tests conducted with the polycarbonate channel plate. The channel height

(a) (b)

Figure 70. Ablation of polycarbonate channel plate (a) after first six tests and (b) after all ten tests with shims attached.

decreased prior to Test 7 by shimming the existing polycarbonate plate to achieve a smaller channel height again. However, the shimmed channel plate quickly opened up again at a faster rate per test due to the increase in mass flow. The polycarbonate thickness was measured at four different times during all testing, and the effective channel height for a given test was extrapolated by assuming that for a given test, the predominant amount of the burning occurred for the latter half of the test and after fuel shut off. In addition to providing uncertainty in the channel height, the mass flux also varied since it was a function of the area as well.

After the testing, the polycarbonate channel plate left residue over the base plate. This soot accumulation, shown in Figure 71, developed near the fuel injectors. This resulted in potential blockage of the hydrogen gaseous fuel. In addition to the channel height variation and injection blockage, the polycarbonate could also have affected the chemistry of the reactant flow as it burned and reacted. Boller [16] analyzed the potential of this effect and concluded that most of the hydrocarbons developed

Table 6. Approximate channel height and mass flux during testing of polycarbonate plate. Values in parentheses represent upper and lower bounds of confidence interval.

Test #	Mass Flow, $\frac{kg}{s}$	Φ	h_c, mm	$\dot{m}''$, $\frac{kg}{m^2 s}$
1	0.32	0.6	6.5 (6.5, 7.0)	75 (70, 75)
2	0.32	0.8	7.4 (7.0, 7.6)	66 (64, 70)
3	0.32	1.0	8.4 (7.6, 8.6)	59 (57, 65)
4	0.22	0.8	8.9 (8.6, 10.0)	37 (33, 39)
5	0.42	0.8	10.0 (9.0, 10.2)	64 (63, 71)
6	0.54	0.8	11.4 (10.2, 11.6)	72 (71, 81)
7	0.32	0.5	4.5 (4.5, 6.5)	108 (75, 108)
8	0.54	0.6	6.9 (6.5, 9.5)	120 (86, 126)
9	0.54	0.6	10.0 (9.5, 12.0)	82 (68, 86)
10	0.87	0.6	13.7 (12.0, 13.9)	63 (59, 68)

from the burning polycarbonate exhausted from the device before it could affect the chemistry.

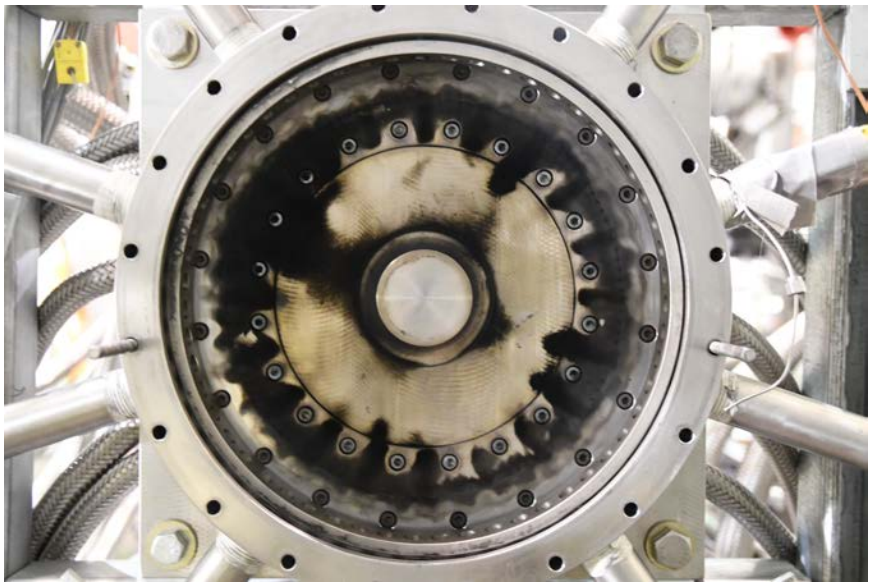

Figure 71. Soot accumulation on base plate after polycarbonate plate testing.

4.5.2 Wave Mode Visualization through Polycarbonate Channel Plate

The first objective of the clear channel plate was to confirm the confinement of the detonation wave suggested by the CTAPs on the stainless steel channel plate.

Figure 72a shows the view of the detonation chamber through the Phantom camera using the clear channel plate compared to the full detonation chamber location, with Figure 72b providing a cross-section with same viewpoints. Due to the installation of the channel plate, the limited view of the detonation chamber prevented visual confirmation of the detonation wave which was confined to the area blocked by the top plate that held the channel plate and sealed the device according to the high static and calculated total pressures located at CTAP 1.

Since the Phantom camera was setup according to the visible chemiluminescence in the detonation chamber, secondary burning and the burning of the polycarbonate provided the peak luminosity values in the high-speed footage rather than the detonation wave. This was concluded based on the changing luminosity throughout the test. Figure 73a provides an image at the beginning of Test 7 during ignition, showing the maximum luminosity for the camera settings of 40,988 frames per second with a 0.9 μs exposure time, while Figure 73b-d show images captured throughout the run. The low luminosity accompanying the one wave mode was due to the camera being able to capture the expansion and secondary burning aft of the detonation wave. As the test progressed and the channel plate ablated, the luminosity increased as the burning in the visible section of the device increased. The final image given in Figure 73e shows the high luminosity seen during shut-off when the device rapidly transitioned through multiple modes with high heat release seen as the remaining fuel combusted. Based on the lack of visibility into the full detonation chamber and the variable luminosity dependent on the amount of secondary and material burning, the polycarbonate channel plate could not be used to confirm the detonation confinement.

Despite the ablation and limited view into the detonation chamber, the polycarbonate channel plate was used to correlate observed ITP frequencies to wave modes. Figure 74 provides the results from Test 1, as described in Table 6. The result for

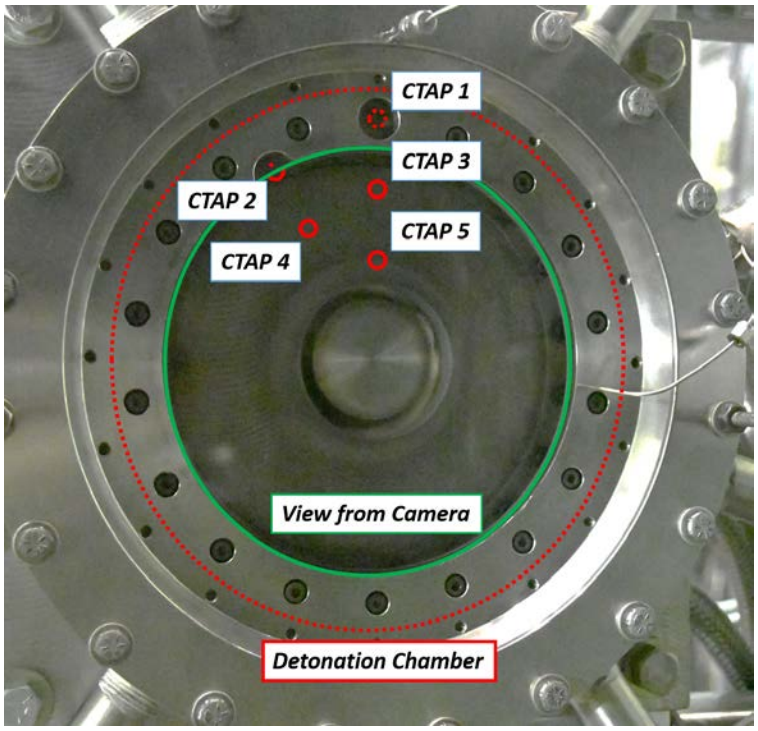

(a)

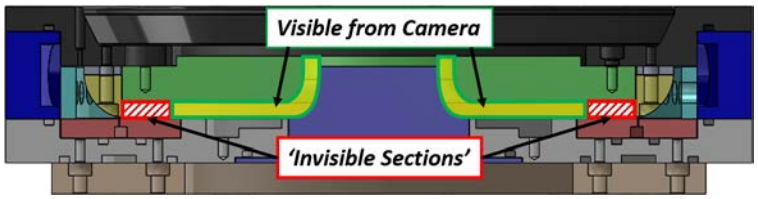

(b)

Figure 72. Visible section of detonation chamber (a) from outside view and (b) through cross-sectional view.

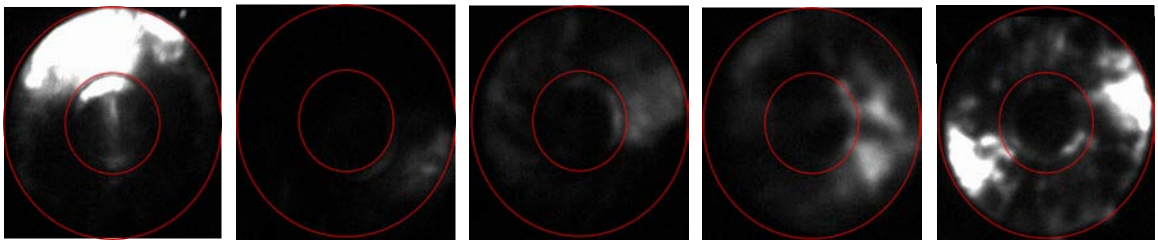

(a) (b) (c) (d) (e)

Figure 73. Progression of luminosity for Test 3 at frames captured (a) $t_a = 0.00$ s, (b) $t_b = 0.05$ s, (c) $t_c = 1.01$ s, (d) $t_d = 1.84$, and (e) $t_e = 1.92$ s from ignition from Phantom camera at 40,988 fps, 0.9 μs exposure, no corrections.

this was a consistent one wave mode operation. The frames captured from the constant height RRDE were digitally enhanced to provide greater visualization of the wave and its associated burning. The ITP was located in the fuel plenum to measure the pressure fluctuations due to a passing detonation wave. The frequency observed during the test using the Phantom camera was 2.4 ±150 kHz, which is within 3% of the 2.47 kHz observed through the ITP.

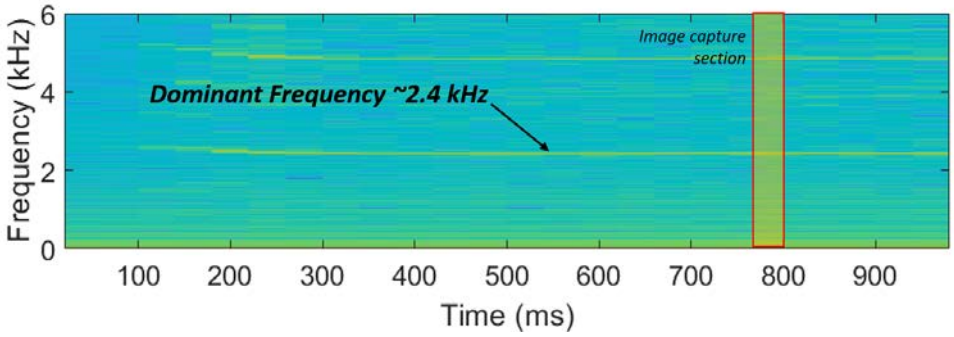

(a)

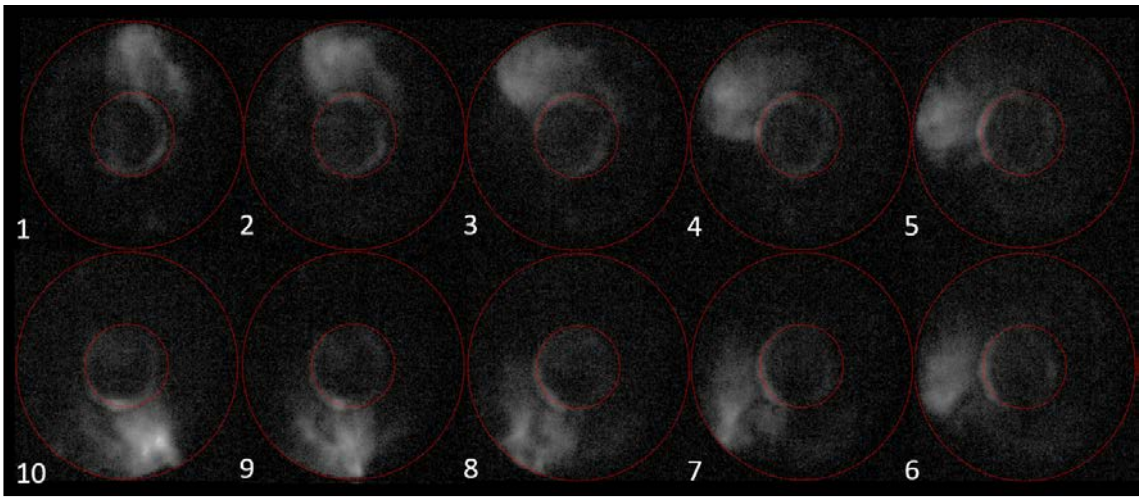

(b)

Figure 74. One wave mode observed during Test 1 through (a) ITP and (b) Phantom camera at 40,988 fps, 0.9 μs exposure with 70% brightness increase, 15% contrast increase.

Figure 75 provides a comparison of the one wave visualized with the flat polycarbonate channel plate (Frames 1-5) to the one wave observed by Boller [16] with

the contoured polycarbonate plate that provided a relatively constant area (Frames a-e). It was assumed that the detonation wave was hidden behind the top plate for the constant height tests, with the increased brightness given in Figure 75 providing the location of the detonation wave by assuming that the higher luminescence was created by the ablation of the plate and secondary burning. For the constant area frames, there is a clearer distinction between the highest luminosity values closer to the centerline and the outer edge of the viewing window. This distinction suggests that the camera was able to capture the bright detonation location and did not capture as much of the secondary burning and ablation that the constant height tests captured. The difference between the easily visible detonation wave in Frames a-e of Figure 75 to the limited luminescence in Frames 1-5 suggest that the one wave was confined to the outer radial location for the constant height geometry.

In Tests 5 and 6, the device experienced a transition from the lower frequency around 2.5 kHz, whose wave modes are given in Figure 76, to a higher frequency of 4.3 kHz, given in Figure 77. In Test 5, the device initiated with a counterclockwise

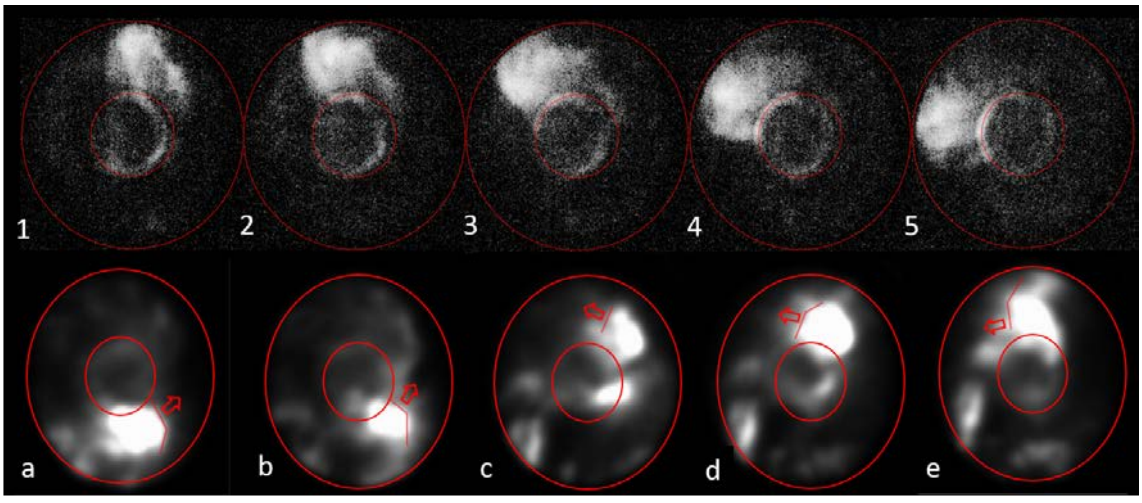

Figure 75. One wave operation captured through polycarbonate channel plate for constant height (1-5) and constant area (a-e) geometries. Frames 1-5 adjusted with 70% brightness increase, 15% contrast increase. Frames a-e modified from Boller [16].

one wave mode to two counter-propagating waves that stabilized to the clockwise one wave mode. This is shown in Figure 76b. This one wave mode transitioned again to two counter-propagating waves, which are shown in Figure 76c.

Despite the presence of the two counter-propagating waves, the frequency obtained through the ITP and observed through the high-speed visualization match the one wave operation at around 2.4 kHz. However, there appeared to be a stronger detonation wave between the two waves that could be the original one wave mode that dictated the frequency and provided the pressure spikes seen by the ITP that corresponded to a one wave mode. Boller et al. [6] suggested that these counter-propagating waves collided and were reflected to appear as 'clapping' modes. This could be possible from the interaction of the gas dynamics of having a combination of reflection and transmission. However, opposing linear shock waves also have the tendency to travel through each other. High-speed visualization by Bennewitz et al. showed counter-propagating waves passing through each other with one dominant (brighter) wave apparent [40]. This would support the indistinction of frequency between the one wave and two counter-propagating wave modes since the dominant frequency observed by the ITP would be the dominant detonation wave. The counter-propagating wave opposite of the dominant detonation wave observed by the ITP would provide relaxed pressure rises in the signal that would be indistinguishable to the noise or harmonics of the dominant wave. However, this observation was not confirmed since the ITP signal recorded through the fuel plenum during the high-speed visualization was too dampened to provide accurate high-frequency pressure change fidelity seen in the detonation chamber.

During Test 5, the device was operating at the two counter-propagating wave mode before transitioning to the higher frequency shown in the spectrogram given in Figure 77a. The two counter-propagating waves transitioned to two counterclockwise waves

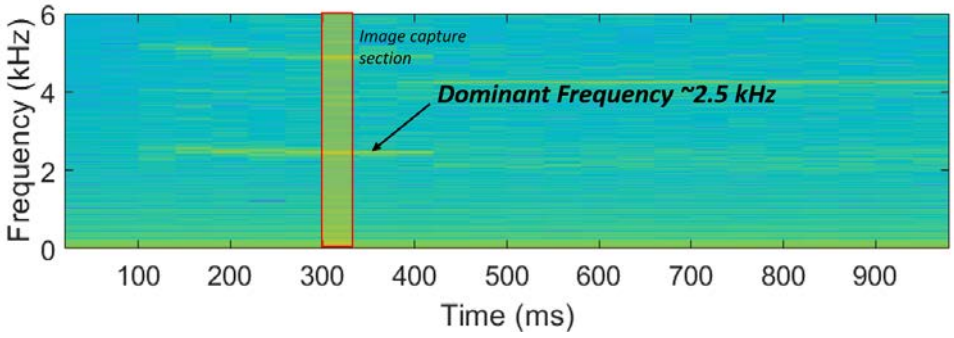

(a)

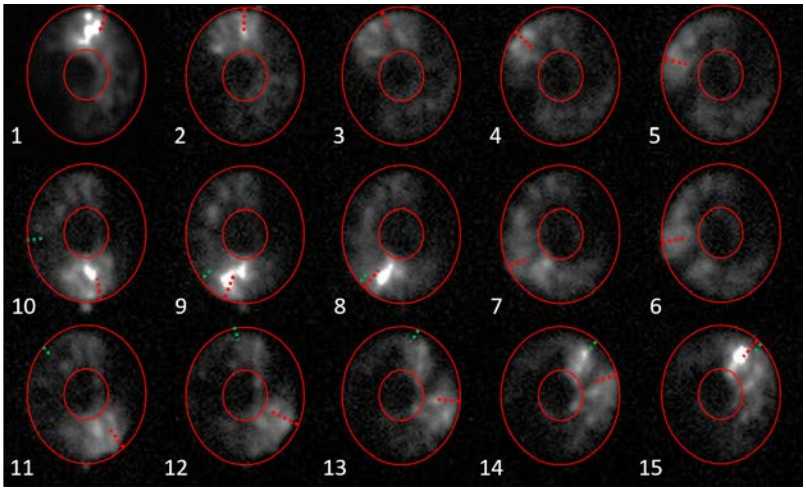

(b)

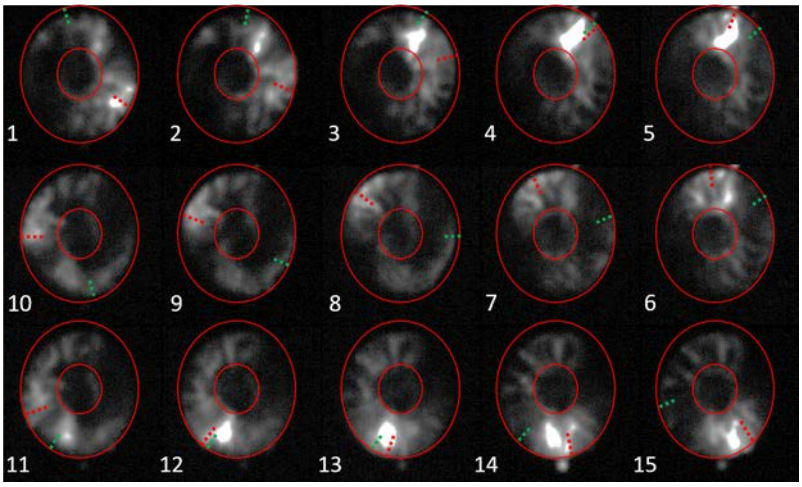

(c)

Figure 76. Test 5 showing 2.4 kHz operation through (a) ITP, (b) one wave transitioning to two counter-propagating waves, and (c) two counter-propagating waves captured at 40,988 fps, 0.9 μs exposure with 40% brightness increase, 40% contrast decrease.

shown in Figure 77b. This wave mode was short-lived before established itself as a four counter-propagating wave mode for the rest of the run. This is seen in Figure 77c. As was seen for the one wave and two counter-propagating wave modes that achieved the same dominant frequency, the two wave and four counter-propagating wave modes both were observed at the same frequency of 4.3 kHz. It was not determined if this counter-propagating phenomenon was a function of the polycarbonate's effect on the flowfield as discussed in Section 4.5.1 or if the stand-alone combustor had operated with these counter-propagating modes while the ITPs suggested one or two waves.

The polycarbonate was shimmed for Tests 7-10 to provide an initially smaller channel height to attempt to observe the three wave modes seen for $h_c = 4.5$ mm. The exposure was limited compared to the first six tests to avoid capturing the secondary burning seen in the previous tests. Three wave modes were successfully seen for all four tests with the shims, with the spectrogram of Test 9 given in Figure 78a with the resulting three waves seen with the high-speed camera shown in Figure 78b. While Figure 78 demonstrates three counterclockwise waves, these co-rotating waves experienced counter-propagating transitions before the waves co-rotated in the opposite direction. This co-rotation was then followed by another counter-propagating transition to reverse the wave direction again, with this cycle of 'clockwise to counter-propagating to counterclockwise to counter-propagating' waves repeating until shut-off. The transition for one direction to another was initiated by one of the three waves having a slightly higher wavespeed than the others, offsetting the initial stability and leading to the counter-propagating waves. This transition could have been initiated by the presence of radial acoustic modes but these modes were not captured for the given experimental setup. The three wave mode was more likely to transition out of the counter-propagating waves to the co-rotating waves due to the inability for the device to support six total waves, with the stronger three waves providing the

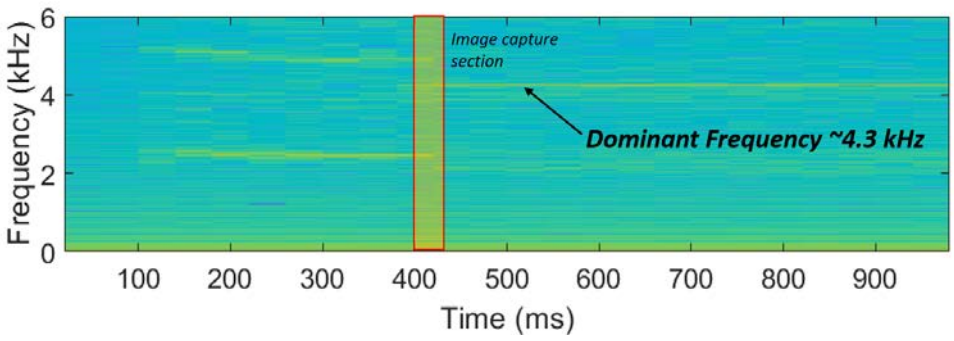

(a)

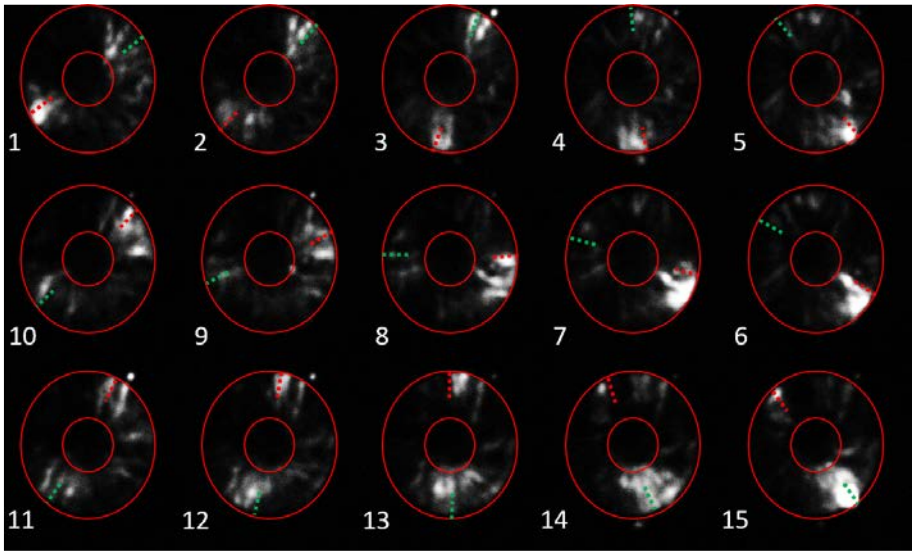

(b)

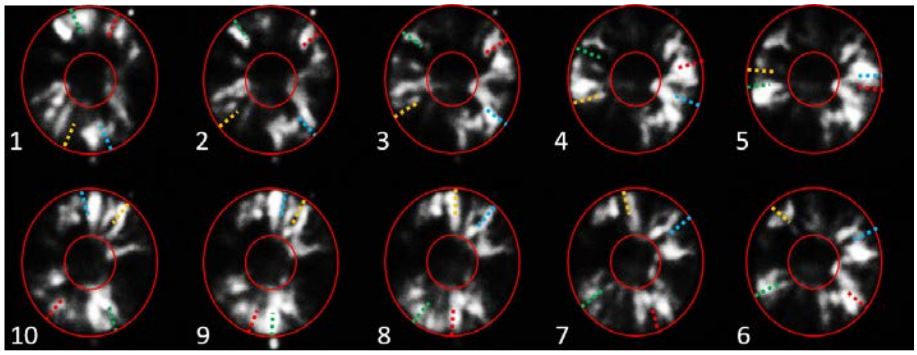

(c)

Figure 77. Test 5 showing 2.4 kHz operation through (a) ITP, (b) one wave transitioning to two counter-propagating waves and (c) two counter-propagating waves captured at 40,988 fps, 0.9 μs exposure with 40% brightness increase, 40% contrast increase.

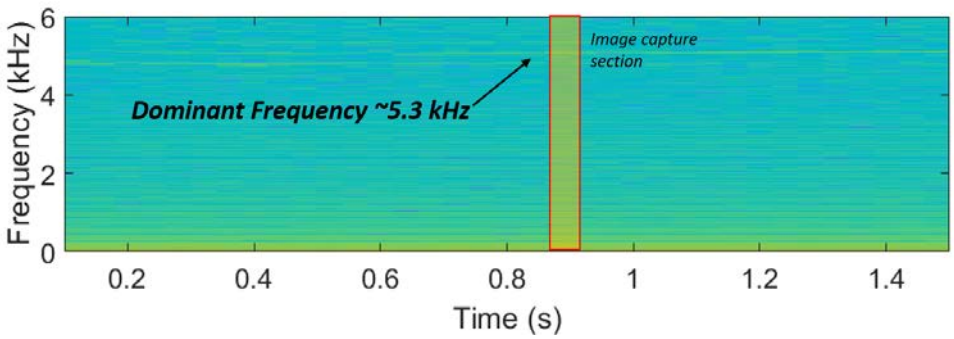

(a)

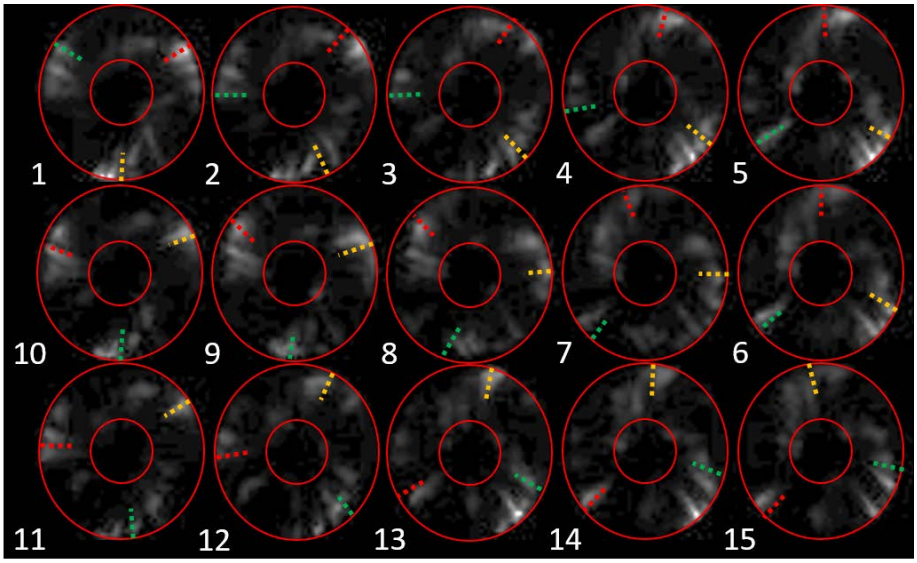

(b)

Figure 78. Three wave mode observed during Test 9 through (a) ITP and (b) Phantom camera at 40,988 fps, 0.7 μs exposure with 70% brightness increase, 15% contrast increase.

transition out of the counter-propagation.

For Tests 7-10, the base plate had been modified so that the guide vanes for the BAT configuration could be installed. While a ring without vanes was used instead of the guide vane ring to continue testing in the stand-alone combustor configuration after the modification, eight fasteners used to constrain this ring were now present in the flowfield. This provided possible recirculation pockets that could have tripped the flow to operate in a three wave mode rather than a one wave mode. For example,

while Test 5 and Test 9 had similar geometries and flow conditions, Test 5 operated at lower wave modes than Test 9. However, this could also be a function of the larger AR_n that was created due to the expansion of the inner diameter of the polycarbonate channel plate. The effect of these fasteners is discussed further in Section 4.6.2 as it relates to the modal operability of the BAT configuration.

4.6 Constant Height Bleed Air Turbine Configuration

While the performance increase of the constant height geometry was seen over the constant area geometry, the relation between the performance of the stand-alone combustor and the bleed air turbine (BAT) configurations needed to be examined. First, the area changes through the cross-sections of the two configurations can be examined to demonstrate their differences.

As it was designed, the channel plates tested for the BAT configuration featured a constant height combustor section, a transition section from the channel height of the combustor to the required channel height of the guide vanes at 13.9 mm, and a turning section that included the guide vanes and the nozzle or turbine. Channel heights for the BAT were measured at the combustor section. The two channel heights that were similar between the two configurations were at $h_c = 4.5$ mm and $h_c = 6.5$ mm. In addition, the BAT was configured at $h_c = 10$ mm to attempt to detonate at a larger channel height that would provide less expansion aft of the combustor section into the guide vanes.

Figure 79 provides the total area changes for channel heights of 4.5 mm, 6.5 mm, and 10.0 mm in the BAT configuration using the largest nozzle with a radius of $r_n = 24.4$ mm. The effective flow area in the stand-alone combustor was calculated by assuming that the bulk flow was traveling purely radially with negligible tangential velocities. For the BAT configuration, the same radial-only velocity assumption was

assumed through the combustor and transition sections. However, as the flow was turned through the guide vanes, the velocity vectors given through CFD were used by assuming the effective area through the vanes occurred perpendicular to these vectors.

The difference in areas for the combustor section are due to the different initial channel heights, similar to the stand-alone combustor. The transition section also

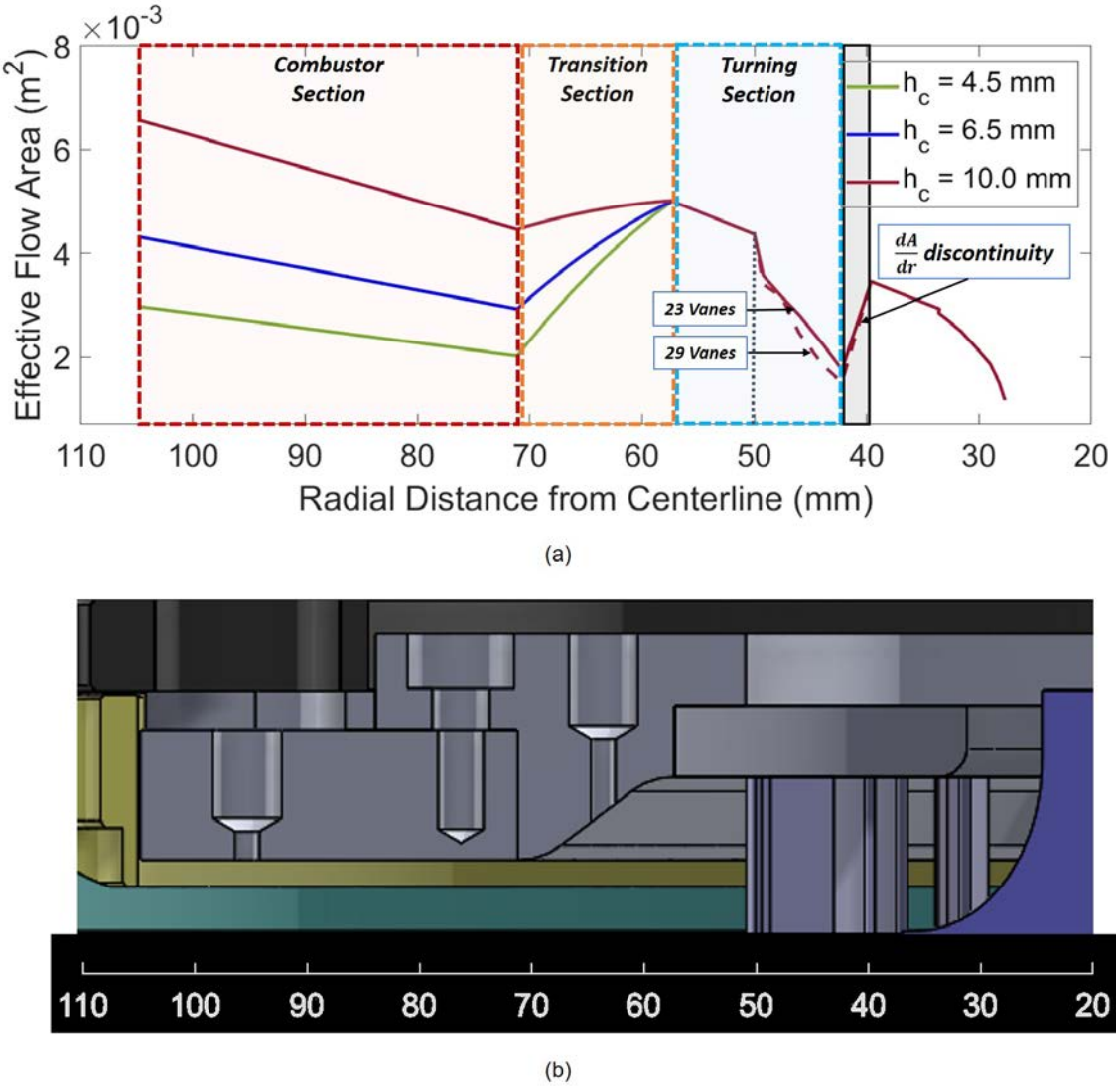

Figure 79. Effective area within detonation chamber for (a) different channel heights of BAT configuration with (b) sample cross-section of BAT configuration.

had different areas since it was dependent on the the initial channel height. All three geometries ended at the same area after the transition section since they all had channel heights of 13.9 mm. The channel height was due to the guide vanes' height which matched the inducer vane height of the proposed radial-inflow turbine (RIT). Overall, the area variation throughout the configuration was not ideal compared to the stand-alone combustor configuration, but attempted the same confinement in the initial constant height section to improve operability while in the BAT configuration.

Closer views of the area variations in the different sections can help examine the differences for each of the channel heights tested. Figure 80 provides the area variation of the BAT configuration through the combustor and transition sections. The area variation through the combustor section was similar to the stand-alone combustor due to the constant channel heights. In the transition section, the area increased since the channel height increased at a greater rate than the radial length of the transition section allowed. The transition section was constrained by the channel height of the combustor section, the required height of 13.9 mm dictated by the guide vanes for the RIT, and the 57 mm radial quartz disk that was used to provide a window into the guide vanes. As seen in the converging-diverging stand-alone combustor geometry at $h_c = 4.5$ mm, which featured a constant height leading to a slight area increase as the flow turned, performance and operability for these area changes was not preferred over a continuously converging section. To maintain a constant area throughout the transition section, the transition section would have to start earlier in the flow, limiting the amount of the constant height combustor, and this would only be possible for $h_c = 10.0$ mm due to the size of the RRDE. Therefore, the desired function of these transition sections was to increase the channel height with minimal losses created by the flow expansion while providing the combustor section as long of a constant height section as possible.

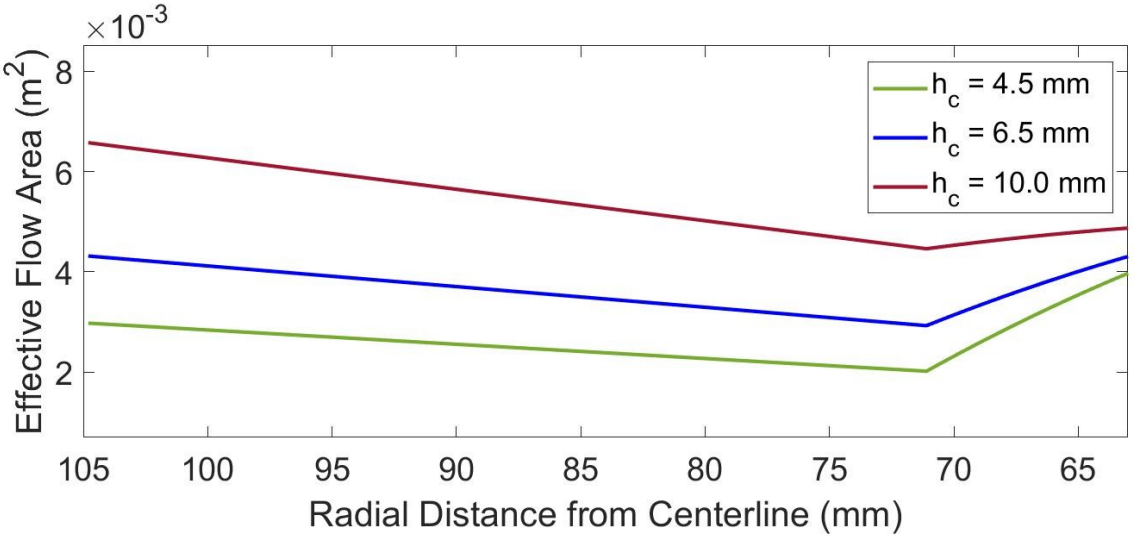

Figure 80. Effective area within combustor and transition sections of turbine channel plate for different channel heights.

While the area variations through the stand-alone combustor provided a constant change in area as the flow traveled radially inward, the inclusion of the guide vanes prevented this simple trend in the BAT configuration. The difference between the stand-alone combustor and BAT channel plates are given in Figure 81a for the two smaller BAT channel heights designed. The changes in the area between the configurations was from the transition and turning sections. From approximately 70 mm to 50 mm from the centerline, where the flow expands until it reaches the guide vanes, it can be seen that there was an opportunity to decrease the area change by having the transition section lead right into the guide vane rather than 6 mm before the guide vane inlet. This 6 mm was given to provide a ledge for the quartz ring to adhere to within the transition channel piece. Therefore, the transition section could redesigned without optical access to stretch the radial length for transition to provide less expansion. Figure 81b provides the area change for the current BAT channel pieces and the previous, constant area turbine channel plate. Previously, it was noted that the increase of the channel height from 4.5 mm to 6.5 mm for the constant area geometry

changed the operability so that the turbine configuration failed to detonate at most test conditions. Based on the area variation, this change in operability was most likely due to the larger volume created.

After the transition sections, the area was the same for all channel heights, which can be seen in Figure 79. The only change through this section depended on the

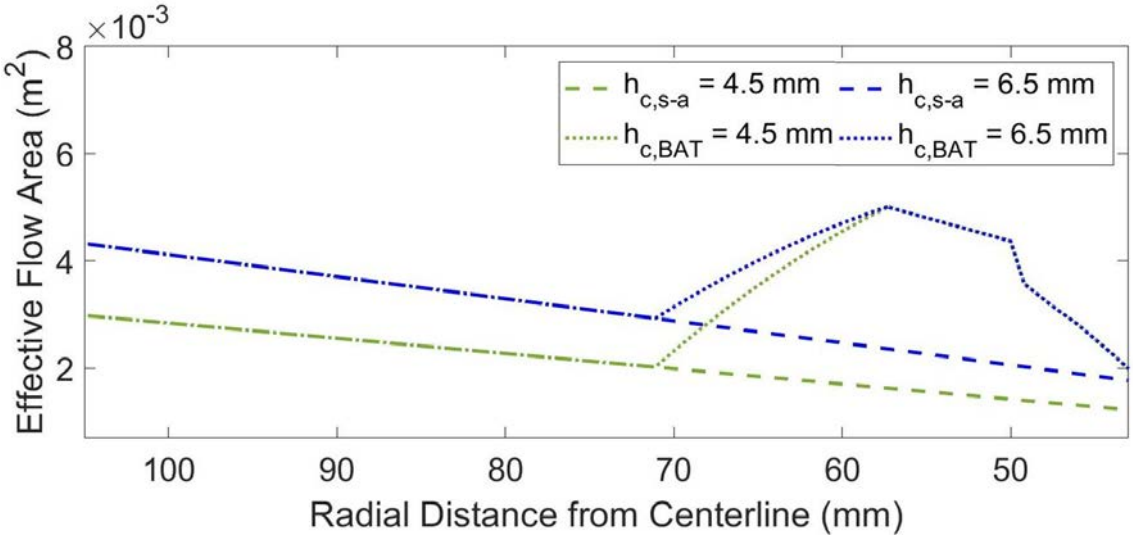

(a)

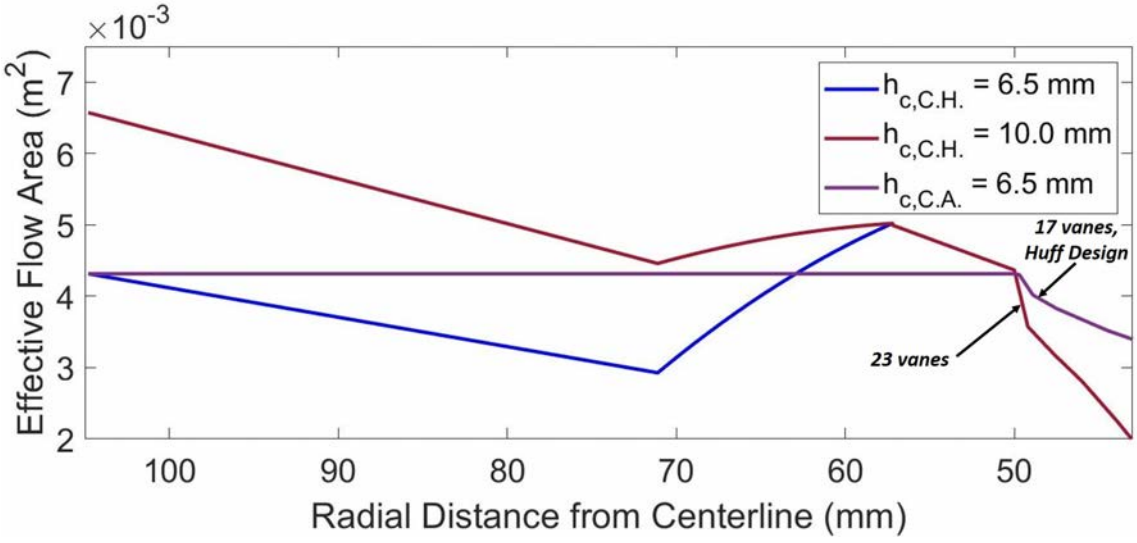

(b)

Figure 81. Comparison of effective area in BAT configuration to (a) stand-alone combustor and (b) constant area turbine channel.

number of guide vanes used. Figure 82 provides the difference in the area variation for the 23 guide vanes compared to the 29 guide vanes. The area decreased at a constant rate just before the guide vanes at 57 mm through a small section of constant height matching the 13.9 mm channel height dictated by the vanes until 50 mm from the centerline. The greatest difference occurred as the flow initially entered the vanes since the flow saw a greater decrease in area for the 29 guide vane ring. After this, the change in area, as the flow was both turned and continued to travel radially inward, was similar between the two guide vane rings. A large increase in area occurred as the flow exited the guide vanes. This resulted in a discontinuity in Figure 79 since the exact change in area, which was dependent on how much the flow was turned and how the flow for a single passage combined with flow through other passes, was not known. This increase in effective area also would occur if a turbine was in place since there is a section aft of the guide vanes where the flow combined without any blockage in area due to the vanes. For the nozzle-BAT configuration, which was used to provide the area changes in Figure 79, the choked condition existed at the exit plane since that was still the location of the smallest effective area.

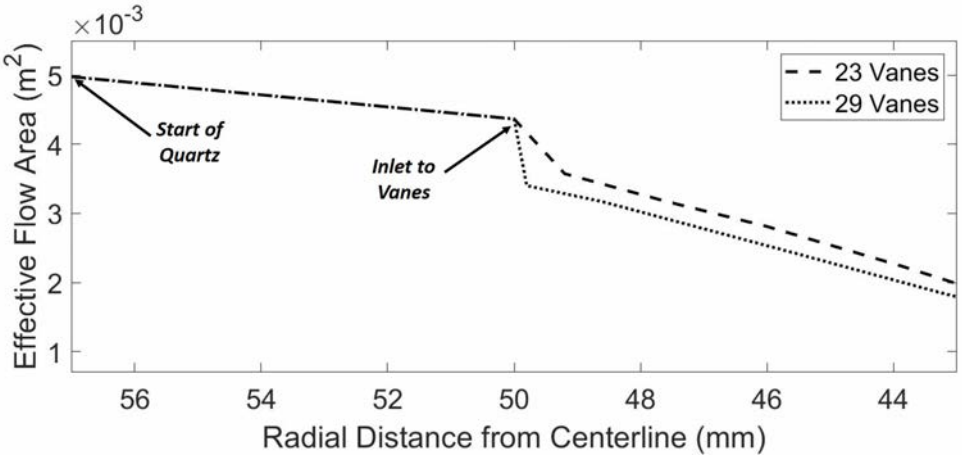

Figure 82. Effective area through guide vanes for the 23 and 29 guide vane rings of BAT configuration.

4.6.1 Operation of BAT configuration with Guide Vanes and Nozzle

The BAT configuration was tested with both the 23 and 29 vane rings with the largest nozzle available, with a radius of $r_n = 24.4$ mm, to simulate blockage from an RIT. While the turbine was not used to determine which vane ring would perform best, the operability and detonation chambers were observed to quantify the device's operation with each ring. This configuration was tested with the quartz disk to perform TFP during testing. The flow rate was set to approximately 0.32 $\frac{kg}{s}$ to match the flow conditions tested by Huff et al. [4] with the constant area BAT RRDE, which was determined on the selected turbocharger's operating map given by Garrett [34]. The operation of the constant area BAT RRDE is given in Figure 83, with successful detonative modes achieved at 75 $\frac{kg}{m^2 s}$ at $\Phi = 0.60$ and and acoustic mode at $\Phi = 0.50$. The flow rate of 0.32 $\frac{kg}{s}$ corresponded to different mass fluxes for the three constant channel heights tested. For $h_c = 10.0$ mm, the mass flux was nominally 50 $\frac{kg}{m^2 s}$. The 6.5 mm channel height had a mass flux of 75 $\frac{kg}{m^2 s}$, matching the constant area BAT configuration, while the 4.5 mm channel height had a mass flux of 100 $\frac{kg}{m^2 s}$.

First, the 10.0 mm channel height was tested. The smaller variation of area across the transition section created the most ideal channel height of the three tested. This larger channel height was not tested for the stand-alone combustor since the flat channel plate was designed based on the constant area geometry's success at channel heights of 4.5 mm and below. The flat channel plate was re-manufactured to provide a 6.5 mm channel height based on its success at smaller channel height, though the channel plate was not modified further due to the depth of the existing fasteners and pressure ports. Therefore, while not fully configured as a flat channel plate, the 10.0 mm channel height was tested without guide vanes.

The 10.0 mm channel height was tested at $AR_t = 0.20$ with the $r_n = 24.4$ mm

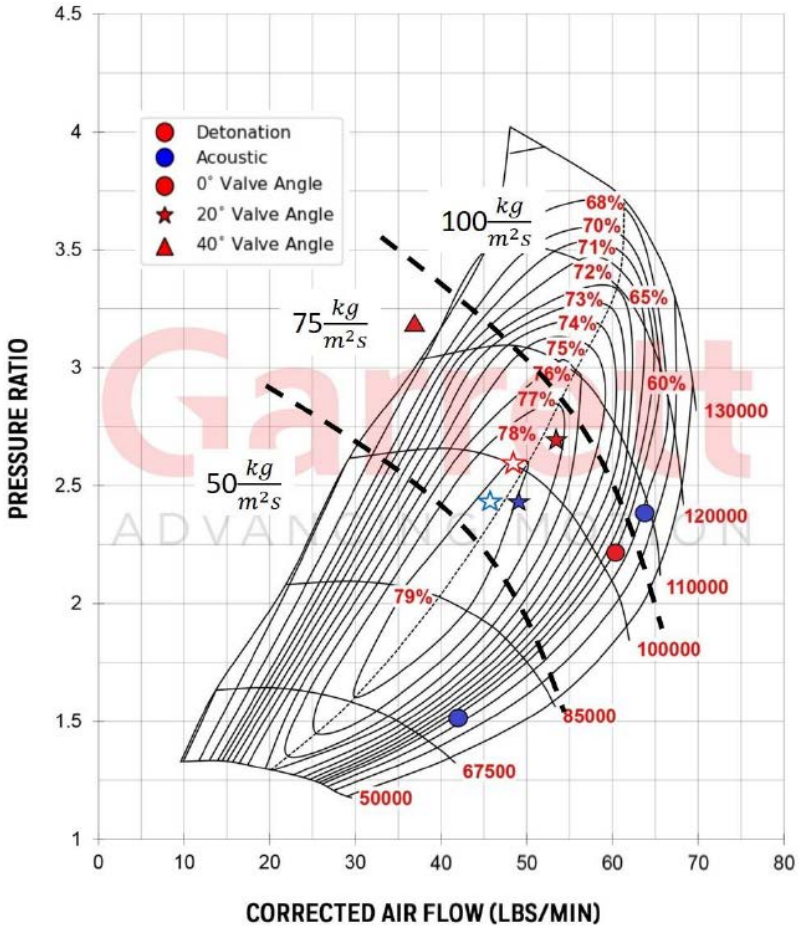

Figure 83. Compressor map from testing of constant area BAT [4].

nozzle and without the guide vanes at $\dot{m}'' = 50\frac{kg}{m^2 s}$ at equivalence ratios between 0.50 and 1.0. The device experienced two different modal operability at this relatively low mass flow rate. An acoustic mode was observed at an equivalence ratio of 0.50. The frequency of this mode was observed to be around 1.9 kHz. The acoustic mode was determined based on the sinusoidal shape of the ITP signals, shown in Figure 84, which was observed by Huff et al. [4] to correlate to an acoustic mode in contrast to a detonation mode that would feature a sharp pressure spike followed by a relaxation section before another sharp pressure spike.

When the equivalence ratio was increased to a value between 0.6 and 1.0, multiple

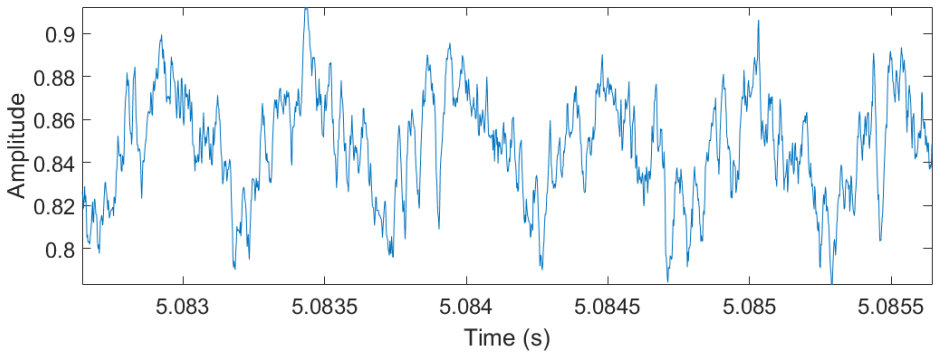

Figure 84. Transient ITP measurement showing an acoustic mode at 1.9 kHz for $h_c = 10.0$ mm, $\Phi = 0.50$.

waves were observed. The transient response of the ITP is given in Figure 85a. Multiple frequencies, given in the FFT plot in Figure 85b, were observed during the test, with the highest frequencies observed at 2.4 kHz and 5.8 kHz for $\Phi = 1.0$. These frequencies occurred at the same time throughout the test as shown in the spectrogram. However, there was no phase angle correlation between the two ITPs at the lower frequency despite its stronger amplitude, and an approximately 135° phase angle difference at 5.8 kHz. This is shown in Figure 85c which provides the cross-correlation between the two offset ITPs. The lower frequency was seen in the ITP signals at a larger time scale and could be due to a continuous acoustic mode operating at both ITP locations in conjunction to the detonative mode. Based on the higher frequencies, cross-correlation, and pressure spikes given in Figure 85a, a dominant three wave mode was assumed for the device when operating for $\Phi = 0.6 - 1.0$, with the observed wave frequency increasing from 5.3 kHz to 5.8 kHz with increasing equivalence ratio. However, the ITPs signals were unable to provide insight as to how the acoustic mode at 2.4 kHz operated with the detonative mode.

With the 10.0 mm channel height characterized without the guide vanes, both the 23 and 29 guide vane rings were tested. First the 23 guide vane ring was examined. Unlike the geometry without the guide vanes, the higher three wave frequency was not

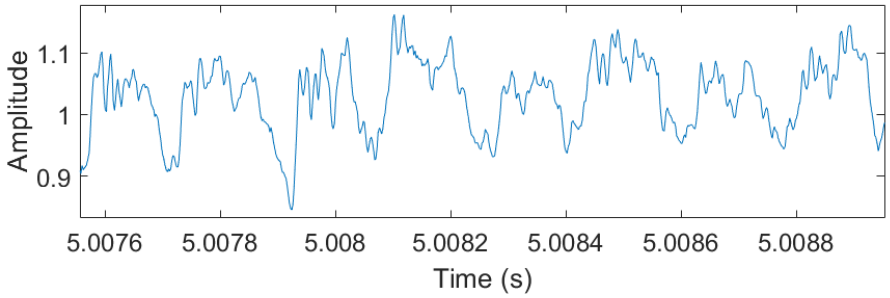

(a)

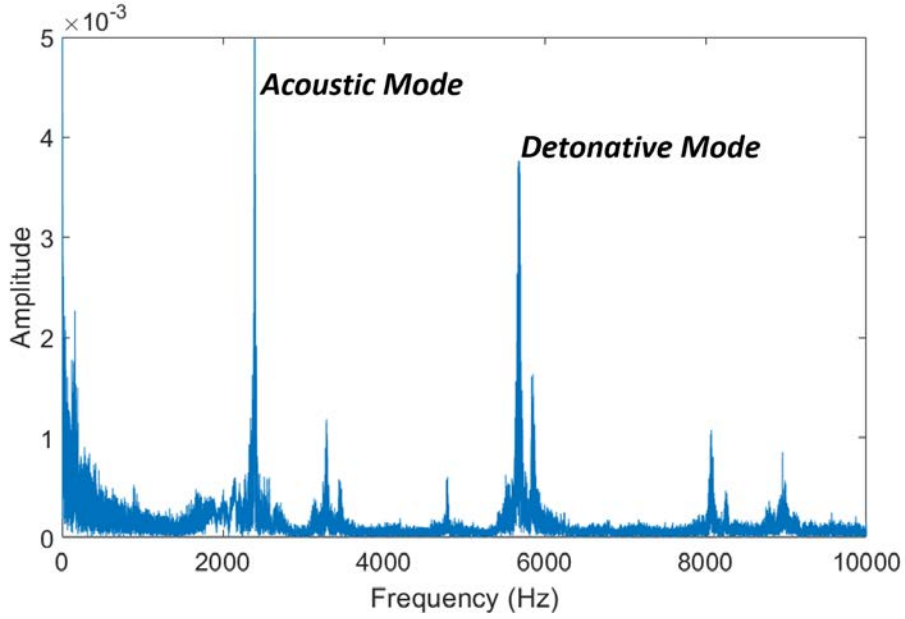

(b)

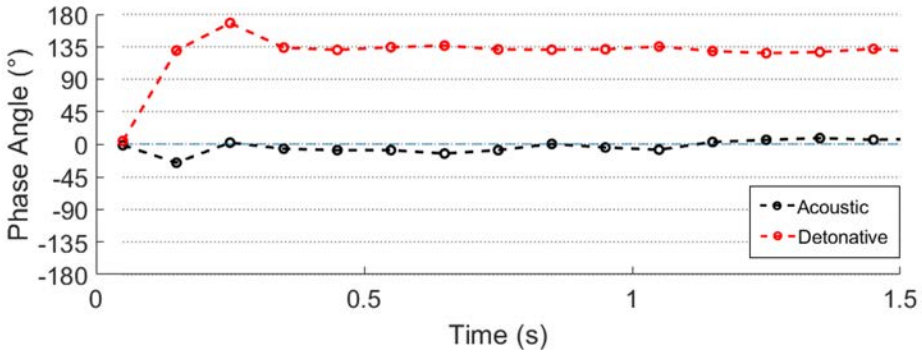

(c)

Figure 85. ITP measurements providing (a) transient signal, (b) FFT, (c) cross-correlation for both acoustic (2.4 kHz) and detonative (5.8 kHz) modes for BAT Configuration at $h_c = 10.0$ mm, $\Phi = 1.0$ with no vanes.

observed for most of the tests. Similar to the no vane geometry, multiple dominant frequencies given in Figure 86a around 1.5 kHz and 4.6 kHz were observed. Unlike the no vane geometry, the lower frequency did provide a correlation, given in Figure 86b, between the two ITPs. The cross-correlation between the two ITPs at 1.5 kHz provided phase angles close to 45°, but closely examining the pressure signals given in Figure 86c show acoustic mode operation. The higher frequency did not correlate to a three wave mode since there was a lack of correlation between the two ITPs with no pressure spikes of significant magnitude at this frequency, seen in Figure 86d.

However, at equivalence ratios greater than 0.6 for the 23 guide vane ring, initial pressure rises were seen when the device first started before it relaxed to its steady state operation. This is seen in the CTAP measurements given in Figure 87a for the 10.0 mm channel height using the 23 guide vane ring at a higher equivalence ratio of 1.0. Using the spectrogram of the same test, given in Figure 87b, the device initially operated at a three wave mode before transitioning into the previously observed acoustic mode. The three wave detonation mode was confirmed through the cross-correlation between the two ITPs which provided a phase angle close to 135°. In addition, the pressure signal from the ITP, shown in Figure 87c, provides sharper pressure rises rather than the sinusoidal behavior seen in Figure 86c. However, due to the limited time the device operated at this three wave mode, the detonation wave mode was unable to sustain itself before it transitioned to an acoustic mode. The initial detonation was able to establish immediately after ignition since the device had a full amount of reactant flow already pressurized within the chamber. As soon as the detonation propagated and began consuming the reactant flow, the device was unable to provide a large enough reactant fill for the large channel height and chamber volume, leading to the acoustic mode until fuel shut off.

The 29 guide vane provided similar operation to the 23 guide vane ring. At

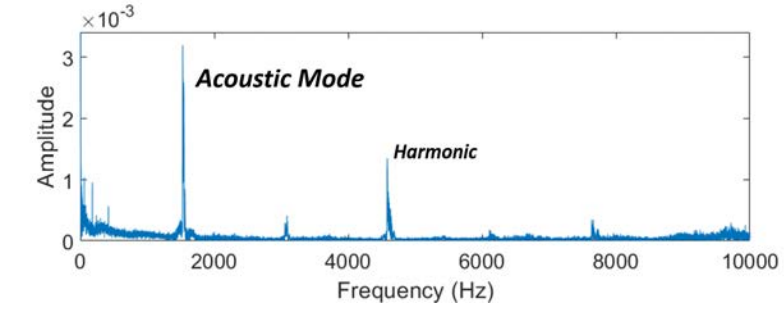

(a)

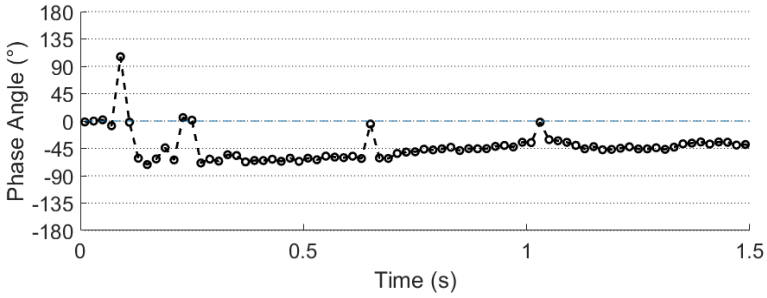

(b)

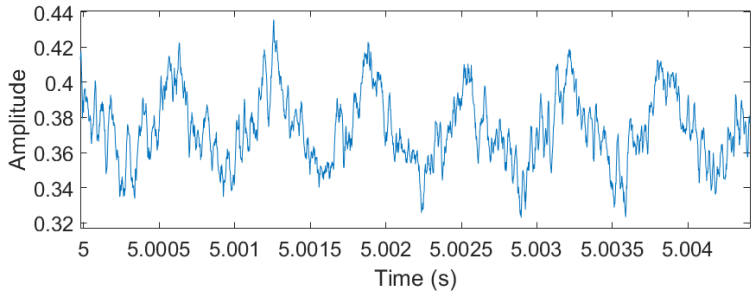

(c)

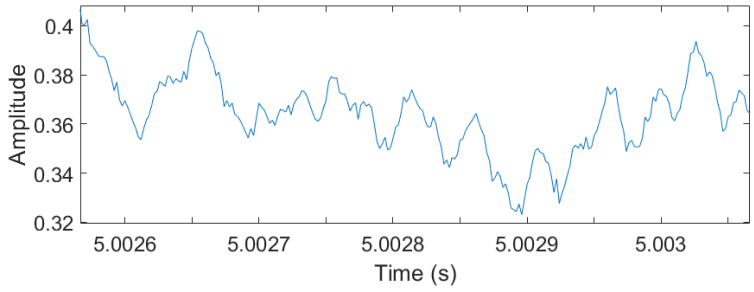

(d)

Figure 86. ITP measurements providing (a) FFT, (b) cross-correlation, (c) transient signal, and (d) focused transient signal for BAT configuration at $h_c = 10.0$ mm, $\Phi = 0.6$ with 23 guide vane ring.

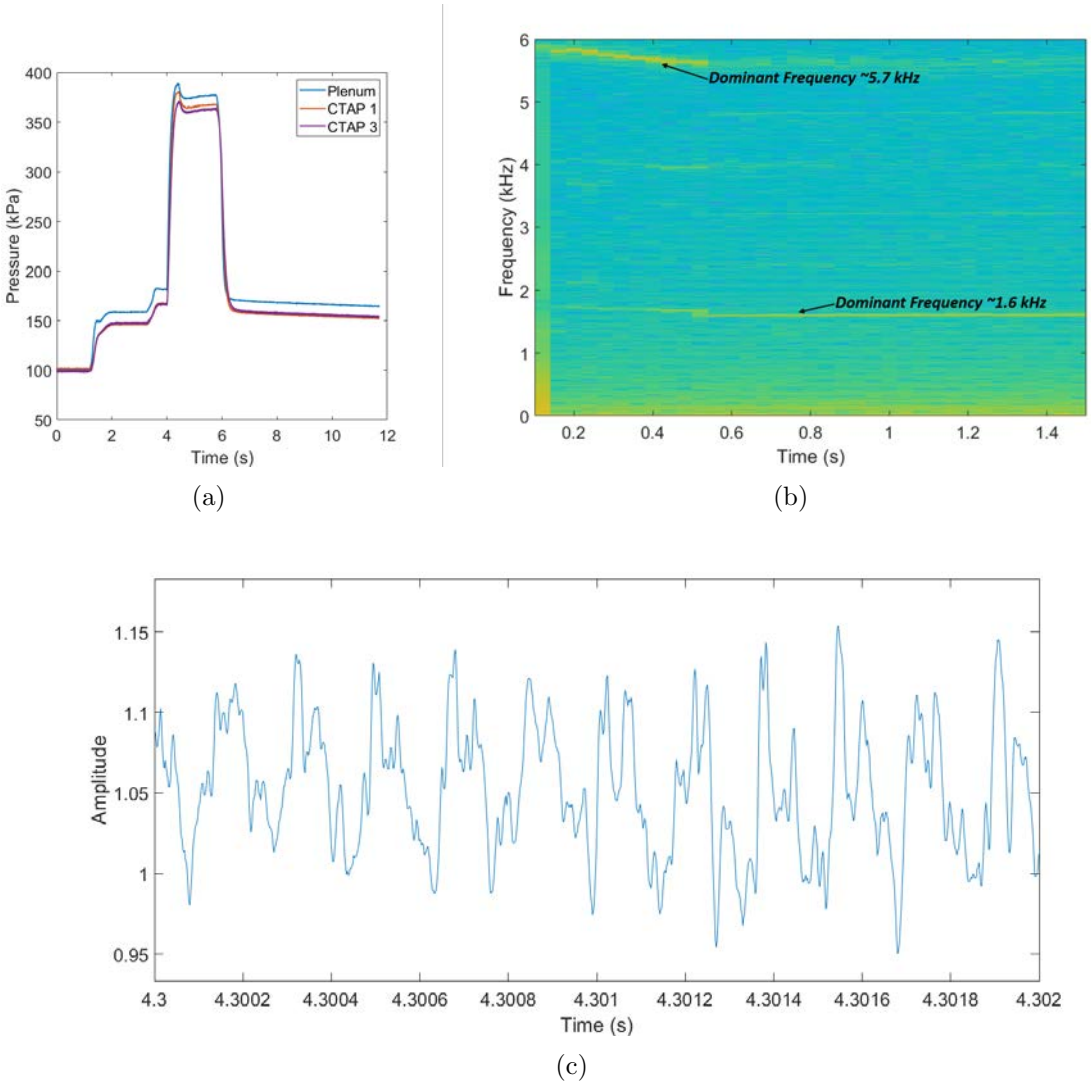

(a) (b)

(c)

Figure 87. Pressure measurements for BAT configuration at $h_c = 10.0$ mm, $\Phi = 1.0$ with (a) CTAP, (b) spectrogram, and (c) transient ITP signal.

equivalence ratios of 0.5 and 0.6, only the acoustic mode at 1.5 kHz was observed, with the three wave mode appearing at the beginning of operation when the device was tested at higher equivalence ratios of 0.7 to 1.0. Furthermore, the frequencies at both the three wave and acoustic modes were similar between the two vanes designs, suggesting similar detonation responses for the two geometries. The exact nature of the acoustic mode was not confirmed at the time of this study. With cross-correlations suggesting a one-wave operation, the small pressure spikes proliferating through the

pressure signal also suggests multiple wave or counter-propagating modes occurring. High-speed visualization into the detonation chamber was not performed for the given hardware, and the quartz disk above the guide vanes did not provide the proper access into the detonation chamber to determine the nature of the mode.

Figure 88a provides example CTAP measurements within the plenum, combustor section, and transition section for the 10.0 mm channel height without vanes. The location of these CTAPs, as discussed in Section 3.3.2, were at radial distances of 9.5 cm, 8.3 cm, and 6.4 cm from the centerline. Relatively stable operation was observed, which could be due to the higher throat height compared to smaller channel heights at the same throat area ratio of $AR_t = 0.20$. Figure 88b provides example CTAP measurements for the 23 guide vane ring at the same mass flux and equivalence ratio shown in Figure 88a, with CTAP measurements for the 29 guide vane ring given in Figure 88c. With the vanes, the device reached similar pressure behavior compared to the no vane geometry. However, for a given equivalence ratio of 0.6, there is a 7% increase in the channel pressures during operation for the 10.0 mm channel height without the vane to the 23 guide vane ring, with a smaller 2% average pressure increase for all CTAPs from the no vane geometry to the 29 guide vane ring.

The change in pressure could be a function of the entire system's response to the different pressure loss areas within the device. Without the vane, the device functioned similar to the stand-alone combustor configuration. When the vanes were added, the system, which was still operating at the same upstream pressure at the air and fuel sonic nozzles and ambient conditions downstream of the device, stabilized the pressure loss provided by the guide vanes by maintaining a larger pressure within the detonation chamber.

Between the two guide vane rings, the difference within the detonation chamber could provide insight on the efficiency of the ring. The pressure decreased an average

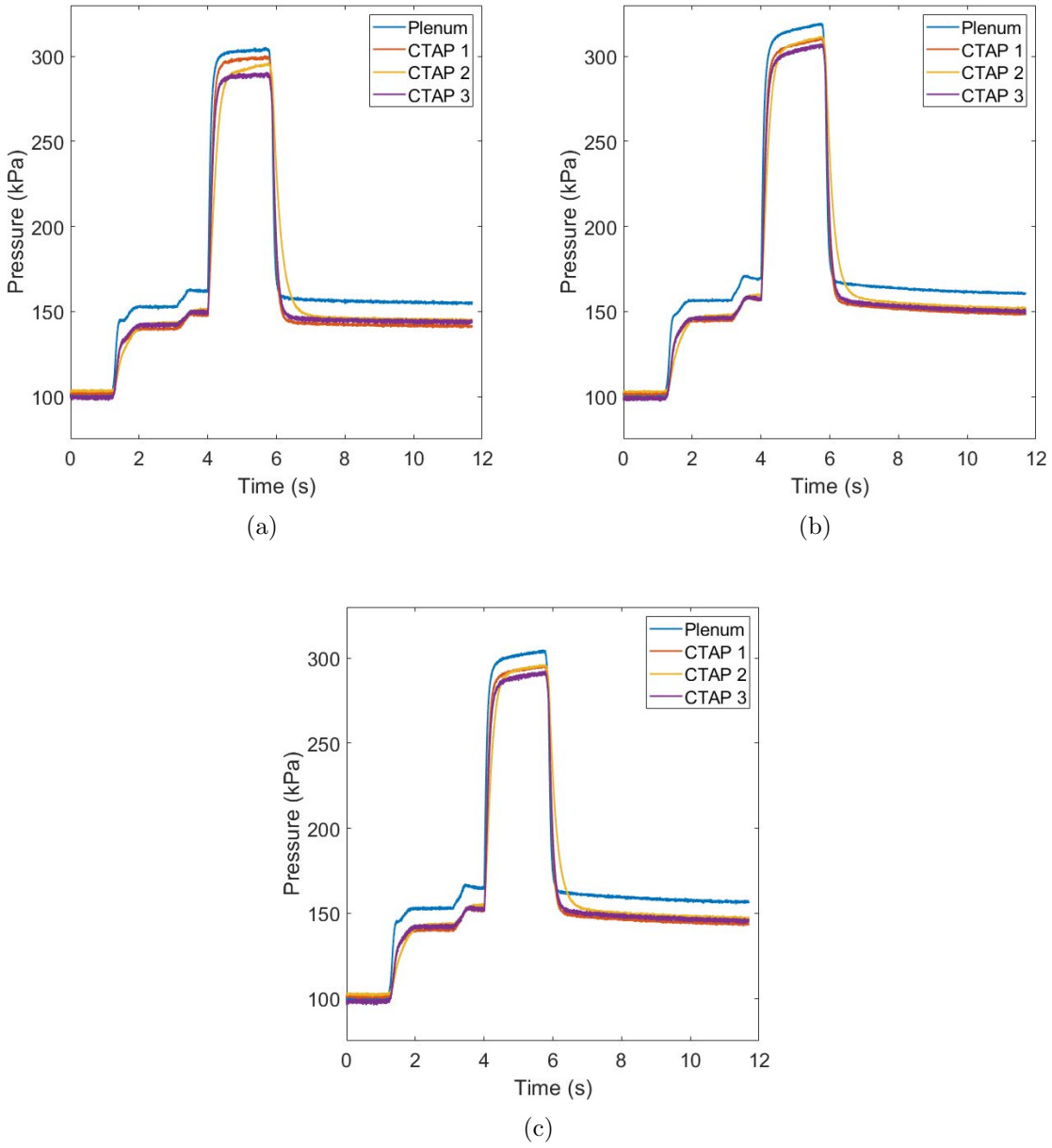

Figure 88. CTAP measurements for BAT configuration at $h_c = 10.0$ mm, $\Phi = 0.6$ with (a) no vanes, (b) 23 vanes, and (c) 29 vanes.

of 5% from the 23 vanes to the 29 vanes. When considering the pressure constraints at the sonic nozzle and from the ambient environment, the CTAP measurements suggest that the 29 guide vane performed better. The lower pressures seen with the higher number of vanes suggested that the 29 vane ring provided a more ideal turning of the

flow. However, the lack of the RIT can affect this assumption since the turned flow would be forced to correct from its circumferential direction downstream of the nozzle and lead to more losses for greater turning. Therefore, to best determine which guide vane ring is more efficient, a turbine is needed and should be considered for future investigations.

Detonation confinement was not confirmed for the 10.0 mm channel height. Initial confinement could have occurred during the detonative mode due to the larger difference between CTAP 1 and CTAP 3 as shown in Figure 87, but during acoustic operation, there was no distinction. As discussed, flowfield visualization into the detonation chamber was not attempted. While the CTAP measurements given in Figure 88 show decreasing static pressures for the acoustic mode as the distance from the centerline decreases, the differences between the CTAP measurements are within the error bounds of the measurements. The total pressures could not be calculated since the relatively high compressible area ratios for h_c10.0 mm, which provided $\frac{A}{A^\star} > 4.2$ at CTAPs 1-3, did not produce subsonic Mach number solutions using Equation 11. Therefore, the total pressures for the BAT configuration were not considered.

To attempt detonative modes rather than the acoustic modes seen in the larger channel height, the BAT was reconfigured to the 6.5 mm channel height with a throat area ratio of $AR_t = 0.20$. The mass flow rate was kept the same to match the required flow of 0.32 $\frac{kg}{s}$ for the proposed RIT; this resulted in a mass flux for $h_c = 6.5$ mm of 75 $\frac{kg}{m^2 s}$.

Both vane designs were tested for the 6.5 mm channel height geometry. Similar frequencies were observed for the same test conditions between the two vane rings. However, the pressures were approximately 6% less for the 29 guide vanes compared to the 23 guide vanes, similar to the differences seen for the 10.0 mm channel height.

The ITP measurements given in Figure 89 were indicative of a detonative oper-

ation. Figure 89a shows a dominant frequency around 5.9 kHz for the entirety of the run. Based on wave mode analysis conducted for the stand-alone combustor, this frequency range was indicative of a three wave mode operation. Furthermore, examining the transient signal given in Figure 89b shows sharp pressure spikes that also suggest a detonative mode. A cross-correlation between the two signals provided a phase angle shift greater than 135°, suggesting that while a three wave mode was dominant, it could also have been influenced by other counter-propagating modes or acoustic mode transitions between changing wave directions that were seen in the high-speed visualization of the stand-alone combustor.

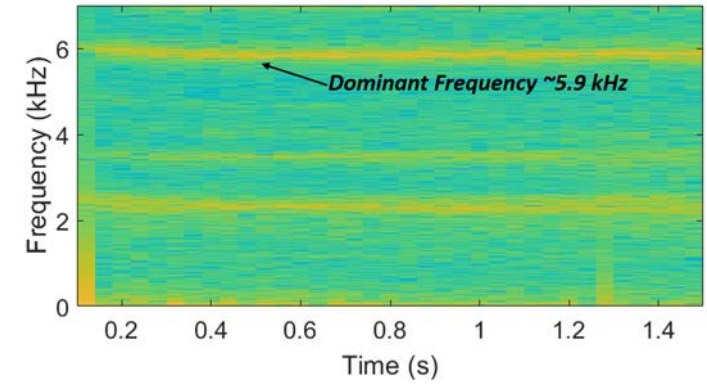

(a)

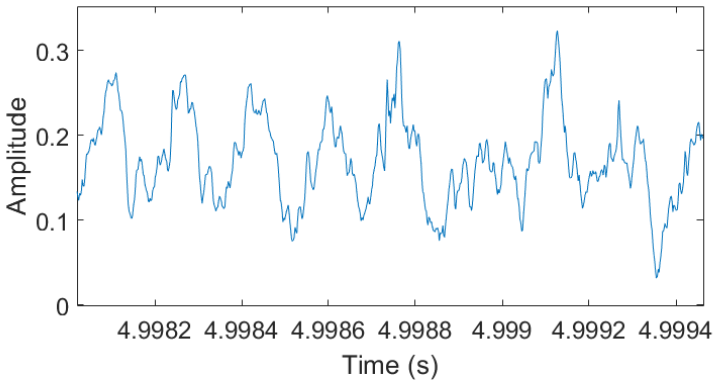

(b)

Figure 89. ITP measurements with (a) spectrogram and (b) transient signal for BAT configuration at $h_c = 6.5$ mm, $\Phi = 1.0$ with 23 guide vane ring.

Figure 90 provides the CTAP measurements for this smaller channel height. It should be noted that CTAP 2 experienced higher lag due to instrumentation error of the tubing, though the correct pressure was eventually measured after one second into the run. The larger channel height had steady operation, while $h_c = 6.5$ mm experienced increasing pressure within the plenum and channel. These pressures were higher for the smaller channel height, which could be a function of the different operational mode or the smaller area within the chamber. Confinement can be assumed for $h_c = 6.5$ mm based on the larger difference of pressure between CTAP 1 and CTAP 2. In addition, the plenum and CTAP 1 were coupled during operation, with a smaller difference of pressure between the two, suggesting that a detonation event occurred at a radially outboard location. This coupling, also seen when the stand-alone combustor was tested at $AR_t = 0.50$ as discussed in Section 4.3, occurred for the smaller channel height despite the larger throat given for $h_c = 10.0$ mm.

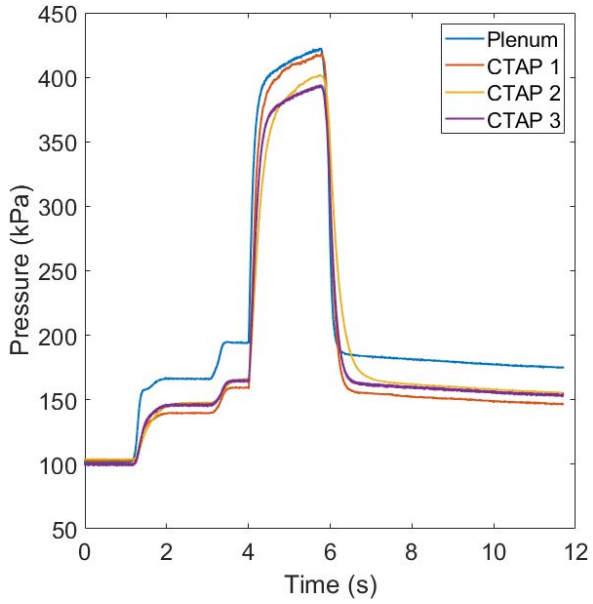

Figure 90. CTAP measurements for BAT configuration at $h_c = 6.5$ mm, $\Phi = 1.0$ with 23 guide vane rings.

4.6.2 Off-Design Mass Flow Testing in BAT Configuration

While the guide vanes and the BAT configuration were designed based on the flow rate of 0.32 $\frac{kg}{s}$ based on the proposed RIT's operating map [34] selected by Huff et al. [4], this turbine was not tested in the constant height RRDE due to the inability of the device to produce the desired single wave mode seen in the stand-alone combustor configuration. Since the turbine was not integrated with the device, the RRDE in BAT configuration was tested at different mass flow rates that could promote a more consistent detonation At $h_c = 10.0$ mm, the mass flux was increased from $50\frac{kg}{m^2s}$ to $75\frac{kg}{m^2s}$ and $100\frac{kg}{m^2s}$, while the mass flux was modified for $h_c = 6.5$ mm from $75\frac{kg}{m^2s}$ to $50\frac{kg}{m^2s}$, $100\frac{kg}{m^2s}$, and $125\frac{kg}{m^2s}$. To reach the higher fuel flow rates needed at the higher mass fluxes, the sonic nozzle for the fuel line was increased from 2.3 mm (0.089 inches) to 3.2 mm (0.125 inches).

At the larger channel height, the device continued to operate at the acoustic mode with a frequency between 1.5-1.6 kHz that was seen when tested at $50\frac{kg}{m^2s}$. In addition, the initial three wave mode that transitioned into this mode continued for most test conditions. In one test case, shown in Figure 91, the device operated at a detonative mode throughout the entire operation. This was accomplished by lowering the flow rate down to $50\frac{kg}{m^2s}$ again at $\Phi = 1.0$. The change in operation could be a function of the devices possible higher temperature, since this test was conducted after the sweep of the higher mass fluxes. Furthermore, the larger fuel sonic nozzle could have influenced the ability for the device to provide continuous fuel flow during operation to maintin the three wave mode operation.

While continuous detonative operation was achieved at $h_c = 6.5$ mm, changing the mass flux was tested to attempt to achieve a single wave mode. This was not achieved when the mass flux was varied from $50\frac{kg}{m^2s}$ - $125\frac{kg}{m^2s}$ and equivalence ratios between 0.50 - 1.0. An area variation was attempted as well by increasing the throat

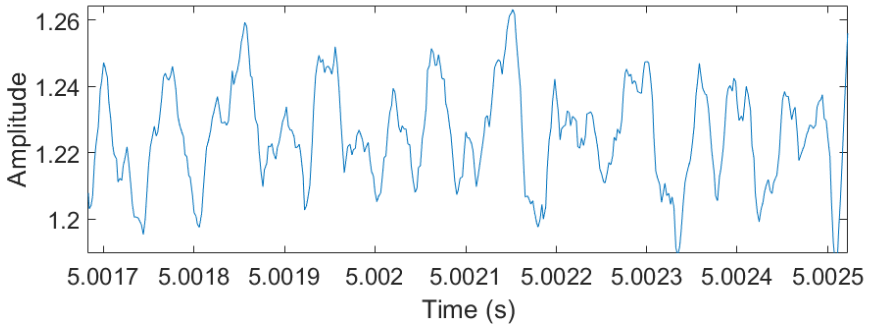

Figure 91. Sample ITP transient signal for BAT configuration at $h_c = 10.0$ mm, $\dot{m}'' = 50\frac{kg}{m^2 s}$, $\Phi = 1.0$.

to $AR_t = 0.31$ which matched the throat height of $h_t = 2.0$ mm that provided $AR_t = 0.20$ for $h_c = 10.0$ mm. This did not change the operation of the device at the same test conditions, with frequencies between 5.7-5.9 kHz seen at the three wave modes that occurred for all tests.

4.7 Thin-Filament Pyrometry on Guide Vanes in BAT Configuration

Thin-Filament Pyrometry (TFP) was performed in conjunction with the operability testing given in Section 4.6. The experimental setup and calibration for TFP is given in Section 2.4.3. Examining TFP within the RDE provided an opportunity to examine the transient response of the temperature due to passing detonation waves, as well as an average temperature downstream from a detonative event. In addition, this research was used to provide recommendations for future implementation of TFP measurements within axial RDEs.

The filaments were placed downstream of the detonation location to separate them from the extreme thermodynamic conditions produced by the detonation. However, there was still concern over the survivability of the filaments due to the impulse from the start of the reactant flow through the device, the initial detonation given by the pre-detonator, and the passing oblique shock waves attached to the detonation

wave during operation. Therefore, the first objective with testing the RRDE with TFP was to determine the filaments survivability within the device. This was tested before consistent operation was recorded by the Phantom high-speed camera.

To test the ability of the filaments to withstand RDE testing, three filaments were installed at three different vane passage in the 23 guide vane ring for a total of nine filaments throughout the vane ring. In one passage, the filaments were installed through the holes in the vanes and were glued fixed in their location. In the other two passages, the filaments were installed through the holes without being glued in place, with one passage having longer filament lengths so that the filament stretched across the vane passages on either side of the main channel to be observed.

The filaments were visually examined after various points in the test procedures. First, cold flow through the device was initiated to test the filament's response to the impulse of the flow. Of the nine total filaments, seven survived these initial tests, with one glued and one free-hanging filament being removed. This loss was most likely due to improper installation or prior fatigued filaments. Next the pre-detonator was fired into the device multiple times, with all filaments surviving this shock. Finally, test runs were conducted. After the first test, the filaments that were glued were destroyed while the remaining free-hanging filaments survived. It was assumed that the constraint created by the glue created larger stresses on the filaments compared to the free-hanging filaments. Therefore, for subsequent testing and for the results reported in this section, the ceramic glue was not used to hold the filaments in the vanes. During testing, the filaments occasionally failed to survive for the entire operation, but it was assumed that the remains of broken filaments still attached to the vanes did not affect the function of the device.

With the survivability of the filaments during start-up and operation established, the filaments were then used to determine the approximate temperature value during

operating at the inlet of the guide vane. These values were compared to the Chapman-Jouguet (CJ) detonation temperatures provided by NASA CEA [32] based on initial conditions of 300 K and 140 kPa seen in the detonation chamber during cold flow for $h_c = 6.5$ mm at 0.43 $\frac{kg}{s}$. The 6.5 mm channel height was used for this comparison since it led to detonative conditions in contrast to the largely acoustic modes for $h_c = 10.0$ mm. The flow rate was used since it provided the largest range of temperatures.

Figure 92 provides the average results from TFP that provided detonative modes, as well as results from the CEA analysis. The TFP value is given as the mean temperature between 0.95-0.98 seconds after the detonation was initiated. The TFP provided temperatures of approximately 68%-79% of the CJ detonation ideal temperatures. Furthermore, the same trend of increasing temperature with increasing equivalence ratio was seen in the TFP data. The difference between the temperatures was expected due to the difference in an ideal detonation as performed by the CEA program compared to the detonation experienced in the RDE; this difference was also seen in the actual pressure rise experienced compared to the burned gas pressures given by CEA. Future analysis should consider the expansion, which can also be calculated through CEA, to provide a complete comparison between what was measured and what was expected. In addition, rather than considering CJ values, the actual pressure as measured by the CTAP should be used upstream of the expansion calculation, and the pressure variation measured by the ITPs could provide expected temperature changes downstream of the expansion at the filaments. These calculated temperature variations could then be compared to the temperature response recorded by the TFP.

Next, the transient response of the filament was examined. As noted in Section 4.6.1, the BAT 10.0 mm channel height failed to provide a continuous detonative event but rather an acoustic mode at steady state operation. A detonative mode

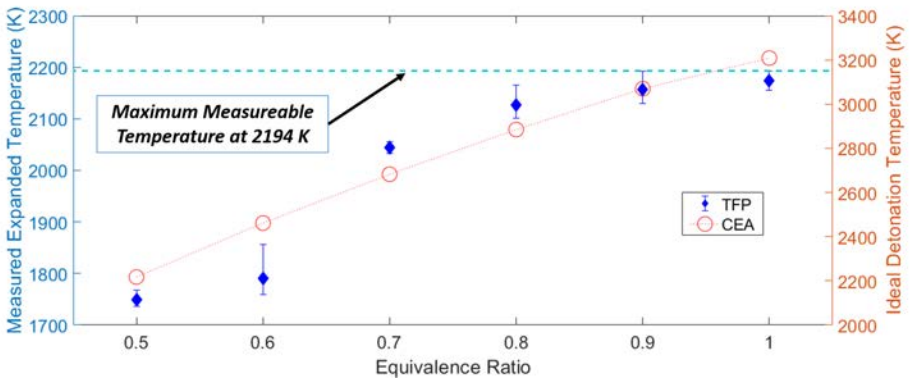

Figure 92. TFP temperature results compared to Chapman-Jouguet detonation temperatures.

did occur at the beginning of higher equivalence ratio runs. This transition from the three wave mode to the acoustic mode seen in the ITP, shown in Figure 87b and given again in Figure 93a, was also captured through the filament's temperature response given in Figure 93b. There was a maximum difference of 93 K observed between maximum and minimum temperatures observed for the test given in Figure 93b. This difference was reflected in the raw images shown in Figures 93c and 93d that represent the intensities recorded by the camera during detonative and acoustic conditions, respectively. The higher heat release apparent in the beginning of the test could be a function of the detonative condition or due to a possibly greater local equivalence ratio initially. However, since the temperature decrease followed the change in operating condition, which was also seen for other tests with initial detonative conditions, it can be assumed that a higher heat release occurred due to the detonative mode compared to the acoustic mode.

In addition, the frequency response of the temperature at the acoustic mode was observed through the filament. This is given in Figure 94, which provides the FFT of the ITP and TFP results for the same test for $h_c = 10.0$ mm at $\dot{m}'' = 50\frac{kg}{m^2 s}$ and $\Phi = 1.0$. While the device operated at two frequencies during the period that TFP

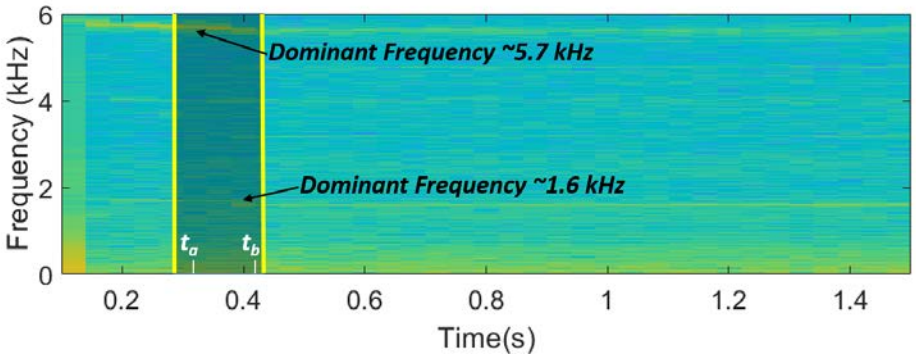

(a)

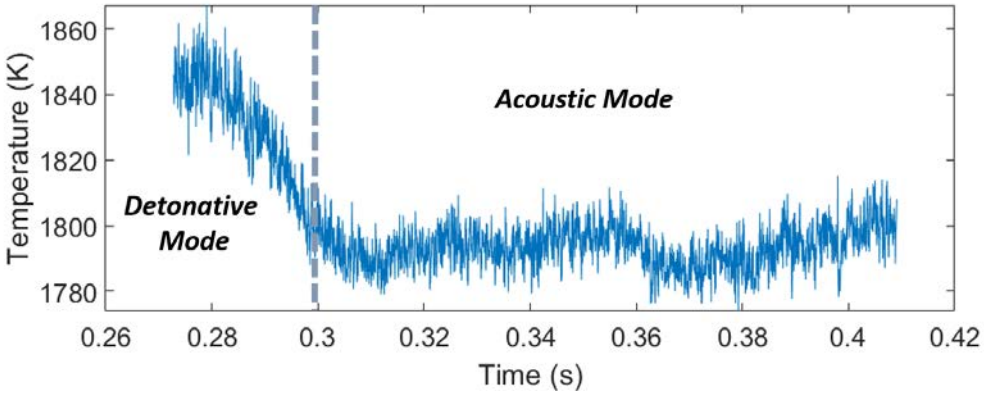

(b)

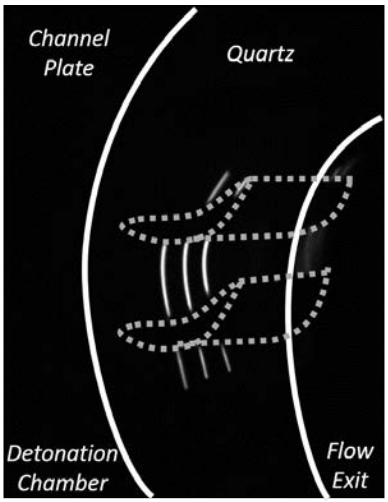

(c)

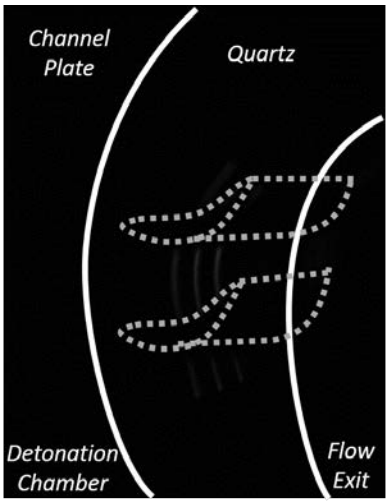

(d)

Figure 93. Results of $h_c = 10.0$ mm at $\dot{m}'' = 50\frac{kg}{m^2 s}$, $\Phi = 1.0$ through (a) spectrogram of ITP, (b) TFP response over time, (c) raw image at $t_a = 0.29$ s, and (d) raw image at $t_b = 0.36$ s.

was performed, as shown in Figure 93, the 5.7 kHz frequency was not observed in the TFP due to the lower number of samples taken during the detonative operation of the RRDE. The agreement of the FFT to provide a dominant frequency of 1.6 kHz for both the ITP and TFP suggests that filaments at 150 μm diameter are able to provide frequency responses at the low frequency range of RDE operation.

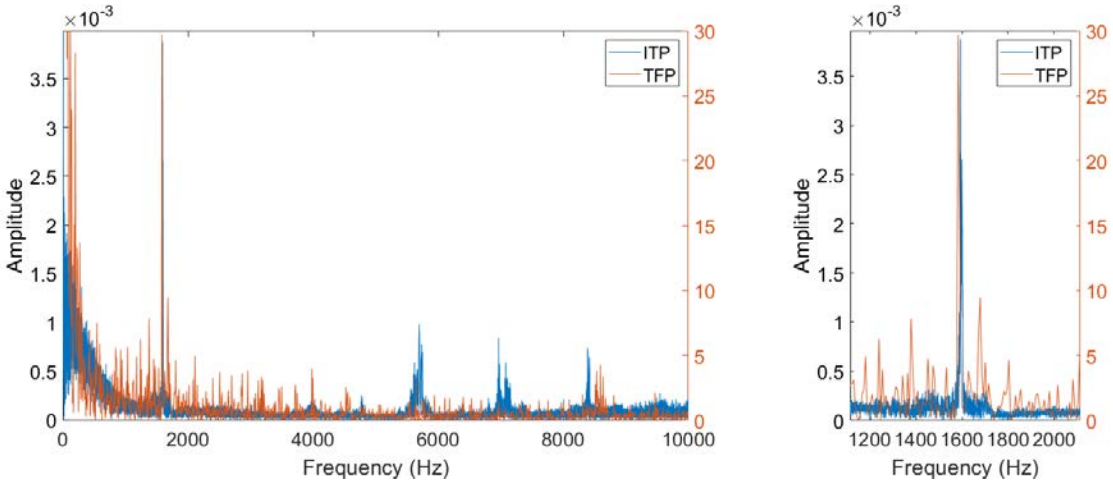

Figure 94. FFT of both ITP and TFP for $h_c = 10.0$ mm at $\dot{m}'' = 50\frac{kg}{m^2 s}$, $\Phi = 1.0$ at 1.6 kHz.

To determine whether the TFP would respond to the detonative modes that operated at almost 6 kHz, TFP data using $h_c = 6.5$ mm was examined. This channel height was used since it provided detonative conditions rather than the acoustic modes seen for $h_c = 10.0$ mm. Figure 95 provides the temperature response measured during detonative conditions for $h_c = 6.5$ mm. Temperature changes that followed the trend provided in Figure 93 did not occur for $h_c = 6.5$ mm. This further suggests that the change from a higher to lower temperature was indicative of a transition from the detonative mode to an acoustic mode.

During multiple tests, the maximum temperature recorded for $h_c = 6.5$ mm approached and presumably exceeded the temperature limits set during calibration. Figure 95a shows an example of TFP data that experienced clipping. The maximum

measurable temperature of 2194 K was restricted based on the maximum luminosity with the selected camera settings and optics. Despite the clipped data, these temperatures were still used for analysis since there were large temperature variations below the maximum measurable limit to provide frequency analysis. The clipping affected the average temperatures, and this was taken into consideration when comparing to expected values.

Figure 95b represents temperature signals that were recorded below 2194 K which were used for statistical analysis compared to acoustic temperature signals. In addition to the overall higher temperatures of the detonative conditions, the temporal variation was greater compared to the acoustic modes. When the temperatures were recorded during an acoustic mode, the average temperature range was 17 K during steady operation. For detonative modes, the average range was 117 K, with a maximum range of 147 K recorded without considering temperature responses that contained random spikes of intensity. Therefore, it can be assumed that detonations, in addition to providing larger pressure rises reflected in the ITP measurements, provide larger fluctuations in the temperature compared to acoustic modes.

Figures 96 and 97 provide the FFT of the ITP and TFP results during detonative modes experienced for $h_c = 10.0$ mm and $h_c = 6.5$ mm, respectively. In Figures 96a-b The TFP provided a frequency peak at 5.7 kHz which was between the dominant frequencies of 5.6-5.7 kHz seen for in the ITP. However, these amplitudes were close to other frequencies within this range. This provided uncertainty whether the peaks were congruent with the detonative mode since the TFP signals were near the noise floor, giving low signal-to-noise ratios. The resolution of the TFP could be improved through a faster capture rate greater than the 22,000 fps that were used initially since the detonative mode was approaching the Nyquist frequency.

Figure 96c shows the low resolution of the TFP compared to the ITP for this

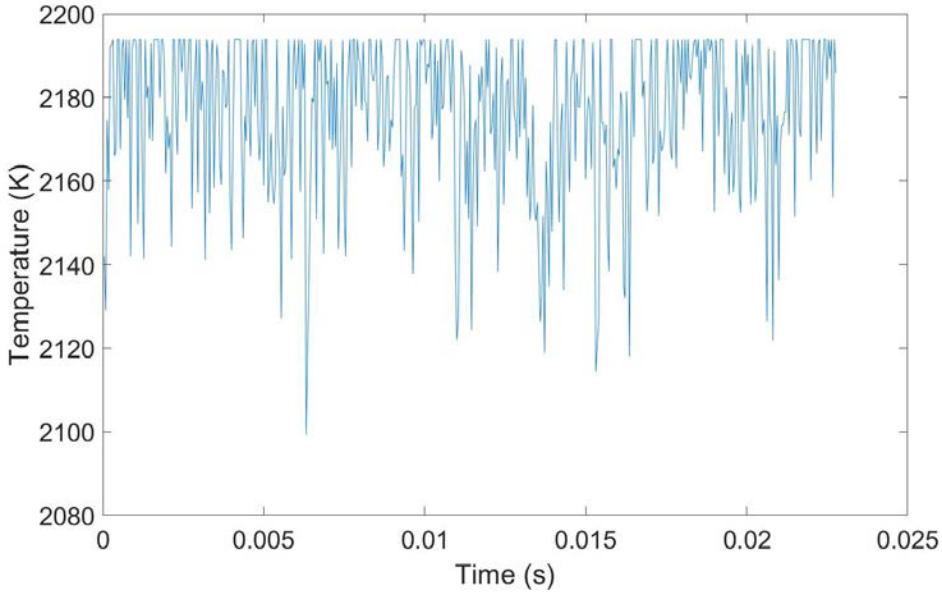

(a)

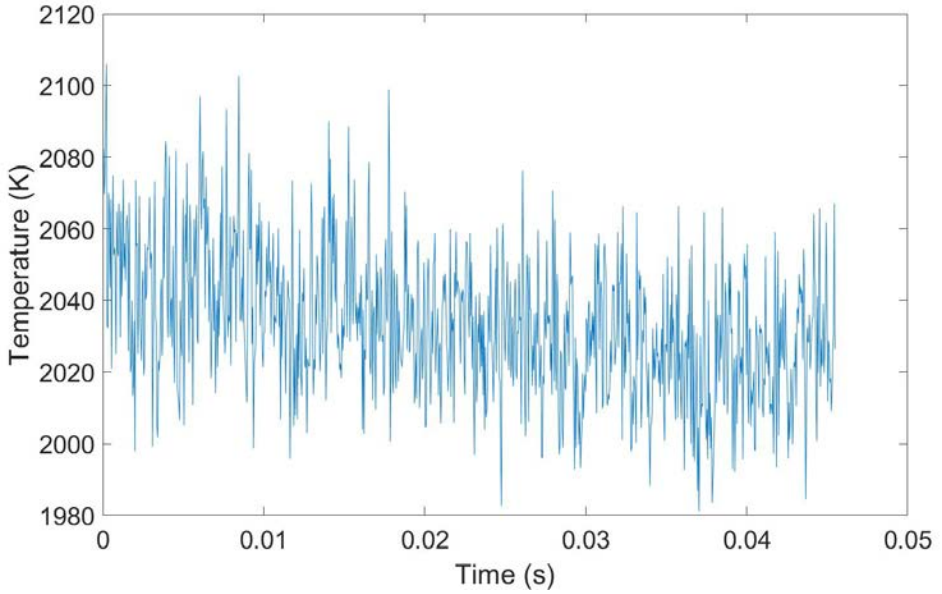

(b)

Figure 95. Temperature response for detonative conditions for $h_c = 6.5$ mm at (a) $\dot{m}'' = 50\frac{kg}{m^2 s}$, $\Phi = 1.0$ and (b) $\dot{m}'' = 100\frac{kg}{m^2 s}$, $\Phi = 0.7$.

relatively high frequency. The transient response of the TFP results given in Figure 97 is shown in Figure 95a and was not focused in due to the clipped signal. The capture rate can be increased by decreasing the camera's resolution. Doing so would

still provide the same calibration equations. Despite the precision error, it was shown that the filaments were able to provide frequency response as high as 5.9 kHz for detonative operation in addition to the low frequency acoustic modes.

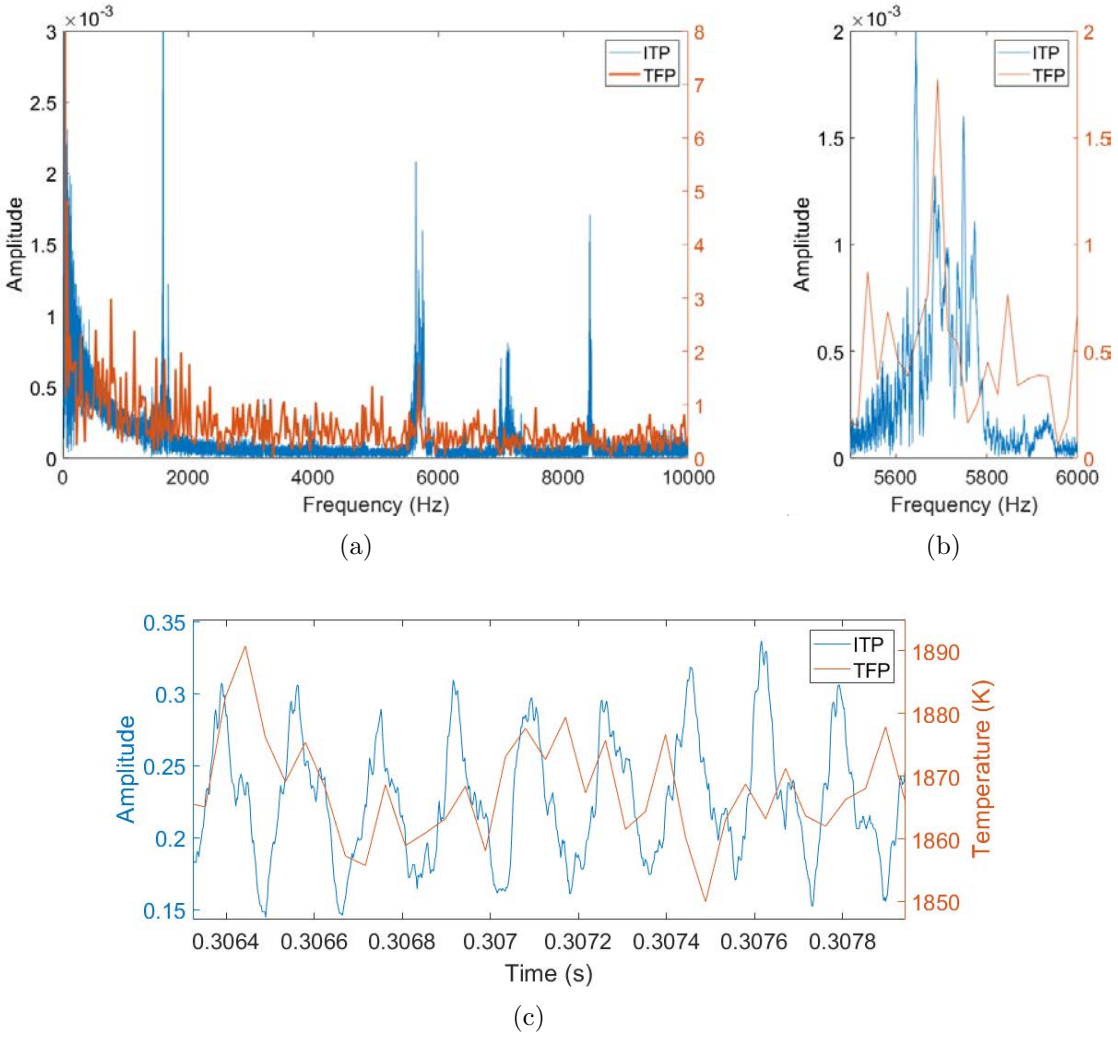

Figure 96. BAT with $h_c = 10.0$ mm at $\dot{m}'' = 50\frac{kg}{m^2 s}$, $\Phi = 1.0$ at 5.7 kHz with (a-b) FFT and (c) transient high-frequency response of both ITP and TFP.

4.8 Influence of Hardware Redesign on Operability

It was noted that the assembly of the guide vanes into the base plate could have affected operation and prevented a single wave mode. To provide visualization for

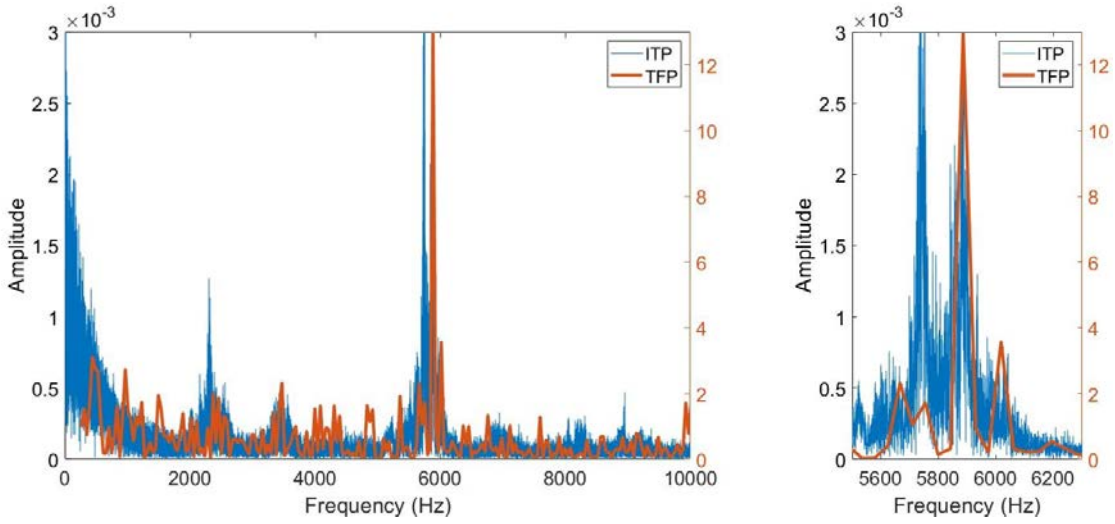

Figure 97. BAT with $h_c = 6.5$ mm at $\dot{m}'' = 50\frac{kg}{m^2 s}$, $\Phi = 1.0$ with (a) FFT and (b) focused frequency range at 5.9 kHz of both ITP and TFP.

TFP into the guide vanes for the BAT configuration, the vane rings were attached to a modified base plate that was tested with both the stand-alone combustor and BAT configurations. Shown in Figure 98, the eight fasteners that attached the rings to the plate were exposed to the flowfield 6.4 cm from the centerline of the device in the transition section, providing potential pockets of recirculation of detonated products that could have tripped the detonation wave to provide three waves, acoustic modes, or multiple counter-propagating waves. The validity of this observation was not directly tested since the exposure to the fasteners was necessary to detach the vane rings to switch between the two designs or to attach filaments between the guide vanes.

In addition to the modal changes suggested by the ITPs, testing with the polycarbonate channel plate after the base plate was modified also experienced transitions to higher wave modes. During the high-speed visualization testing conducted for the stand-alone combustor given in Section 4.5.2, the device conducted differently at similar channel heights and flow conditions between clear channel plate Tests 5 and 9.

Test 5 produced one and two waves while Test 9 produced only three waves. Tests 7-10 were tested after the modifications were made to the base plate. Therefore, these tests could have also been affected by the new holes created downstream of the detonation.

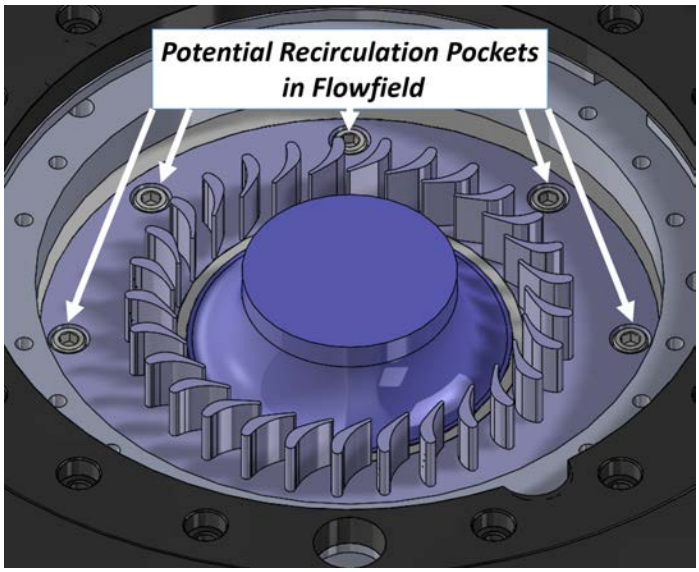

Figure 98. CAD view of vane ring fasteners in BAT configuration.

To attempt to alleviate the influence of these potential recirculation pockets on the modal operability of the device, all exposed fastener holes within the detonation chamber were covered with ultra-high temperature RTV silicone, as shown in Figure 99. In addition to the fasteners holding down the vane rings, the fasteners closest to the throat which held the fuel mounting ring were also covered. The influence of these holes near the throat could not be compared to a baseline without the fastener holes, unlike the mounting ring holes, since they have always been exposed based on Huff's initial design [5]. The RTV was cured with a handheld torch and allowed to rest for three days before testing. However, the sealant did not survive past the initial series of tests, with the fasteners being exposed after the first test. Future implementation of this method should pursue a high-temperature cure in a ceramic oven to ensure

that the RTV has set on the components before testing within the RDE.

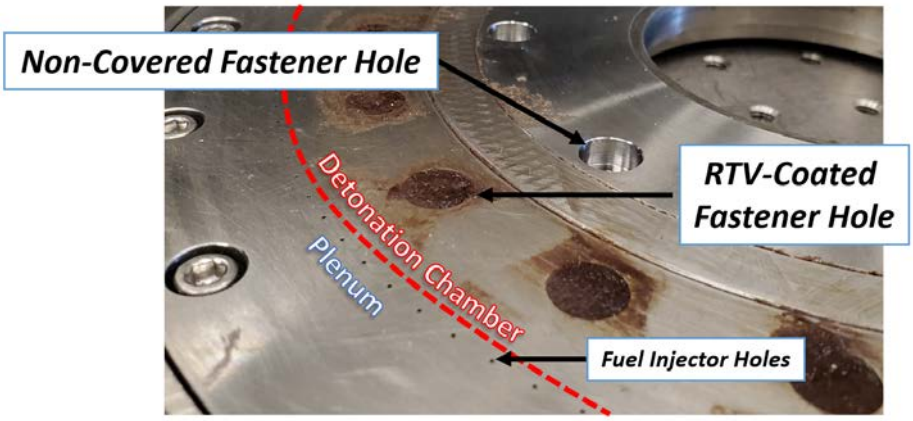

Figure 99. Fasteners holes in detonation chamber to be covered with RTV.

The first test with the RTV sealant was conducted at $\dot{m}'' = 100\frac{kg}{m^2 s}$ and $\Phi = 0.7$ at $h_c = 6.5$ mm. Since this was the only test that had all the holes covered during part of operation, this test can be used to examine if the fasteners provided an influence on the operation and whether the RTV would prevent transitions. Previously, before the base plate was modified to hold vane rings, this test condition operated at a one wave mode. With the modifications and the sealant, the frequency response, shown in the spectrogram in Figure 100a, showed that a transition of operating modes occurred 0.8 seconds into operation. The cross-correlation given in Figure 99b, as well as the relative frequency bands, suggest that this test transitioned from a one wave mode to a three wave or acoustic mode. The one wave mode was not seen past 0.2 seconds for future tests. Based on the lack of repeatability of operation modes after the base plate was modified, it was concluded that the fasteners holes affected the modal operability. Therefore, a solution should be developed to cover the exposed holes during operation if future testing of the RRDE is desired.

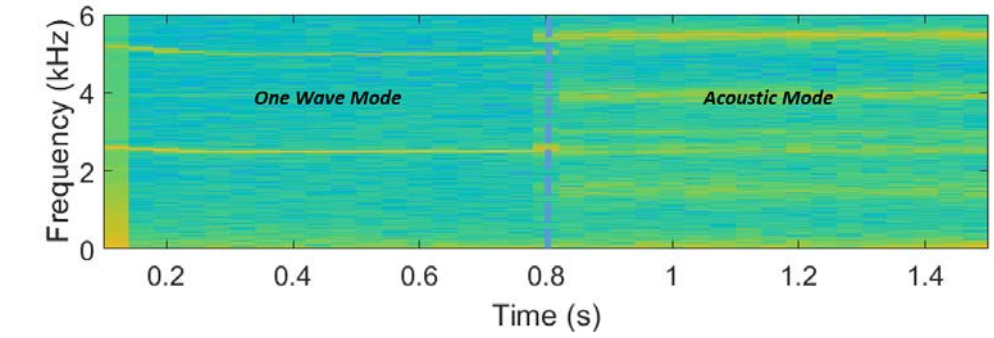

(a)

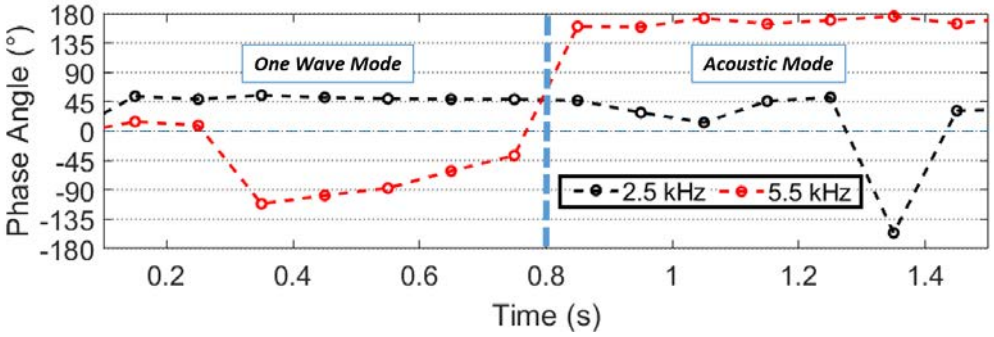

(b)

Figure 100. Mode transition due to fastener holes shown through (a) spectrogram and (b) cross-correlation for the stand-alone combustor with $h_c = 6.5$ mm at $\dot{m}'' = 100 \frac{kg}{m^2 s}$, $\Phi = 0.7$.

V. Conclusion

Current research in Rotating Detonation Engines (RDE) strives to provide a more thermally efficient power unit compared to systems with deflagrative combustors. This is accomplished by operating a thermodynamic denotative combustion cycle that ideally features pressure-gaining combustion compared to the constant pressure Brayton cycle seen in modern gas-turbine engines. In addition, RDEs excel at providing rapid power response with minimal start up times. The Radial Rotating Detonation Engine (RRDE) provides a more compact form of this pressure-gain combustion compared to typically researched axial RDEs since the reactants and detonated products flow radially before exhausting axially through a nozzle or radial turbine. This flow configuration provides an opportunity to employ the RRDE as a thermodynamically efficient, rapid response, compact auxiliary power unit (APU) for use onboard aircraft where space is constrained and transient energy dense output is required.

Previous studies of the RRDE was distinguished by a constant area detonation chamber created by an increasing channel height as the radial distance from the centerline decreased [3]. As a stand-alone combustor, the device successfully operated at a variety of mass fluxes and equivalence ratios while observing multiple modes with one, two and three waves [3]. In addition, when the RRDE was implemented with a radial-inflow turbine, the larger area required as a result of the required guide vane height and constant area geometry resulted in limited operability of the RRDE with relative low thermal efficiencies, less than 40% [4]. Further research was conducted on the constant area RRDE with a clear channel plate that determined that detonation confinement occurred for multiple wave modes that propagated at an outer radial location within the detonation chamber [6]. This promoted the current study to investigate detonation confinement in the RRDE.

This RRDE was reconfigured to feature a flat channel plate that led to a constant

height, decreasing area detonation chamber geometry. The device was tested using H_2-Air at mass fluxes between $50\frac{kg}{m^2s}$ and $200\frac{kg}{m^2s}$ and equivalence ratios between 0.5 and 1.0. The current research of the constant height RRDE was conducted on two separate configurations for the device. The configuration that used a nozzle and a flat channel plate without any turbomachinery was considered the stand-alone combustor while the inclusion of guide vanes for a radial inflow turbine considered the bleed air turbine (BAT) configuration.

5.1 Objectives and Results

The first objective was to demonstrate detonation confinement within the outer radial location of the RRDE for all test conditions. The RRDE was reconfigured with a flat channel plate in the stand-alone combustor configuration to create a constant height, decreasing area detonation chamber geometry. This was tested at various geometries with channel heights between 4.5-6.5 mm, throat area ratios between 0.20 and 0.50, and nozzle area ratios between 0.76 and 1.2. The flow conditions were set at mass fluxes between $50\frac{kg}{m^2s}$ and $200\frac{kg}{m^2s}$ and equivalence ratios between 0.5 and 1.0. Detonation confinement was confirmed for all tests through the capillary tube average pressure (CTAP) measurements that showed higher static pressure values at the two pressure ports farthest from the centerline. The confinement occurred despite the size of the detonation chamber, the injector restriction, and the area changes created by the nozzle. In contrast, the constant area RRDE previously tested [3] had higher pressure values at the CTAPs located closer to the centerline, with flowfield visualization demonstrating a variable radial location for the detonation wave in the constant area detonation chamber [6]. High-speed visualization was attempted for the constant height geometry with a clear, polycarbonate channel plate to confirm detonation confinement, but the top plate obscured the main area for the confined

detonation which made finding the exact location difficult to locate. The lack of luminosity within the visible section of the detonation chamber did suggest that the detonation was located toward the outer portion of the device.

The second objective was to determine the modal operability of the constant height geometry RRDE in the stand-alone combustor configuration. While the top plate of the device obscured the main detonation event during the high-speed visualization tests with the clear channel plate, the chemiluminescence from the secondary burning and secondary shocks attached to the main detonation wave were visible. This visual data, in addition to infinite tube pressure (ITP) measurements, were used to determine the operability of the constant height geometry at channel heights of 4.5, 5.5, and 6.5 mm. At $h_c = 4.5$ mm, the constant height geometry had an increase in the number of waves compared to the constant area RRDE at $h_c = 4.5$ mm at the same flow conditions. As tested by Huff [5], the constant area RRDE saw an increase in wave modes as the mass flux increased or equivalence ratio decreased. This trend continued for the constant height RRDE, with a greater number of three wave modes occurring in the constant height RRDE at $h_c = 4.5$ mm compared to the constant area RRDE at $h_c = 4.5$ mm. These three wave conditions occurred at mass fluxes greater than $50\frac{kg}{m^2s}$ and equivalence ratios less than 0.8, though it was not shown whether these three wave modes were a full detonative mode or an acoustic mode. Increasing the constant channel height to 5.5 mm saw a decrease in three wave modes to equivalence ratios less than 0.7, with no three wave modes observed for the 6.5 mm channel height. Despite the initial goal of maintaining multiple waves, high-speed visualization suggested that these three wave modes were unstable and transitioned between detonative and acoustic modes. Furthermore, the smaller channel height of 4.5 mm that operated primarily at three waves had unsteady operation due to the inability to use a large enough nozzle to provide a continuously converging area

throughout the chamber.

The third objective was to develop potential pressure gain combustion in the stand-alone combustor configuration that was not previously achieved in the constant area geometry. Pressure gain was not achieved, but the total pressure loss decreased for all constant height geometry tests compared to the constant area geometry. When considering EAP, the constant height channel height of 4.5 mm had pressure loss decreases as high as 75% compared to the constant area geometry at 4.5 mm for similar flow conditions. The 5.5 mm channel height had greater improvements as high as 92% decrease in pressure loss. This suggested that a continuously converging flow area, which was possible for $h_c = 5.5$ mm, increased performance. Compared to the 6.5 mm channel height with the same blockage, the RRDE at $h_c = 5.5$ mm continued to have the highest performance with up to 80% improvement in pressure loss. Increasing the channel height while maintaining a constant throat height showed a 20%-50% depending on the equivalence ratio since the expansion and subsequent pressure loss aft of the throat increased. When the channel height remained constant at 6.5 mm and the throat increased, the larger throat area ratio increased performance by decreasing overall pressure loss by more than 90%. For most tests, a nozzle was used to provide a continuously converging area from the inlet of the detonation chamber to the exhaust. Decreasing the radius of the nozzle from a converging section to a overall converging-diverging section increased the pressure loss by 42% as the choked condition relocated closer within the detonation chamber, showing that moving the minimum area away from the combustion section increased performance.

For the last two objectives, the BAT configuration was explored. The fourth objective was to successfully detonate and maintain detonation confinement within the RRDE with guide vanes. This RRDE configuration with the largest channel height tested of $h_c = 10.0$ mm provided a short duration of detonation at equivalence

ratios above 0.6 before relaxing to an acoustic mode. At $h_c = 6.5$ mm, the device consistently operated at higher frequencies up to 6 kHz, suggesting three wave modes. This occurred at the mass flow rate of 0.32 $\frac{kg}{s}$, required by the desired radial inflow turbine which resulted in mass fluxes of $50\frac{kg}{m^2 s}$ for $h_c = 10.0$ mm and $75\frac{kg}{m^2 s}$ for $h_c = 6.5$ mm. To determine if other off-design flow conditions would lead to detonative conditions for the larger channel height of 10.0 mm, the mass flux was increased up to $100\frac{kg}{m^2 s}$, but the device continued to operate at predominately acoustic conditions. These results provided guidance to redesign the turbine channel to have less area variation upstream of the guide vanes.

The final objective was to determine if thin-filament pyrometry (TFP) is a viable technique to characterize the temperature of the flow downstream of the detonation event and if TFP is able to capture the transient temperature response due to a rotating detonation event. TFP was successfully implemented within the guide vanes and was able to withstand the initial shock of the flow, pre-detonation event, and operation of the device while in a detonative and acoustic mode. Temperature was shown to increase with increasing equivalence ratios from 0.5 to 1.0, with the highest temperature of 2194 K measured during detonative modes at equivalence ratio of 0.9 and 1.0. These temperatures were approximately 68%-79% of the Chapman-Jouguet detonation temperatures, though the filament temperatures were not corrected based on the convective heat transfer from the product gases. The filaments were able to measure fluctuations of the temperature through the flowfield, and the TFP responses showed congruence at both the acoustic modes around 1.6 kHz and the detonative modes up to 5.9 kHz.

5.2 Recommendations for Future Work

The results presented in this document provide initial steps in developing a suitable RRDE for use as a pressure-gain APU. To further accomplish this goal, future research can be conducted to better configure the device. Due to the reactivity of the polycarbonate to the combusted flowfield, a direct correlation could not be made between the flow conditions tested by the steel channel plate and the tests conducted with the polycarbonate, clear channel plate. A quartz channel plate should be used in lieu of the polycarbonate channel plate to both confirm detonation confinement suggested by the CTAPs as well as examine the modal operability at various test conditions. If tested as a constant height RRDE, the quartz plate would have lower production cost due to lower machining requirements and the quartz could be implemented without tapping holes through the plate by using high-temperature Room-Temperature-Vulcanizing (RTV) silicone. In addition to providing a correlation between the ITP data and high-speed visualization, the quartz plate would provide insight on transitions from one and two rotating detonations to the counter-propagating modes that provided similar frequency responses.

A more comprehensive study on the device's Equivalent Available Pressure (EAP) can be performed to provide high confidence for future pressure gain values obtained from the plenum pressure and EAP. One method would be to confirm the assumed choked conditions at the nozzle of the RRDE. This assumption was used in this study to calculate the EAP by using compressible area ratios. Determining the location of the choked point can be obtained by purposefully instrumenting a channel plate to provide thermodynamic properties at locations downstream of the detonation chamber. In addition, thrust can be measured in conjunction to pressure measurements aft of the detonation chamber to calculate EAP as suggested by Kaemming et al. [31].

Next, the BAT configuration should be reexamined to develop a suitable APU. This research provided newly designed guide vanes that increased solidity and turning compared to previous vanes designed by Huff et al. [4]. The RRDE should be tested with a radial inflow turbine using both vane sets to determine the efficiency of this research's guide vanes compared to the constant area's vanes.

The BAT configuration could also be redesigned to make use of the constant height's detonation confinement with the constant area's ability to detonate at lower mass flow rates. A future design could implement both a constant height constraint aft of the throat that leads to a constant area detonation chamber up to the guide vanes. In addition, the guide vanes can be modified to have an increasing vane height so that the expansion from the constant height section to the inlet of the turbomachinery is not as large. If possible, rather than using an off-the-shelf turbocharger, a unique radial inflow turbine could be designed to accept the higher flow rates that are optimized for either the constant height or constant area RRDE. Another solution would be to design the RRDE based on the 0.32 $\frac{kg}{s}$ design flow rate of the off-the-shelf turbocharger. This could be achieved by creating a larger diameter RRDE that has the ability to start at a smaller constant channel height. The larger diameter would allow for a less aggressive expansion due to a longer radial change from the combustion section to the turning section.

With the guide vanes, thinner filaments can be tested to determine if a smaller diameter filament would still be able to survive testing while providing a temperature response at a high enough frequency to respond to multiple waves. In addition, expanding the temperature range to measure temperatures lower than 1710 K and higher than 2194 K would provide responses not seen in this study. This includes the temperature change during start-up and shut-off, as well as higher temperatures that occurred during detonative conditions but were limited to the maximum intensity set

during the calibration. The range could be optimized through the experimental setup of the calibration equipment, the camera location, and the filters and camera settings used.

5.3 Summary

The RRDE successfully demonstrated the use of a constant height, decreasing area detonation chamber created by a flat channel plate. This constant height geometry provided detonation confinement while operating at multiple wave modes. The performance of the device increased compared to the constant area geometry, with the pressure loss decreasing towards potential pressure-gain from the plenum to the area just upstream of the nozzle. While operating with turbomachinery, the RRDE showed less potential for continuous detonative performance, but the device provided trends for future development of an optimized configuration with both constant height and constant area sections. This research allowed for the continued progression of the RRDE as a thermodynamically efficient, rapid response, compact APU.

Appendix A. Thin Filament Pyrometry Calibration and Analysis

The following procedures in this Appendix were created primarily by Dr. Larry P. Goss of Innovative Scientific Solutions, Inc. The calibration, experimental setup, and results were developed through personal communication with Dr. Goss from October 2019 - February 2020, with the discussion provided in Chapter IV created by the author.

Calibration of the Phantom camera as a single wavelength pyrometer was accomplished using a calibrated tungsten filament light bulb. The light bulb was calibrated using the non-optical method described by Izarra and Gitton [41]. The color temperature (at 650 nm) of the lamp as a function of power supply amperage is shown in Figure 101. A secondary optical calibration was carried out using a disappearing filament pyrometer [42] and the results of which showed very good agreement with the non-optical approach [41]. The phantom camera was fitted with a 650 nm filter and the emission from the light bulb captured as a function of the current supplied by a 12 Volt power supply.

The calibrated lamp was placed in the experimental setup such that its emission passed through the same optical path as the thin filament and its brightness was captured as a function of lamp color temperature. The resulting camera calibration is shown in Figure 102 and was used to derive the SiC filament temperature during the RDE operation.

The SiC filament temperature is determined by using the fitted equation shown in Figure 102. The filament temperature is typically lower than the gas temperature due to the heat balance between filament and surrounding gases. An estimate of the heat balance can be obtained with a knowledge of the gas velocity and composition. This correction factor was not included in this analysis.

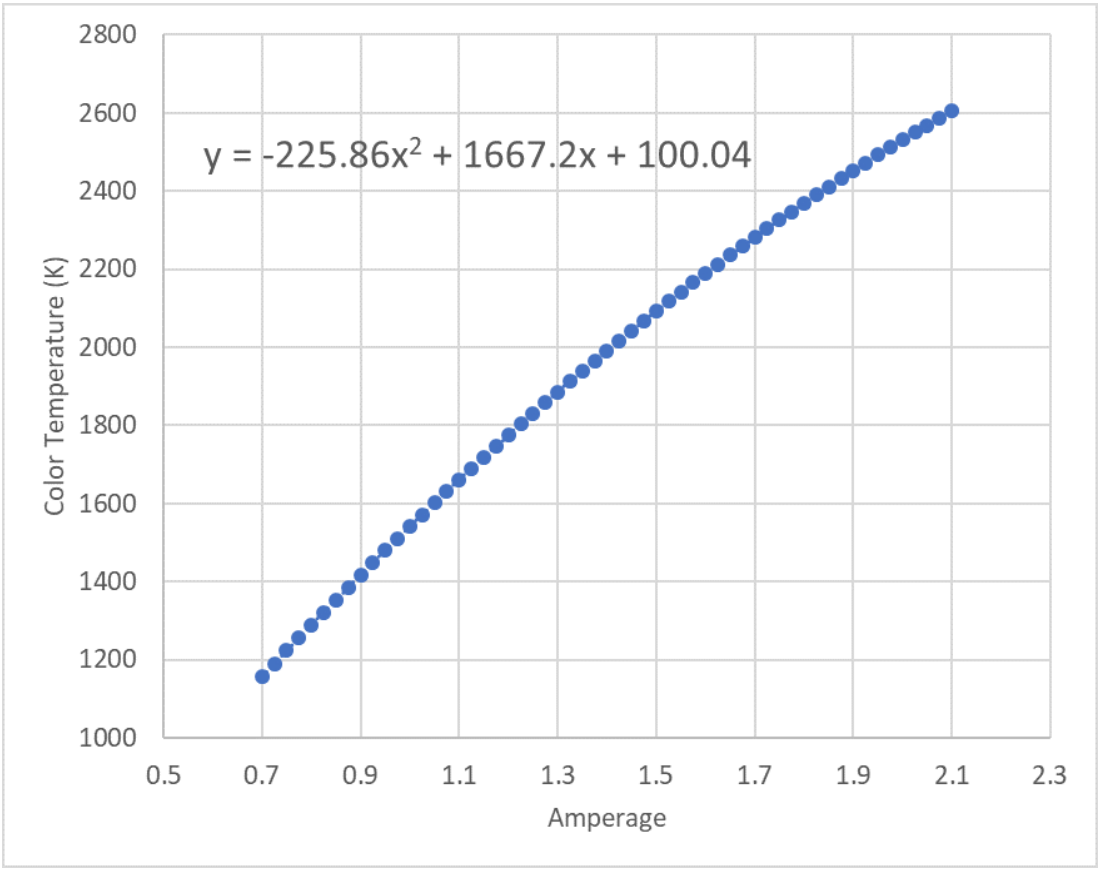

Figure 101. Color temperature of tungsten lamp at 650 nm as a function of the 12 V power supply amperage.

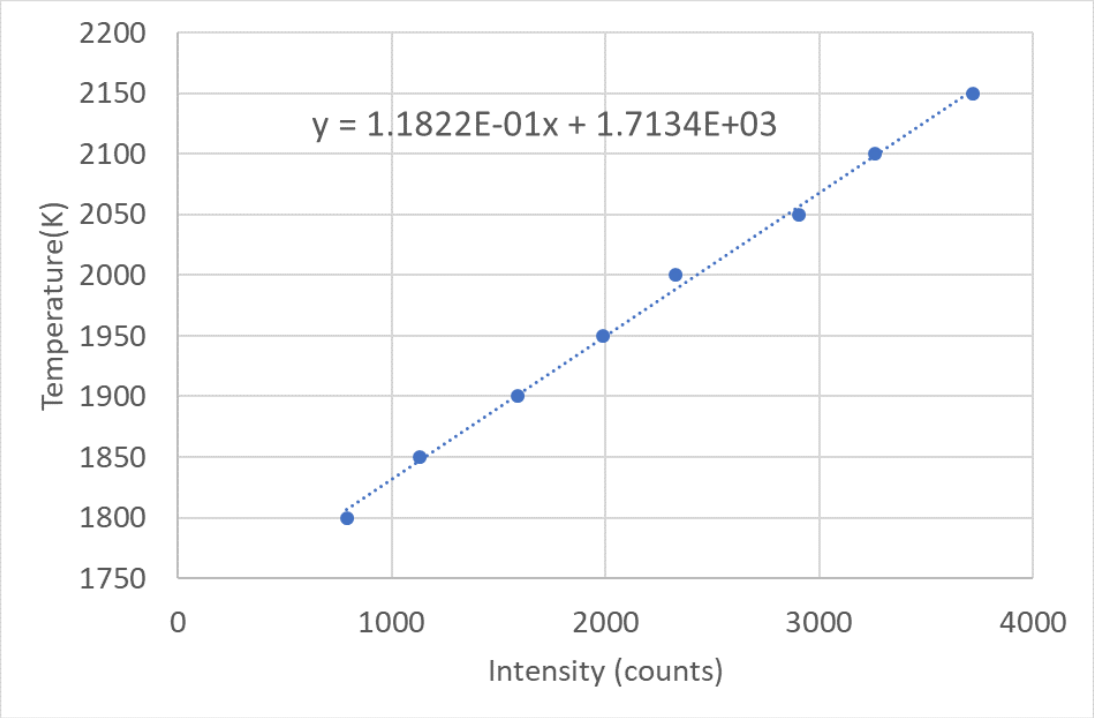

Figure 102. Calibration Curve for Phantom Pyrometer at 650 nm Using Tungsten Lamp.

Bibliography

1. Rankin, B. A., Fotia, M. L., Naples, A. G., Stevens, C. A., Hoke, J. L., Kaemming, T. A., Theuerkauf, S. W., and Schauer, F. R., "Overview of Performance, Application, and Analysis of Rotating Detonation Engine Technologies," *Journal of Propulsion and Power*, Vol. 33, No. 1, 2017, pp. 131–143.

2. Nakagami, S., Matsuoka, K., Kasahara, J., Kumazawa, Y., Fujii, J., Matsuo, A., and Funaki, I., "Experimental Visualization of the Structure of Rotating Detonation Waves in a Disk-Shaped Combustor," *Journal of Propulsion and Power*, Vol. 33, No. 1, 2017, pp. 80–88.

3. Huff, R., Polanka, M. D., McClearn, M. J., Schauer, F. R., Fotia, M. L., and Hoke, J. L., "Design and Operation of a Radial Rotating Detonation Engine," *Journal of Propulsion and Power*, Vol. 35, No. 6, 2019, pp. 1143–1150.

4. Huff, R., Schauer, F. R., Boller, S. A., Polanka, M. D., Fotia, M. L., and Hoke, J. L., "Exit Condition Measurements of a Radial Rotating Detonation Engine Bleed Air Turbine," *AIAA Scitech 2019 Forum*, AIAA 2019-1011, San Diego, 2019.

5. Huff, R., "Design, Buildup, and Testing of a Radial Rotating Detonation Engine for a Compact Auxiliary Power Unit," Master's Thesis, Air Force Institute of Technology, 2018.

6. Boller, S. A., Polanka, M. D., Huff, R., Schauer, F. R., Fotia, M. L., and Hoke, J. L., "Experimental Flow Visualization in a Radial Rotating Detonation Engine," *AIAA Scitech 2019 Forum*, AIAA 2019-1253, San Diego, 2019.

7. Fotia, M. L., Hoke, J. L., and Schauer, F. R., "Experimental Performance Scaling of Rotating Detonation Engines Operated on Gaseous Fuels," *Journal of Propulsion and Power*, Vol. 33, No. 5, 2017.

8. Kailasanath, K., "Recent Developments in the Research on Rotating-Detonation-Wave Engines," *55th AIAA Aerospace Sciences Meeting*, AIAA 2017-0784, Grapevine, 2017.

9. Schwer, D. and Kailasanath, K., "Numerical Investigation of Rotating Detonation Engines," *46th AIAA/ASME/SAE/ASEE Joint Propulsion Conference & Exhibit*, AIAA 2010-6880, Nashville, 2010.

10. Naples, A., Hoke, J., Karnesky, J., and Schauer, F., "Flowfield Characterization of a Rotating Detonation Engine," *51st AIAA Aerospace Sciences Meeting*, AIAA 2013-278, Grapevine, 2013.

11. Turns, S. R., *An Introduction to Combustion: Concepts and Applications*, McGraw-Hill, New York, 3rd ed., 2011.

12. Lee, J. H., *The Detonation Phenomenon*, Cambridge University Press, New York, 2008.

13. Schwer, D. A. and Kailasanath, K., "Rotating Detonation-Wave Engines," *NRL Review*, 2011.

14. Vutthivithayarak, R., Braun, E., and Lu, F., "Examination of the Various Cycles for Pulse Detonation Engines," *47th AIAA/ASME/SAE/ASEE Joint Propulsion Conference & Exhibit*, AIAA 2011-6064, San Diego, 2011.

15. Wintenberger, E. and Shepherd, J. E., "Thermodynamic Cycle Analysis for Propagating Detonations," *Journal of Propulsion and Power*, Vol. 22, No. 3, 2006, pp. 694–697.

16. Boller, S. A., "Flow Behavior in Radial Rotating Detonation Engines," Master's Thesis, Air Force Institute of Technology, 2019.

17. Cho, K. Y., Codoni, J. R., Rankin, B. A., Hoke, J., and Schauer, F., "Effects of Lateral Relief of Detonation in a Thin Channel," *55th AIAA Aerospace Sciences Meeting*, AIAA 2017-0373, Grapevine, 2017.

18. Reynaud, M., Virot, F., and Chinnayya, A., "Interactions of a Detonation Wave Confined by a High-Temperature Compressible Layer," *26th ICDERS*, Boston, 2017.

19. Mattingly, J. D., *Elements of Propulsion: Gas Turbines and Rockets*, AIAA, Reston, 2nd ed., 2006.

20. Aungier, R. H., *Turbine Aerodynamics: Axial-Flow and Radial-Flow Turbine Design and Analysis*, ASME Press, New York, 2005.

21. Huff, R., Polanka, M. D., McClearn, M. J., Schauer, F. R., Fotia, M. L., and Hoke, J. L., "A Disk Rotating Detonation Engine Part 2: Operation," *2018 AIAA Aerospace Sciences Meeting*, AIAA 2018-1607, Kissimmee, 2018.

22. Huff, R., Polanka, M. D., McClearn, M. J., Schauer, F. R., Fotia, M. L., and Hoke, J. L., "A Radial Rotating Detonation Engine Driven Bleed Air Turbine," *Joint Propulsion Conference*, AIAA 2018-4879, Cincinnati, 2018.

23. "Sonic Nozzles - FlowMaxx Engineering," 2019.

24. Yin, Z. Q., Li, D. S., Meng, J. L., and Lou, M., "Discharge Coefficient of Small Sonic Nozzles," *Thermal Science*, Vol. 18, No. 5, 2014, pp. 1505–1510.

25. Stevens, C. A., Fotia, M. L., Hoke, J. L., and Schauer, F. R., "Comparison of Transient Response of Pressure Measurement Techniques with Application to Detonation Waves," *53rd AIAA Aerospace Sciences Meeting*, AIAA 2015-1102, Kissimmee, 2015.

26. Kiel, G., "Total-Head Meter with Small Sensitivity to Yaw," *Luftfahrtforschung*, 1935.

27. Goss, L. P., Vilimpoc, V., Sarka, B., and Lynn, W. F., "Thin-Filament Pyrometry: A Novel Thermometry Technique for Combusting Flows," *Journal of Engineering for Gas Turbines and Power*, Vol. 111, 1989, pp. 46–52.

28. Vilimpoc, V., Goss, L. P., and Sarka, B., "Spatial Temperature-Profile Measurements by the Thin-Filament-Pyrometry Technique," *Optics Letters*, Vol. 13, No. 2, 1988, pp. 93–95.

29. "Saber-Rig Experimental Campaign," Innovative Scientific Solutions, Inc., Dayton, 2014.

30. Huff, R., Polanka, M. D., McClearn, M. J., Schauer, F. R., Fotia, M., and Hoke, J. L., "A Disk Rotating Detonation Engine Part 1: Design and Buildup," *2018 AIAA Aerospace Sciences Meeting*, AIAA 2018-0633, Kissimmee, 2018.

31. Kaemming, T. A. and Paxson, D. E., "Determining the Pressure Gain of Pressure Gain Combustion," *Joint Propulsion Conference*, AIAA 2018-4567, Cincinnati, 2018.

32. Snyder, C., "CEARUN," 2019.

33. Andrus, I. Q., *Design and Experimentation of a Premixed Rotating Detonation Engine*, Ph.D. thesis, Air Force Institute of Technology, 2016.

34. "GTX3582R GEN II Mid Frame Turbocharger - Garrett Motion," 2019.

35. Spalart, P. R. and Allmaras, S. R., "One-Equation Turbulence Model for Aerodynamic Flows," *Recherche aerospatiale*, 1994.

36. "Aremco — New Ceramabond 569 Bonds & Coats Platinum Resistance Heaters," 2011.

37. Kaneshige, M. and Shepherd, J. E., "Detonation Database," Tech. rep., GALCIT, 1997.

38. Muraleetharan, K., Polanka, M. D., Schauer, F. R., and Huff, R., "Detonation Confinement using a Flat Channel Plate in a Radial Rotating Detonation Engine," *AIAA Scitech 2020 Forum*, AIAA 2020-0200, Orlando, 2020.

39. Fotia, M. L., Schauer, F. R., Kaemming, T. A., and Hoke, J. L., "Experimental Study of the Performance of a Rotating Detonation Engine with Nozzle," *Journal of Propulsion and Power*, Vol. 32, No. 3, 2016, pp. 674–681.

40. Bennewitz, J. W., Bigler, B. R., Hargus, W. A., Danczyk, S. A., and Smith, R. D., "Characterization of Detonation Wave Propagation in a Rotating Detonation Rocket Engine using Direct High-Speed Imaging," *Joint Propulsion Conference*, AIAA 2018-4688, Cincinnati, 2018.

41. de Izarra, C. and Gitton, J.-M., "Calibration and Temperature Profile of a Tungsten Filament Lamp," *European Journal of Physics*, Vol. 31, 2010, pp. 933–942.

42. "Disappearing Filament Optical Pyrometer," PYRO MicroTherm, Pyrometer LLC, Ewing, 2019.

REPORT DOCUMENTATION PAGE

Form Approved
OMB No. 0704–0188

1. REPORT DATE *(DD–MM–YYYY)*	2. REPORT TYPE	3. DATES COVERED *(From — To)*
26-03-2020	Master's Thesis	Oct 2018 Mar 2020

4. TITLE AND SUBTITLE

DETONATION CONFINEMENT IN A
RADIAL ROTATING DETONATION ENGINE

5a. CONTRACT NUMBER

5b. GRANT NUMBER

5c. PROGRAM ELEMENT NUMBER

6. AUTHOR(S)

Kavi Muraleetharan, 2d Lt

5d. PROJECT NUMBER

5e. TASK NUMBER

5f. WORK UNIT NUMBER

7. PERFORMING ORGANIZATION NAME(S) AND ADDRESS(ES)

Air Force Institute of Technology
Graduate School of Engineering and Management (AFIT/EN)
2950 Hobson Way
WPAFB OH 45433-7765

8. PERFORMING ORGANIZATION REPORT NUMBER

AFIT-ENY-MS-20-M-273

9. SPONSORING / MONITORING AGENCY NAME(S) AND ADDRESS(ES)

Air Force Research Lab Aerospace Directorate
Combustion Branch, Turbine Engine Division
1790 Loop Road North
WPAFB OH 45433-7765

10. SPONSOR/MONITOR'S ACRONYM(S)

AFRL/RQTC

11. SPONSOR/MONITOR'S REPORT NUMBER(S)

12. DISTRIBUTION / AVAILABILITY STATEMENT

DISTRIBUTION STATEMENT A:
APPROVED FOR PUBLIC RELEASE; DISTRIBUTION UNLIMITED.

13. SUPPLEMENTARY NOTES

14. ABSTRACT

Radial Rotating Detonation Engines (RRDE) have provided an opportunity for use of a pressure-gain combustor in a more compact form compared to an axial RDE. A successfully tested RRDE was modified from its constant area detonation chamber to a decreasing area design as the flow travelled radially inward to confine the detonation wave to a more radially outward position to improve combustion time and efficiency. The detonation chamber featured a flat channel plate that reduced the flow's effective cross-sectional area by almost 65% from its inlet to the turbine inlet plane. The constant channel height improved total pressure loss as high as 92% over the constant area geometry for similar flow conditions and increased the RRDE's ability to operate at larger channel heights. Guide vanes were introduced downstream of the combustion section by modifying the flat channel plate with modular channel plates. While in this configuration, the RRDE operated at both detonative and acoustic wave modes. Thin-filament pyrometry (TFP) was also performed to measure transient temperature responses during operation. The successful implementation of the filaments provided temperature measurements during detonative modes up to 2194 K at the guide vanes and frequency responses captured through TFP between 1.6-5.9 kHz.

15. SUBJECT TERMS

Rotating Detonation Engine, Radial Rotating Detonation Engine, Disk Rotating Detonation Engine, Combustion, Pressure-Gain Combustion, Thin-Filament Pyrometry

16. SECURITY CLASSIFICATION OF:			17. LIMITATION OF ABSTRACT	18. NUMBER OF PAGES	19a. NAME OF RESPONSIBLE PERSON
a. REPORT	b. ABSTRACT	c. THIS PAGE			Dr. Marc D. Polanka, AFIT/ENY
U	U	U	UU	194	19b. TELEPHONE NUMBER *(include area code)* (937) 255-3636, x4714; marc.polanka@at.edu